PONTIFÍCIA UNIVERSIDADE CATÓLICA
DO RIO DE JANEIRO

Damien Foiny

**Coupled Systems in Mechanics :
Fluid Structure Interactions**

Dissertação de Mestrado

Dissertation presented to the Programa de Pós–graduação em Engenharia Mecânica of PUC-Rio in partial fulfillment of the requirements for the degree of Mestre em Engenharia Mecânica.

Advisor   :   Prof. Rubens Sampaio Filho
Co-advisor: Profa. Roberta de Queiroz Lima

Rio de Janeiro
August 2017

Damien Foiny

**Coupled Systems in Mechanics :
Fluid Structure Interactions**

Dissertation presented to the Programa de Pós–graduação em Engenharia Mecânica of PUC-Rio in partial fulfillment of the requirements for the degree of Mestre em Engenharia Mecânica. Approved by the undersigned Examination Committee.

Prof. Rubens Sampaio Filho
Advisor
Departamento de Engenharia Mecânica – PUC-Rio

Profa. Roberta de Queiroz Lima
Co-advisor
Departamento de Engenharia Mecânica – PUC-Rio

Prof. Daniel Alves Castello
UFRJ

Prof. Thiago Gamboa Ritto
UFRJ

Prof. Márcio da Silveira Carvalho
Vice Dean of Graduate Studies
Centro Técnico Científico – PUC-Rio

Rio de Janeiro, August 22th, 2017

Damien Foiny

Graduated from the Department of Mechanical Engineering of the National Institute of Applied Sciences of Rouen in France (INSA-Rouen, Institut National des Sciences Appliquées), has been working for the last two years in the Laboratory of Dynamics and Vibrations of the PUC-Rio on the subject of this dissertation and several articles published in conferences.

To my little mussel, my parents and my brother.

Acknowledgments

First, I would like to thank my advisor, Prof. Rubens Sampaio, for everything he has done for me during these two years on the academic point of view but also in so many different aspects, which were essential to my development as a professional. I am conscious of the opportunity he gave me to work in his Laboratory and I am infinitely grateful for that .

Then I wish to thank Prof. Roberta Lima, which is my co-advisor in this work, for all her support and hints during my studies at the Laboratory of Dynamics and Vibrations. Her help in many cases was the key of my success during these two years.

Thank to the PUC-Rio and to CAPES, CNPq and FAPERJ for the support during these two years and for all the conducted projects.

I would like also to thank my colleagues at the Laboratory for helping my integration in the group, especially Gustavo Wagner with whom I have worked a lot in several articles and whom even helped in this dissertation. All of them worked with a remarkable good mood every day during all this period and I really appreciated working with them.

Also, I would like to thank my parents who always supported me in this project and gave me all the keys to succeed and bring this work until the end. Since the beginning of this adventure in Brazil, they have always trusted in me and accepted my choices.

Finally, as one of the most important persons for the success of this project, I would like to thank my girlfriend Ana Luiza. She supported me every day and helped me to overcome my doubts during these years.

Abstract

Foiny, Damien; Sampaio Filho, Rubens (Advisor); de Queiroz Lima, Roberta (Co-Advisor). **Coupled Systems in Mechanics : Fluid Structure Interactions**. Rio de Janeiro, 2017. 141p. Dissertação de Mestrado – Departamento de Engenharia Mecânica, Pontifícia Universidade Católica do Rio de Janeiro.

Fluid-structure interactions are very common in mechanical and civil engineering because many structures, as bridges, offshore risers, transmission lines or wind turbines are directly in contact with a fluid, which can be air, which will be source of wind, or water, which will perturb the structure through waves. An important role of the engineer is to prevent structure failure due to instabilities created by the fluid-structure interactions. This work will first present all the basic concepts needed for the study of fluid-structure interaction problems. Thus, a dimensional analysis of those problems is performed and also all the equations governing such cases are presented. Then, thanks to the dimensional analysis made, a classification of problems, namely based on the reduced velocity, can be done and some conclusions concerning the consequences of the fluid-structure interactions can be drawn in terms of stability or, which is more interesting, instability. Indeed, using simplified models one can show static and dynamic flow-induced instabilities that may be critical for the structure. The final parts of the work will present a specific non-linear structure, a suspension bridge. First the formulation of a simplified one-dimensional model is explained and then, through a finite element discretization, a dynamical study is performed. Also, some conclusions are made concerning the dynamic of suspension bridges. The last part of this work presents a method that was an important source of publication for us, the Smooth Decomposition method.

Keywords

Fluid-Structure Interactions; Smooth Decomposition; Coupled Systems; Suspension Bridge;

Resumo

Foiny, Damien; Sampaio Filho, Rubens; de Queiroz Lima, Roberta. **Sistemas Acoplados em Mecânica : Interações Fluido-Estrutura**. Rio de Janeiro, 2017. 141p. Dissertação de Mestrado – Departamento de Engenharia Mecânica, Pontifícia Universidade Católica do Rio de Janeiro.

As interações fluido-estrutura são muito comuns na engenharia mecânica e civil porque muitas estruturas, como pontes, plataformas de petróleo, linhas de transmissão ou turbinas eólicas, estão diretamente em contato com um fluido, que pode ser o ar, no caso de vento, ou água, que irá perturbar a estrutura através de ondas. Um papel importante do engenheiro é prevenir a falha da estrutura devido às instabilidades criadas pelas interações fluido-estrutura. Este trabalho apresentará em primeiro lugar todos os conceitos básicos necessários para o estudo de problemas de interação fluido-estrutura. Assim, é realizada uma análise dimensional visando classificar os problemas de fluido-estrutura. A classificação é baseada na velocidade reduzida, e algumas conclusões sobre as conseqüências das interações fluido-estrutura podem ser feitas em termos de estabilidade ou, o que é mais interessante, de instabilidade. De fato, usando modelos simplificados, pode-se mostrar instabilidades estáticas e dinâmicas, induzidas por fluxo, que podem ser críticas para a estrutura. As partes finais do trabalho apresentarão uma estrutura não-linear específica, uma ponte suspensa. Primeiro, a formulação de um modelo simplificado unidimensional é explicada e, em seguida, através de uma discretização por elementos finitos, é realizado um estudo dinâmico. Além disso, algumas conclusões são apresentadas sobre a dinâmica das pontes suspensas. A última parte deste trabalho apresenta um método que foi uma importante fonte de publicação para nós, o método de decomposição regular.

Palavras-chave

Interações Fluido-Estrutura; Decomposição Regular; Sistemas Acoplados; Ponte suspensa;

Table of contents

List of figures

List of tables

1
Introduction

Solid structures as bridges, buildings, offshore risers, transmissions lines, wind or marine current turbines and so on, are directly in contact with fluid, which could be water, air or both of them. These fluids are generally in motion and create fluid flows such as waves or wind. Those flows can then generate forces called flow-induced forces and also vibrations (as said in[38] or in [49]), flow-induced vibrations. One can generalize these phenomena under the terminology flow-induced instabilities. As for any mechanical system, these forces and vibrations may be of small or large amplitude which can be source of different type of damage [15], from fatigue and fretting wear (in the case of small amplitude forces and vibrations), which will occur in the long term, to other consequences in a much shorter term in the case of large forces and vibrations. In both cases, these damages can lead to dramatic consequences for the structure and the most radical one is the collapse of the structure.

In many cases, before the collapse of the structure one has observed a brutal and sudden change in the behavior of the structure dynamic. This phenomena can be explained if one considers self-excited vibrations. Indeed, on one side of the flow velocity threshold, the structure dissipates the instabilities and its dynamic is not really impacted, when, on the other side of this threshold, these instabilities may grow and the dynamic of the structure is completely different. Thus, understand how this kind of phenomena appears is really important considering the damage they can cause.

The main source of flow-induced instabilities is related to cross-flow, when the flow is normal to the long axis of the structure. The particularity of cross-flow-induced instabilities is that they occur in natural conditions (e.g. wind for flexible bridges, waves for offshore risers) and not necessary for extreme natural conditions such as strong winds, hurricanes or huge waves. Indeed, if the structure was not well designed, standard conditions of wind and waves can create cross-flow-induced instabilities. This is the reason why engineers and designers involved in such projects need to know all the concepts behind fluid-structure interactions.
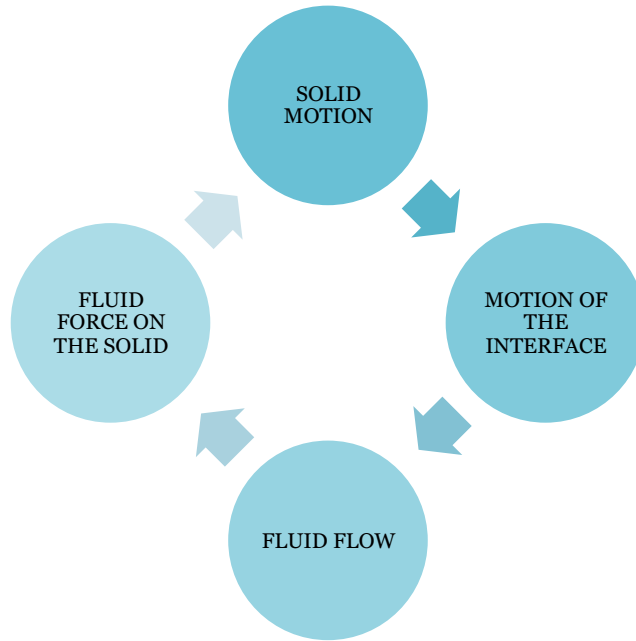
Figure 1.1: Diagram of the principle of fluid-solid interactions.

First of all, one should remind how fluid-solid or fluid-structure interactions occur in coupled systems (as said in [53]). Usually, this kind of interactions is represented as an infinite circle (see Fig.1.1) made of four main parts: the solid domain, the fluid domain, the fluid forces acting on the solid and the solid forces acting on the fluid through the motion of the solid. To better explain this process, one can take a simple example. Considering for instance a garden hose with water flow inside, the different steps can be identified. First the fluid flow will create a force on the tube of the hose. Due to this fluid force, the hose will be deformed and thus the dynamic of the solid domain will be impacted. This deformation will thus affect the fluid-solid interface which will be different. This modification of the interface will finally perturb the fluid flow and so on. This is a simple example of the whole process of fluid-solid interaction problems.

All this problem is governed by differential equations and some sets of boundary conditions which are presented later in this discussion. The objective of this dissertation is, for the first part, to present some basic concepts of fluid-structure interactions in terms of dimensional analysis which will lead to dimensionless variables and some dimensionless numbers. Also, in this part, one will find the equations governing general fluid-structure interactions problems.

Then, in the second chapter, for different situations and conditions of fluid-structure interactions systems, some consequences and characteristic

phenomena will be presented. Thus, several cross-flow-induced instabilities will appear and their causes are going to be explained. The influence of some characteristic dimensionless numbers is taken as comparison base and a classification of fluid-solid interaction problems can be done.

Usually, fluid-structure interactions can be classified into different types depending on various characteristic non-dimensional numbers of the system. This will be better explained in the second chapter, but, basically, according to the common classification, the characteristic non-dimensional numbers of the system will define if the coupling between the fluid and structure is weak or strong. Depending on this consideration, several assumptions can be made.

After describing in detail the basic concepts of fluid-structure interactions, one will focus on a numerical case. The fourth chapter of the dissertation will present a numerical model of a suspension bridge which is a structure that can suffer from fluid-structure interactions. This type of mechanical system is quite interesting because it can be modeled in a relatively simple way and because some non-linearities should be considered. One of the objectives of this dissertation is to observe the influence of the non-linearities on the motion of the structure. The fifth chapter will remind some basic concepts of the finite element formulation that will be used to solved the mechanical system presented in the fourth chapter. Then the sixth chapter will focus on some simulations and some conclusions will be drawn, namely concerning the non-linearity of the system. Also, a representation of a fluid-structure interaction phenomenon will be investigated for several conditions of the non-linearity in the system. Finally, the last chapter will focus on the energy partition during the simulations. To do this, a modal analysis tool that works for non-linear systems may be used. Thus, one proposes to use the Smooth Decomposition method. This method was an important topic of our research during the last past years at the Laboratory.

2
Fluid-structure interactions

In order to start on solid basis the study of fluid-structure interactions, one should start with a fundamental tool for this kind of problem, the dimensional analysis. After this, the equations relative to fluid-structure interactions problem are discussed. For this chapter the theory is based namely on [3] and [61].

2.1
Dimensional analysis

In order to better understand and investigate the interactions between fluid and structure or fluid and solid, one could be interested in simplify the problems. Dimensional analysis (presented in [35]) is a powerful tool to classify problems. It is very helpful for such classifications according to some dimensionless numbers. This part will explain and present the dimensional analysis and its application for several problems. The discussion is based on [19] and [61] for the theory of the method and also for its application on the specific case of fluid-structure interaction problems.

The objective of this method is to simplify the formulation of the problem and its equations. This method consists of reducing the number of variables in the problem taking care of the dependence between them. This is very common in fluid mechanics problems.

To apply this method one can follow some basic steps. To begin, one needs to identify the variables which are relevant for describing the problem and then relate them to the physical laws that govern the system. Of course, one important step of the procedure consists of identifying the variables or parameters that will be the most relevant to observe the results, discuss and interpret the solutions of the problem.

One important and essential tool for this method is the Pi-Theorem (also called π-Theorem or Buckingham's Pi-Theorem). This formulation will lead to dimensionless numbers, that will allow a classification of problems. With this classification it is possible to identify some characteristic phenomena and thus do some simplifications.

2.1.1
Buckingham's Pi-theorem

This method and this theorem state the number of π-quantities remaining after the dimensional analysis. This number is equal to the difference between the number of quantities involved in the problem and the maximum number of them that are dimensionally independent. It is quite obvious that the number of π-quantities is smaller or equal to the number of fundamental dimensions needed to write dimensional equations. This statement can be express as:

$$P = N - R, \tag{2-1}$$

where N is the number of physical variables involved in the problem written with R fundamental units. The number of π-quantities P corresponds to the number of dimensionless variables expressed from the original ones. The way to choose the variables taken into account in the dimensionless analysis is presented later on, but first let's state the Pi-Theorem.

<u>Pi-theorem statement:</u> Let R be the number of fundamental dimensions required to describe the physical variables and x_1, x_2, ..., x_N represent N physical variables in the relation:

$$f(x_1, x_2, ..., x_N) = 0. \tag{2-2}$$

The physical relation f may be also expressed as a relation of P dimensionless products (called π-products) such as:

$$F(X_1, X_2, ..., X_P) = 0, \tag{2-3}$$

where $P = N - R$. Each π-product X_k is a dimensionless product of a set of $(k+1)$ physical variables. Calling p_1, p_2, ..., p_N the selected sets of k physical variables which leads to:

$$\begin{aligned}
X_1 &= F_1(p_1, p_2, ..., p_k, p_{k+1}) \\
X_2 &= F_2(p_1, p_2, ..., p_k, p_{k+2}) \\
&\vdots \\
X_P &= F_P(p_1, p_2, ..., p_k, p_N)
\end{aligned} \tag{2-4}$$

The choice of the repeating variables p_1, p_2, ..., p_k should be such that they include all the k dimensions used in the problem. The dependent variables should appear in only one of the π-products.

Basically, the dimensional analysis is based on the fact that for a given equation, both sides of the equal-sign have the same dimension. Then, the different terms involved in the equation have the same dimension too.

Considering this, one can then express a dimensionless equation. For example, let's consider three different quantities called x_1, x_2 and x_3 related as following:

$$x_1 + x_2 = x_3 \tag{2-5}$$

Then, dividing the entire equation (2-5) by x_3 leads to a dimensionless equation equivalent to the previous one:

$$\frac{x_1}{x_3} + \frac{x_2}{x_3} = 1. \tag{2-6}$$

This simple illustration of the method of dimensional analysis shows that manipulating the terms respecting their dimensions, one can find dimensionless terms and expressions. At this step, it is important to discuss more about dimensions and dimensional homogeneity.

2.1.2
Dimensions and dimensional homogeneity

First one should introduce the concept of dimension of a given quantity. According to the Maxwell convention, if x is a physical quantity, then its dimension is written $[x]$. Thus, for simple variables, one can easily define a table with the dimension of common physical variables such as length, mass or time (this part only focuses on the variables involved in fluid-structure interaction problems but this discussion can be realized for any kind of problem such as electrical or magnetic systems). Doing this, one defines a dimension table of a given class. For each problem type one can limit the class according to the variables involved.

The mathematical model of fluid-structure interaction usually deals with dimensions of length, mass, time, frequency, velocity, acceleration, force, etc. All these physical quantities are written in Table 2.1. As it is quite obvious, each physical variable can be written as a combination of the units of the class. One says that physical variables are power law monomials. Thus, for any physical variable x, its dimension can be expressed thanks to the following expression called dimension homogeneity:

$$[x] = CL^\alpha M^\beta T^\gamma, \tag{2-7}$$

where C, α, β and γ are constants (directly linked to the involved system of units). This expression is the central point of dimensional analysis. All the following dimensionless variables and equations of this section are written thanks to this formulation.

Quantity	Physical meaning	Dimension
l, x	Length	L
m	Mass	M
t	Time	T
v, u	Velocity	LT^{-1}
a	Acceleration	LT^{-2}
F	Force	MLT^{-2}
ρ	Mass density	ML^{-3}
p	Pressure	$ML^{-1}T^{-2}$
k	Stiffness	$ML^{2}T^{-2}$
f, ω	Frequency	T^{-1}

Table 2.1: Dimension table of class Length-Mass-Time.

Knowing this, one can express the dimension matrix of any system. For example, let's consider the physical system involving the physical variables $x_1, x_2, ..., x_N$. As seen before, each dimension of each variable can be expressed as a combination of the LMT-class dimensions such as :

$$[x_i] = L^{\alpha_i} M^{\beta_i} T^{\gamma_i}. \tag{2-8}$$

Then the dimension matrix can be written as :

$$M_D = \begin{bmatrix} \alpha_1 & \alpha_2 & \cdots & \alpha_N \\ \beta_1 & \beta_2 & \cdots & \beta_N \\ \gamma_1 & \gamma_2 & \cdots & \gamma_N \end{bmatrix}. \tag{2-9}$$

From this matrix one can deduce the number of dimensionless variables P necessary to describe the problem such as $P = N - R$ where:

$$R = rank(M_D). \tag{2-10}$$

At this step one knows exactly the number of dimensionless variables necessary to describe the problem but does not know what they are. The Pi-Theorem does not give this information. How to choose the dimensionless variables is presented later in this section. One can only determine the exponents of each physical variable involved to describe the dimensionless quantities with the kernel of the dimension matrix, called K_e, such as:

$$\begin{bmatrix} [X_1] & [X_2] & ... & [X_P] \end{bmatrix} = K_e \begin{bmatrix} x_1 & x_2 & ... & x_N \end{bmatrix}. \tag{2-11}$$

Doing this does not mean that the dimensionless numbers obtained from this expression are the most convenient for the problem. Actually this result does

only permit to get a linear expression for all the exponents. To illustrate the method of Pi-Theorem, let's present two simple examples.

Example 1 - Dimensional analysis of a static 1dof-mass-spring system:
This is a really simple case but it permits to understand how to apply this theorem. Let's assume that the displacement of the mass is the unknown of the problem. The system is described with its mass m, the stiffness of the spring k, the external constant force F and the constant displacement x.
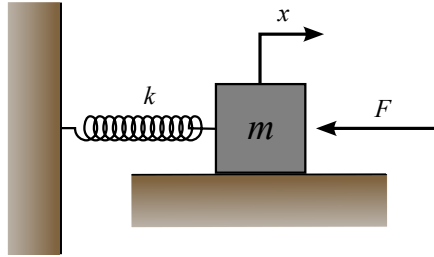
Figure 2.1: Simple 1-dof mass spring forced system.

Quantity	Physical meaning	Dimension
m	Mass	M
k	Stiffness	MT^{-2}
F	Force	LMT^{-2}
x	Displacement	L

Table 2.2: Dimension table of class LMT for the mass-spring system.

Thus, this system has four physical quantities that define it (cf. Table 2.2), thus $N = 4$. The equation governing the displacement of the system can be written as:

$$g(m, k, F, x) = 0. \tag{2-12}$$

One can build up the dimension matrix M_D thanks to the constant α, β and γ of each variable and get:

$$M_D = \begin{bmatrix} 0 & 0 & 1 & 1 \\ 1 & 1 & 1 & 0 \\ 0 & -2 & -2 & 0 \end{bmatrix}, \tag{2-13}$$

where the rows represent the three independent dimensions of the system and the columns represent the four parameters involved to describe the problem. Then one can determine how many dimensionless variable are necessary to describe the problem. Let's first calculate the rank of this matrix:

$$R = rank(M_D) = 3. \tag{2-14}$$

Thus, the number of dimensionless variables needed is:

$$P = N - R = 1. \tag{2-15}$$

That means that this problem can be expressed only with one dimensionless variable. Now, calculating the kernel of the M_D called K_e, one finds the exponents of each physical variables that lead to a dimensionless number. In this case,

$$K_e = \begin{bmatrix} 0 & -1 & 1 & 1 \end{bmatrix}^T, \tag{2-16}$$

then,

$$[X] = [m]^0 [k]^{-1} [F]^1 [x]^1 \Rightarrow X = \frac{Fx}{k} \tag{2-17}$$

As it is well known, the equation governing such a problem is $F = -kx$ which is coherent with (2-17). Considering the dimension of each physical quantity, one can deduce the dimension of X and verify that it is well dimensionless:

$$[X] = \frac{MLT^{-2} \times L}{ML^2T^{-2}} = 1. \tag{2-18}$$

At this step, the dimensional analysis gives the relation between the four physical variables involved in the problem. The dimensionless equation governing the system is:

$$G(X) = 0, \tag{2-19}$$

and thanks to (2-17) one can affirm that the displacement is not a function of the mass since the exponent relative to the mass is zero. But it is important to note that this method does not tell which variable we should use later in the problem, it only gives a relation between all the physical variables. It is important to verify the physical meaning of each dimensionless variable before doing further calculations. Also, this method does not give the system of units that should be used.

Example 2 - Dimensional analysis of a flow around a cylinder: Let's consider a cylinder in a fluid flow as presented in Fig.2.2. In this example, several physical variables (dimensional quantities) such as the upstream velocity U, the density of the fluid ρ, its viscosity μ and the diameter of the cylinder L are present. Now, considering the drag D_r (force exerted by the flow on the solid), five physical variables ($N = 5$) should be taken into account. The governing equation for the drag is then:

$$g(D_r, U, \rho, \mu, L) = 0, \tag{2-20}$$
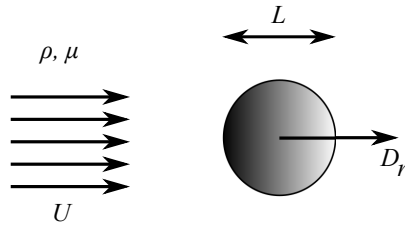
Figure 2.2: Cylinder in a cross flow.

Quantity	Physical meaning	Dimension
D_r	Drag Force	LMT^{-2}
U	Velocity	LT^{-1}
ρ	Density	ML^{-3}
μ	Viscosity	$ML^{-1}T^{-1}$
L	Length	L

Table 2.3: Dimension table of class LMT for a flow around a cylinder.

which is dimensional. The dimension table (Cf. Table 2.3) can be built as in the previous example. Now, thanks to this table one can build up the dimension matrix M_D with all the constant α, β and γ of each physical variable. Therefore, the rank of this matrix can be calculated and gives R. Then,

$$M_D = \begin{bmatrix} 1 & 1 & -3 & -1 & 1 \\ 1 & 0 & 1 & 1 & 0 \\ -2 & -1 & 0 & -1 & 0 \end{bmatrix}, \tag{2-21}$$

$$R = rank(M_D) = 3. \tag{2-22}$$

Finally, the number of dimensionless variables needed to define the problem is calculated as

$$P = N - R = 2. \tag{2-23}$$

At this step, one knows that two dimensional variables are needed to define the problem but does not know them. Calculating the kernel K_e of the dimension matrix will lead to:

$$K_e = \begin{bmatrix} -1 & 2 & 1 & 0 & 2 \\ -1 & 0 & -1 & 2 & 0 \end{bmatrix}^T. \tag{2-24}$$

Using the properties of the kernel (cf. the box called "Property of the kernel"), one can use other exponents more suitable and more comfortable which will lead to dimensionless variables with physical meaning only multiplying by a given constant.

> **Property of the kernel:** Let's consider a linear application f of a vector space A into a vector space B. The kernel K_e of f is defined as:
>
> $$K_e = \{x \in A | f(x) = 0\}$$
>
> One can also write that if K_e is a kernel of f then αK_e will also verify this property for $\forall \alpha \in \mathbb{R}$.

Indeed, for this problem, the drag function can be written thanks to the drag coefficient C_D and the Reynolds number R_E. With the first column of the kernel of the dimension matrix one can write the dimension of the first dimensionless variable X_1 as (using the property of the kernel and multiplying this column by -1):

$$[X_1] = [D_r]^1[U]^{-2}[\rho]^{-1}[\mu]^0[L]^{-2} \Rightarrow X_1 = \frac{D_r}{\rho U^2 L^2}, \qquad (2\text{-}25)$$

as it is well known, this quantity is the drag coefficient C_D. With the second column of the kernel, one can write the dimension of the second dimensionless variable X_2 as:

$$[X_2] = [D_r]^{-1}[U]^0[\rho]^{-1}[\mu]^2[L]^0 \Rightarrow X_2 = \frac{\mu^2}{D_r \rho}, \qquad (2\text{-}26)$$

but this quantity does not have any physical meaning. Reorganizing things in a different way:

$$[X_2] = \frac{[\rho][U][L]}{[\mu]} \times \frac{[\mu]^3}{[D_r][\rho]^2[U][L]}, \qquad (2\text{-}27)$$

after verifying that the second term of the expression is equal to 1, one can simplify it which leads to:

$$X_2 = \frac{\rho U L}{\mu}, \qquad (2\text{-}28)$$

here one recognizes the Reynolds number. Thus, the problem with five dimensional variables can be written with two dimensionless variables only as:

$$G(C_D, R_E) = 0. \qquad (2\text{-}29)$$

2.1.3
Some common dimensionless numbers

Now the basic concepts of dimensional analysis were stand out, let's focus on some common dimensionless numbers usually found in fluid dynamics and, therefore, in fluid-structure interactions in mechanical systems. Later, using these numbers, one will be able to classify problems and then to do some simplifications that will be useful. Indeed, those considerations will permit to identify some physical phenomena.

2.1.3.1
Reynolds number

A very common dimensionless number in fluid mechanics is the Reynolds number noted here as R_E. Considering a cylinder with a diameter L in a fluid flow of reference velocity U_0, the Reynolds number can be written as:

$$R_E = \frac{\rho U_0 L}{\mu}, \tag{2-30}$$

where ρ represents the density and μ the viscosity of the fluid involved. This number indicates the regime of the flow from laminar to turbulent and allows to classify the topology of the fluid around the cylinder. Depending on the value of the Reynolds number, for instance, one can easily determine if the flow will creep (for small R_E) or if it will be detached (for high R_E) from the cylinder as presented in Figure 2.3.
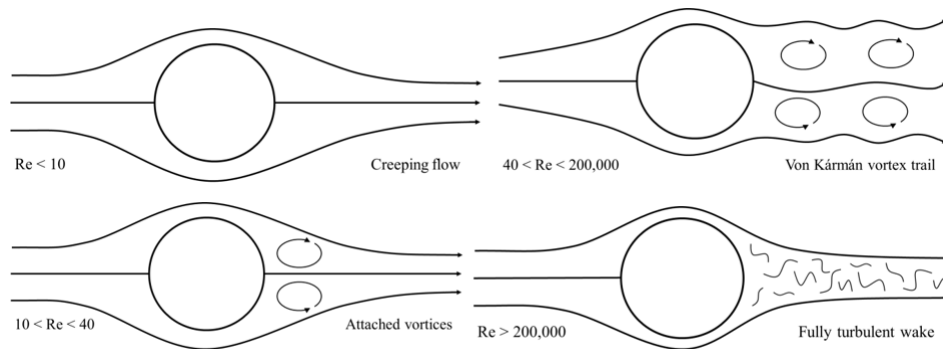
Figure 2.3: Evolution of the fluid topology in relation to the Reynolds number.
Source: *http://www.et4u.org/Toy_information/Cylinder_flow.html*,
consulted July, 3rd of 2017

2.1.3.2
Cauchy number

The Cauchy number is also a very common dimensionless number generally used for compressible flows. Usually noted C_A, this number can be written as the ratio between the inertial and elastic forces:

$$C_A = \frac{\rho U_0^2}{K}, \tag{2-31}$$

where ρ represents the density of the fluid, U_0 the reference flow velocity and K is the bulk modulus of elasticity. It is quite interesting to note that for isentropic processes, the Cauchy number is equal to another dimensionless number, the Mach number.

2.1.3.3
Froude number

An other common dimensionless number is the Froude number representing the ratio of the flow inertia and an external field, for instance the gravity field. Usually noted F_R, this number can be written as:

$$F_R = \frac{U_0}{\sqrt{gL}}, \tag{2-32}$$

where U_0 is the reference flow velocity, g the gravity field and L the characteristic length.

2.1.4
Dimensionless variables in the fluid domain

In order to define the variables of the system, let's consider the fluid-solid system as two separated systems which means that there is no mass transfer between them. Thus, one considers the decoupled problem first. Then for each domain, one needs to specify the physical quantities involved in the system.

The quantities are all related through the physical laws and differential equations presented later in the next chapters. These quantities are specific for the problems studied here. It is clear that for other problems, this list could be much longer and could include, for the fluid domain, temperature or pressure for instance.

An important point is to understand how to pass from the physical quantities defined before to the dimensionless variables. Once again, this step can be done separately for both domains, the fluid and the solid and then associate them to form the complete system.

Let's start with the fluid domain. Table 2.4 shows the physical variables that will be considered. All of them are related with physical laws (which means by differential equations) which can be written as the following dimensional equation:

$$g_F(x, t, U, \mu, L, g, \rho_F, U_0) = 0. \tag{2-33}$$

Observe that this law represents a pure fluid system since no variables from the solid are involved yet. Then, the objective is to perform the dimensional analysis of this law (made of eight physical variables, $N_F = 8$). First the LMT-class dimension table is built for this pure fluid system. Then the dimension matrix and the quantity of dimensionless variables are computed as

Quantity	Physical meaning	Dimension
x	Coordinates	L
t	Time	T
U	Velocity field	LT^{-1}
μ	Viscosity	$L^{-1}MT^{-1}$
L	Length	L
g	Gravity	LT^{-2}
ρ_F	Density	$L^{-3}M$
U_0	Velocity	LT^{-1}

Table 2.4: Dimension table of LMT-class for the fluid domain.

$$M_{D_F} = \begin{bmatrix} 1 & 0 & 1 & -1 & 1 & 1 & -3 & 1 \\ 0 & 0 & 0 & 1 & 0 & 0 & 1 & 0 \\ 0 & 1 & -1 & -1 & 0 & -2 & 0 & -1 \end{bmatrix}, \tag{2-34}$$

$$R_F = rank(M_{D_F}) = 3. \tag{2-35}$$

Thus, the number of dimensionless variables needed to describe the fluid domain P_F can be calculated as:

$$P_F = N_F - R_F = 5. \tag{2-36}$$

The physical law presented in (2-33) can now be written in its dimensionless form as:

$$G_F(X_1, X_2, X_3, X_4, X_5) = 0, \tag{2-37}$$

where the X_i's are dimensionless variables. Now the X_i's should be found and defined. The objective of this step is to give to the dimensionless variables a physical meaning in order to turn the interpretation of the results easier. Having two different velocities and two length involved in the problem, respectively (U, U_0) and (x, L), two dimensionless variables can be written as:

$$X_1 = \frac{U}{U_0}, \qquad\qquad X_2 = \frac{x}{L}. \tag{2-38}$$

For the third dimensionless variable, one can consider the dimensionless time ratio $\frac{t}{T_{fluid}}$, where T_{fluid} is the convection time in the fluid, which is a relevant information, written as:

$$T_{fluid} = \frac{L}{U_0} \implies \frac{t}{T_{fluid}} = \frac{U_0 t}{L}. \tag{2-39}$$

The third dimensionless variable which is a time ratio for the fluid can be written as a function of velocity and time as:

$$X_3 = \frac{U_0 t}{L}. \tag{2-40}$$

Concerning the two remaining dimensionless variables, one should keep in mind that all the physical variables of the law (2-33) have to be used to write the X_i's. Then one of them can be the Reynolds number R_E:

$$X_4 = R_E = \frac{\rho_F U_0 L}{\mu}, \tag{2-41}$$

and the last one can be the Froude number F_R for instance:

$$X_5 = F_R = \frac{U_0}{\sqrt{gL}}. \tag{2-42}$$

Finally, all the physical variables presented in the Table 2.4 are used and the following dimensionless law can be written and represents the pure fluid system:

$$G_F\left(\frac{U}{U_0}, \frac{x}{L}, \frac{U_0 t}{L}, \frac{\rho_F U_0 L}{\mu}, \frac{U_0}{\sqrt{gL}}\right) = 0. \tag{2-43}$$

2.1.5
Dimensionless variables in the solid domain

Considering only the solid domain, the typical physical variables involved in mechanical systems are presented in Table 2.5. These variables are related by physical laws (differential equations) which can be written as the following dimensional equation:

$$g_S(x, t, \xi, E, L, g, \rho_S, \xi_0) = 0. \tag{2-44}$$

Here, one can consider that for continuous systems, the stiffness term is the Young modulus of the material for instance and the density term is the mass per volume unit of it. Indeed, considering a simple 1-dof mass-spring system for instance, the stiffness is $E = \frac{k}{l}$, where k is the stiffness of the spring and l its length, and the density is $\rho_S = \frac{m}{l^3}$, where m is the mass.

This law (2-44) represents a pure solid or structure system since no variables from the fluid are involved. To perform the dimensional analysis of this law (made of eight physical variables, $N_S = 8$), first the LMT-class dimension table is built and then, the dimension matrix and the quantity of dimensionless variables are computed. The results found are

$$M_{D_S} = \begin{bmatrix} 1 & 0 & 1 & -1 & 1 & 1 & -3 & 1 \\ 0 & 0 & 0 & 1 & 0 & 0 & 1 & 0 \\ 0 & 1 & 0 & -2 & 0 & -2 & 0 & 0 \end{bmatrix}, \tag{2-45}$$

Quantity	Physical meaning	Dimension
x	Coordinates	L
t	Time	T
ξ	Displacement field	L
E	Stiffness	$L^{-1}MT^{-2}$
L	Length	L
g	Gravity	LT^{-2}
ρ_S	Density	$L^{-3}M$
ξ_0	Displacement data	L

Table 2.5: Dimension table of class LMT for the solid domain.

$$R_S = rank(M_{D_F}) = 3. \tag{2-46}$$

The number of dimensionless variables needed to describe the fluid domain P_S can be calculated as:

$$P_S = N_S - R_S = 5. \tag{2-47}$$

The physical law presented in Eq.(2-44) can now be written in its dimensionless form as:

$$G_S(Y_1, Y_2, Y_3, Y_4, Y_5) = 0, \tag{2-48}$$

where the Y_i's are dimensionless variables. Now the Y_i's should be found and defined. Since several terms are expressed as length, two dimensionless variables can be written as:

$$Y_1 = \frac{\xi}{L}, \qquad\qquad Y_2 = \frac{x}{L}. \tag{2-49}$$

For the third dimensionless variable, as done before for the fluid, one can consider the dimensionless time ratio $\frac{t}{T_{solid}}$, where T_{solid} is the time needed to an elastic wave to cross the solid, with the velocity $c = \sqrt{\frac{E}{\rho_s}}$. This term is written as:

$$T_{solid} = \frac{L}{c} \implies \frac{t}{T_{solid}} = \frac{t\sqrt{\frac{E}{\rho_s}}}{L}. \tag{2-50}$$

Then, a third dimensionless variable which is a time ratio for the solid can be written as a function of stiffness and time as:

$$Y_3 = \frac{t\sqrt{\frac{E}{\rho_S}}}{L}. \tag{2-51}$$

The ratio between the displacement data and the length scale of the system called by D (displacement number) will be used to define the fourth dimensionless variable. It is written as:

$$Y_4 = D = \frac{\xi_0}{L}. \tag{2-52}$$

The fifth dimensionless variable wil be called the elastogravity number G_E and it is written as:

$$Y_5 = G_E = \frac{\rho_S g L}{E}. \tag{2-53}$$

All the physical variables presented in the Table 2.5 are used and the following dimensionless law can be written and represents the pure fluid system:

$$G_S \left(\frac{\xi}{L}, \frac{x}{L}, \frac{t\sqrt{E/\rho_S}}{L}, \frac{\xi_0}{L}, \frac{\rho_S g L}{E} \right) = 0. \tag{2-54}$$

2.1.6
Dimensionless variables for the coupled fluid-solid system

Combining both domains (fluid and solid), one can find a set of twelve different dimensional quantities. Five of them come from the fluid domain and other five come from the solid domain. The two remaining are related with the coupling. They are the variables of greater interest of the couped system (the fluid velocity field and the displacement of the solid). Then for each of those two, one can write the physical law. For the fluid velocity field U:

$$g(U, x, t, \mu, \rho_F, U_0, L, g, E, \rho_S, \xi_0) = 0. \tag{2-55}$$

To perform the dimensional analysis, first one needs to find the number of dimensionless quantities needed using the dimension matrix (calculating the rank of the matrix). Here, eight quantities are necessary to write the dimensionless law. Then one can write, with the dimensionless numbers used before:

$$G \left(\frac{U}{U_0}, \frac{x}{L}, \frac{U_0 t}{L}, \frac{\rho_S U_0 L}{\mu}, \frac{U_0}{\sqrt{gL}}, \frac{\xi_0}{L}, \frac{\rho_S g L}{E}, A \right) = 0, \tag{2-56}$$

where the five first quantities are dimensionless numbers related to the fluid domain, then two related to the solid domain and the last one, A, linked to the interface, which is related to both the fluid and the solid (it has to be related simultaneously to the fluid and the solid otherwise it would have appeared before).

This last dimensionless quantity can take several forms that should be chosen on its relevance in relation to the physical system. Thus, A can be:

- the **mass number** M, which is the ratio between the two densities. Observe that M will vary directly on the fluid (air, water, ...). One can write it as:

$$M = \frac{\rho_F}{\rho_S}. \tag{2-57}$$

This dimensionless number shows, for instance, that it is different to move in water than to move in air.

– the **reduced velocity** U_R, which is the ratio between the reference fluid velocity U_0 and the velocity of elastic wave in the solid:

$$U_R = \frac{U_0}{\sqrt{E/\rho_S}} = \frac{U_0}{c}. \tag{2-58}$$

The reduced velocity contains the information between the two dynamics (the fluid and the solid ones) and thus how they are related. Of course, using the length scale L, one can write the reduced velocity as:

$$U_R = \frac{T_{solid}}{T_{fluid}}, \tag{2-59}$$

which is an important form using the two time scales.

– the **Cauchy number** C_A presented before as the ratio between the fluid load and the stiffness of the solid:

$$C_A = \frac{\rho_F U_0^2}{E}. \tag{2-60}$$

The dimensionless numbers enable a classification of problems. One example already presented is the Reynolds number (Figure 2.3) which anticipates the behavior of the fluid. The classification of physical problems will permit to use simplified models to represent the systems.

2.2
Standard equations for the fluid, the solid domains and the interface

In this part, the equations involved in fluid-structure interaction problems will be presented using [19] and [27]. As this kind of problem is composed of three main domains: the fluid domain, the solid or structure and, the interface between them, three types of equation can be distinguished. This part will focus on the equations for some specific problems treated in this context.

2.2.1
Fluid equations

The fluid domain is governed by several conservation equations. In this present document, an homogeneous fluid is considered and its temperature is not taken into account. Thus, the main governing equations for this specific domain are:

– the **mass balance**, also called continuity equation (considered here for an incompressible fluid);

– the **momentum balance**, also called Cauchy equation (which relates the inertia with the local loads).

Both together form the well known Navier-Stokes equations. To have a more complete mathematical model, boundary conditions should be taken into account. In this work, neither the energy conservation equation nor the species balance equation will be considered.

Mass balance: Considering a volume V of a fluid bounded by the surface S. The mass of the fluid is m_F and can be written as:

$$m_F = \int_V \rho_F dV, \tag{2-61}$$

where ρ_F represents the volumetric mass (i.e. the mass per unit volume). Then the variation in time of mass inside the volume, called δm_F, can be express as:

$$\delta m_F = \pm \frac{d}{dt} \int_V \rho_F dV = \pm \int_V \frac{d\rho_F}{dt} dV. \tag{2-62}$$

The sign of this expression depends on the variation of the fluid mass, increasing or decreasing. The fluid mass involved in the problem may be constant then, the variation of fluid mass inside the given volume must be equal to the mass flux Φ_m passing through the surface S:

$$\Phi_m = \pm \int_S \rho_F U dS = \pm \int_V \nabla \left(\rho_F U \right) dV, \tag{2-63}$$

where U represents the velocity of fluid particles. To pass from the integral on the surface to one on the volume, one uses the Green's formula. Note that if the total mass is decreasing, $\delta m_F \leq 0$ then $\Phi_m \geq 0$. If the mass is increasing, $\delta m_F \geq 0$ and $\Phi_m \leq 0$. At this step, saying that the mass is conserved, leads to the following sequence:

$$\delta m_F = \Phi_m \Rightarrow \int_V \frac{d\rho_F}{dt} dV = -\int_V \nabla \left(\rho_F U \right) dV. \tag{2-64}$$

This expression can be written without the integrals which leads to:

$$\frac{d\rho_F}{dt} + \nabla \left(\rho_F U \right) = 0. \tag{2-65}$$

In this document, it will be considered that the fluids involved are not compressible, i.e. ρ_F is constant, then $\frac{d\rho_F}{dt} = 0$. The final form for the mass conversation is:

$$\nabla U = div(U) = 0. \tag{2-66}$$

Dimensionless formulation of the mass conservation: considering that $\tilde{U}$ notes the dimensionless velocity field such as:

$$\tilde{U} = \frac{U}{U_0},$$

where U_0 is a reference velocity field (it can be the initial field) one can write:

$$div\left(\tilde{U}\right) = 0. \tag{2-67}$$

This equation will be used later on and all along the fluid-structure interactions sections to describe the mass conservation. Note that the tilde notation $\tilde{\square}$ denotes the dimensionless quantities in the fluid domain. For the quantities of the solid domain, it will be used the bar notation $\bar{\square}$.

Momentum balance: Let's consider a volume V of a fluid element bounded by the surface S characterized by the flow U. The momentum M_F of this fluid is written as:

$$M_F = \int_V \rho_F U dV. \tag{2-68}$$

The variation in time of M_F can be written thanks to the notation δ and the volumetric mass density of the fluid ρ_F:

$$\delta M_F = \frac{d}{dt}\int_V \rho_F U dV = \int_V \rho_F \frac{dU}{dt} dV. \tag{2-69}$$

It will be considered that this variation of momentum is equal to the acting forces on this element which are of two different types: the external ones and the internal ones. In the problems addressed here, the unique external force acting on this element is linked to the gravity g and it is written as:

$$f_E = -\int_V \rho_F g e_z dV. \tag{2-70}$$

Concerning the internal forces, only one will be taken into account. It is acting directly on the surface S of the fluid element and can be expressed with the stress tensor Π as:

$$f_I = \int_S \Pi dS = \int_V \nabla \Pi dV. \tag{2-71}$$

Then, the total force acting on the element can be found as the sum of the external and the internal forces. Rewriting the surface integral as a volume integral using the operator ∇ one get:

$$F = \int_V \left(-\rho_F g e_z + \nabla\Pi\right) dV. \tag{2-72}$$

Finally, combining Eqs. (2-68) and (2-72) one can obtain:

$$\rho_F \frac{dU}{dt} = -\rho_F g e_z + \nabla\Pi. \tag{2-73}$$

From literature [19], one can easily find the expression of the stress tensor for fluid element for an incompressible fluid with constant viscosity. The results is:

$$\nabla \Pi = -\nabla P + \mu \Delta U, \tag{2-74}$$

where P is the pressure and μ the dynamic viscosity. Finally, the momentum conservation equation is:

$$\rho_F \frac{dU}{dt} = -\rho_F g e_z - \nabla P + \mu \Delta U. \tag{2-75}$$

Dimensionless formulation of the momentum balance: considering the equation (2-75), one can replace the physical quantities by the following dimensionless ratios:

$$\tilde{U} = \frac{U}{U_0}, \qquad \tilde{P} = \frac{P}{\rho_F U_0^2}, \qquad \bar{t} = \frac{t}{L/c}, \qquad \tilde{x} = \frac{x}{L}.$$

Then the dimensionless form of the momentum balance equation is:

$$\rho_F \frac{d\left(\tilde{U} U_0\right)}{d\left(\bar{t}\frac{L}{c}\right)} = -\rho_F g e_z - \frac{1}{L}\nabla\left(\tilde{P}\rho_F U_0^2\right) + \frac{\mu}{L^2}\Delta\left(\tilde{U} U_0\right). \tag{2-76}$$

Note that here, for no major reason, the characteristic time of the solid is considered to scale the equations. After some simplifications and variable changes, one gets:

$$\frac{c}{U_0}\frac{d\tilde{U}}{d\bar{t}} = -\frac{gL}{U_0^2}e_z - \nabla\tilde{P} + \frac{\mu}{\rho_F U_0 L}\Delta\tilde{U}. \tag{2-77}$$

This expression can then be rewritten as a function of the characteristic dimensionless numbers such as:

$$\frac{1}{U_R}\frac{d\tilde{U}}{d\bar{t}} = -\frac{1}{F_R^2}e_z - \nabla\tilde{P} + \frac{1}{R_E}\Delta\tilde{U}, \tag{2-78}$$

where one recognizes the reduced velocity, the Froude and the Reynolds numbers.

2.2.2
Solid equations

This section presents the equations for the solid domain, using [21]. Several approximations will be made. One example is that instead of using the continuous mechanics equations that would combine perfectly with the fluid equations, modal approximations will be used. The objective is to simplify the mathematical model and speed up computational experiments. The first modal approximation that will be presented is the simplest one, the single mode approximation.

Single mode approximation: In the single mode approximation, that can be found in [29] or [41], the displacement of the solid ξ (function of the position x and the time in dynamic problems) is written as function of modal displacement q and modal shape φ (which is a function of the position x). Then:

$$\xi(x,t) = q(t)\varphi(x). \tag{2-79}$$

The dynamics of the solid is described by the equation of motion:

$$m\frac{d^2q}{dt^2} + kq = f, \tag{2-80}$$

where m is the modal mass, k the modal stiffness and f the modal force written as:

$$f = \int F\varphi dx. \tag{2-81}$$

Note that the modal shape is usually known from experiments or from numerical simulations.

Dimensionless formulation of the solid equations: considering the following dimensionless variables linked to the solid domain,

$$\bar{q} = \frac{q}{\xi_0}, \qquad \bar{f} = \frac{f}{k\xi_0}, \qquad \bar{t} = \frac{t}{T_{solid}},$$

where, $T_{solid} = \sqrt{\frac{m}{k}}$, one can write the equation of motion as:

$$m\left[\sqrt{\frac{k}{m}}\right]^2 \xi_0 \frac{d^2\bar{q}}{d\bar{t}^2} + k\xi_0\bar{q} = k\xi_0\bar{f}. \tag{2-82}$$

Simplifying, the oscillator equation in terms of dimensionless modal displacement;

$$\frac{d^2\bar{q}}{d\bar{t}^2} + \bar{q} = \bar{f}. \tag{2-83}$$

Of course, one could think in using more than one mode for the approximation. This will be done to explain one type of instability later on.

2.2.3
Interface equations

At the interface between the fluid and the solid, one shall define the continuity equations that will link the dynamic of the fluid and solid. Two different conditions are used, one kinematic and other dynamic.

Kinematic condition: The kinematic condition connects directly the velocities (the fluid velocity at the interface and the solid interface velocity). In this

region, these two velocities must be equal. Then, saying that there is no mixing possible between the two domains and also there is no sliding of one on the other. This condition is simply a velocity equality:

$$U = \frac{d\xi}{dt}. \tag{2-84}$$

Using the single mode approximation this equality can be written as:

$$U = \frac{dq}{dt}\varphi, \tag{2-85}$$

where q is the modal displacement, function of time t and φ is the modal shape, function of the position x.

Dimensionless formulation of the kinematic condition: considering the following dimensionless variables:

$$\tilde{U} = \frac{U}{U_0}, \qquad\qquad \bar{t} = \frac{t}{L/c}, \qquad\qquad \bar{q} = \frac{q}{\xi_0},$$

one can find the dimensionless form on the kinematic condition equation at the interface as:

$$\tilde{U}U_0 = \frac{d\left(\bar{q}\xi_0\right)}{d\left(\bar{t}\frac{L}{c}\right)}\varphi. \tag{2-86}$$

Simplifying, one can write the dimensionless form of the kinematic condition as:

$$\frac{U_0}{c}\tilde{U} = \frac{\xi_0}{L}\frac{d\bar{q}}{d\bar{t}}\varphi, \tag{2-87}$$

which is equivalent to:

$$U_R\tilde{U} = D\frac{d\bar{q}}{d\bar{t}}\varphi. \tag{2-88}$$

Observe that the reduced velocity and the displacement number appear in this formulation.

Dynamic condition: This condition states an equilibrium between forces at the interface region. Then one needs the forces from the fluid acting on the solid f_F and the solid force induced by the displacement of the interface. In the fluid domain, the force acting on the interface is composed of pressure and viscosity forces. Then:

$$f_F = \left[-PI + \mu\left(\nabla U + \nabla^T U\right)\right]n, \tag{2-89}$$

where n is the normal to the interface. On the solid domain, one shall consider the modal force f only. The equation consists of equalizing the sum, on the whole interface called Γ_S, of all the fluid forces projected on the modal shape φ with the modal force. We get:

$$\int_{\Gamma_S} \left(\left[-PI + \mu \left(\nabla U + \nabla^T U \right) \right] n \right) \varphi dS = f. \tag{2-90}$$

Dimensionless formulation of the dynamic condition: considering the following dimensionless variables,

$$\tilde{U} = \frac{U}{U_0}, \qquad \tilde{P} = \frac{P}{\rho_F U_0^2}, \qquad \bar{x} = \frac{x}{L}, \qquad \bar{f} = \frac{f}{k\xi_0},$$

one can write, taking care of the integral over the interface (which leads to scaled term on this variable and an extra L-term):

$$\int_{\bar{\Gamma}_S} \left(\left[-\tilde{P}\rho_F U_0^2 I + \mu \left(\frac{1}{L} \nabla \left(\tilde{U} U_0 \right) + \frac{1}{L} \nabla^T \left(\tilde{U} U_0 \right) \right) \right] n \right) \varphi L d\bar{S} = \bar{f} k \xi_0. \tag{2-91}$$

Simplifying, one obtains:

$$\int_{\bar{\Gamma}_S} \left(\frac{\rho_F U_0^2}{k} \left[-\tilde{P}I + \frac{\mu}{\rho_F U_0 L} \left(\nabla \tilde{U} + \nabla^T \tilde{U} \right) \right] n \right) \varphi d\bar{S} = \frac{\xi_0}{L} \bar{f}, \tag{2-92}$$

and finally, using the characteristic dimensionless numbers (Cauchy, Reynolds and displacement numbers):

$$\int_{\bar{\Gamma}_S} \left(C_A \left[-\tilde{P}I + \frac{1}{R_E} \left(\nabla \tilde{U} + \nabla^T \tilde{U} \right) \right] n \right) \varphi d\bar{S} = D\bar{f}. \tag{2-93}$$

In this chapter, the main equations involved in fluid-solid interaction problems have been presented in their classical form and in their dimensionless form. The dimensionless numbers that appear in the fomulations can be used to classify problems. These numbers are often the variables of interest in sensistivity studies and varying them one can observe their influence on the dynamic of the system.

3
Classification of fluid-structure interaction problems

The previous chapter presented the basic concepts of fluid-structure interactions and some dimensionless numbers used to classify problems. This chapter shows how such classification can be done using the reduced velocity. It will be investigated the influence of this dimensionless parameter in the stability of the solid motion.

3.1
Small reduced velocity: still fluid

As seen before, the reduced velocity is an important dimensionless number that can be used to classify problems since it compares the time scales of the solid and the fluid. Recall that it is written as:

$$U_R = \frac{T_{solid}}{T_{fluid}} = \frac{U_0}{c}, \tag{3-1}$$

where U_0 is the reference upstream velocity and, c is the velocity of elastic waves in the solid. First, let's consider the simplest case to study the influence of the reduced velocity to fluid-solid interaction systems, the case where the motion of the fluid is so slow compared to the dynamic of the solid. One can say that the fluid appears to be not moving in comparison to the motion of the solid.

In relation to the solid dynamic, it can be considered that the displacement ξ and the reference displacement ξ_0 have the same order of magnitude, i.e. $\xi = o(\xi_0)$, where the notation $o(\square)$ indicates the order of magnitude. A similar hypothesis can be considered for the dynamic of the fluid, in a wat that $U = o(U_0)$. The kinematic condition at the interface, that relates both of them, leads to:

$$U = o(U_0) = o\left(\frac{\xi_0}{T_{solid}}\right). \tag{3-2}$$

To consider that the reduced velocity is small means that the time evolution of the fluid, called T_{fluid}, is much longer than the time evolution of the solid T_{solid}. Then, one can define a limit case where the fluid can be considered as a still fluid (it is moving but this occurs so slowly). Thus the dynamic of the fluid in this case is only related and due to the dynamic of the solid. Thus:

$$U_0 << \frac{\xi_0}{T_{solid}}. \tag{3-3}$$

Reorganizing the equation, one gets:

$$U_R << D. \tag{3-4}$$

Finally, one can neglect the proper dynamic of the fluid and consider that only the interaction with the solid governs the fluid domain. This leads to an uncoupled fluid dynamics and thus to new equations. Those new equations will be simplified thanks to this new consideration.

Since small reduced velocity is being considered (meaning that the variable U_0 is not relevant), the dimensionless numbers should be rewritten. Indeed, instead of using the reference velocity field of the fluid, one should use the characteristic velocity in the solid domain c or also $\frac{L}{T_{solid}}$. Then, the following new dimensionless number can be defined:

$$R_E \Longrightarrow S_T = \frac{\rho_F c L}{\mu} = \frac{\rho_F L^2}{T_{solid}\mu}, \tag{3-5}$$

$$F_R \Longrightarrow F_D = \frac{c}{\sqrt{gL}} = \frac{L}{T_{solid}\sqrt{gL}}, \tag{3-6}$$

$$C_A \Longrightarrow M = \frac{\rho_F c^2}{E} = \frac{\rho_F}{\rho_S}. \tag{3-7}$$

Those numbers are respectively, the Stokes number, the dynamic Froude number and, the mass number. The fluid dimensionless variables must be rewritten taking into account the consideration about U_0. Thus one gets:

$$\bar{U} = \frac{U}{c}, \tag{3-8}$$

$$\bar{P} = \frac{P}{\rho_F c^2}, \tag{3-9}$$

$$\bar{x} = \frac{x}{L}. \tag{3-10}$$

Note that the notation $\tilde{\Box}$ is no more used since the quantities are scaled with the reference velocity in the solid domain. Only $\bar{\Box}$ appears. To obtain the uncoupled fluid dynamics, it will be considered small motion of the solid which means little change in the solid shape and consequently $D << 1$.

Besides of this, the three variables P, U and ξ will be expanded as an asymptotic expansion thanks to the displacement number D. Indeed, the asymptotic expansion of a function y gives:

$$y(x, \epsilon) \approx y_0(x) + \epsilon y_1(x) + \epsilon^2 y_2(x) + ... \tag{3-11}$$

For the pressure field the asymptotic expansion in $D << 1$ is:

$$P = P_0 + Dp + D^2..., \tag{3-12}$$

for the velocity field one can write

$$U = 0 + Du + D^2..., \tag{3-13}$$

Specific set of equation for small reduced velocity: using the new dimensionless variables defined before, one can express the mass balance and the momentum balance for the fluid domain as:

$$div\left(\bar{U}\right) = 0, \tag{3-14}$$

$$\frac{d\bar{U}}{d\bar{t}} = -\frac{1}{F_D^2}e_z - \nabla\bar{P} + \frac{1}{S_T}\Delta\bar{U}. \tag{3-15}$$

At the interface, one can rewrite the kinematic condition and the dynamic condition as:

$$\bar{U} = D\frac{d\bar{q}}{d\bar{t}}\varphi, \tag{3-16}$$

$$\int_{\bar{\Gamma}_S} M\left(-\bar{P}I + \frac{1}{S_T}\left(\nabla\bar{U} + \nabla^T\bar{U}\right)\right)n\varphi d\bar{S} = D\bar{f}. \tag{3-17}$$

Finally, the equation for the solid is:

$$\frac{d^2\bar{q}}{d\bar{t}^2} + \bar{q} = \bar{f}. \tag{3-18}$$

<u>Note</u>: from now until the end of the section concerning small reduced velocity, the notation $\bar{\Box}$ will not appear in order to simplify the notation. But the equations are still dimensionless.

and finally the expansion of the displacement of the solid is:

$$\xi = 0 + Dq\varphi + D^2... \tag{3-19}$$

Considering only the term of zero order in the three expansions, the momentum balance equation becomes:

$$0 = -\frac{1}{F_D^2}e_z - \nabla P_0 + 0. \tag{3-20}$$

Now, the equations at the 1st-order should be written. To write the mass balance, the momentum equations and the kinematic condition at the interface, there is no major difficulty and one gets for the mass balance:

$$div\left(u\right) = 0, \tag{3-21}$$

for the momentum balance at the 1st-order in D one has:

$$\frac{du}{dt} = -\nabla p + \frac{1}{S_T}\Delta u \tag{3-22}$$

and finally, for the kinematic condition at the 1st-order in D is:

$$u = \frac{dq}{dt}\varphi \tag{3-23}$$

For the dynamic condition, as it involves the description of the interface one should be careful. The pression and the velocity have to be written at the new position of the interface. To find this expression, one can linearize (considering the simplest form of the interface deformation, as a simple translation) the pressure field and the velocity field as:

$$\begin{aligned} P\left(x + Dq\varphi\right) &\simeq P_0\left(x + Dq\varphi\right) + Dp\left(x + Dq\varphi\right) + D^2... \\ &\simeq P_0(x) + Dq\varphi\nabla P_0(x) + Dp(x) + ... \end{aligned} \tag{3-24}$$

$$\begin{aligned} U\left(x + Dq\varphi\right) &\simeq 0 + Du\left(x + Dq\varphi\right) + D^2... \\ &\simeq 0 + Du(x) + ... \end{aligned} \tag{3-25}$$

Then, at the first order expansion one gets the following equation for the dynamic condition at the interface:

$$M\int_{\Gamma_S}\left(-pI + \frac{1}{S_T}\left(\nabla u + \nabla^T u\right)\right)n\varphi dS - Mq\varphi\int_{\Gamma_S}\left(\nabla P_0\right)n\varphi dS = f, \tag{3-26}$$

the equation for the solid domain still unchanged:

$$\frac{d^2q}{dt^2} + q = f. \tag{3-27}$$

Concerning the dynamic condition equation (3-26), one can distinguish two different terms in the left hand side. The first one is the first integral which represents the projection of the fluid force on the modal shape resulting from the viscous stress. Note that with the considerations made in this part, the pression field p and the velocity field u are only due to the motion of the solid (recall that here a still fluid is considered). Thus, this term represents the response of the fluid to the solid motion.

The second term is the second integral which depends on P_0. Observe that it does not depend on the dynamic of the fluid due to the solid motion but it is linked to the motion of the solid due to a pre-stressed fluid. This term has been calculated in the simplest case of the translation in the fluid, by expanding only the fluid stress in term of the position of the interface. A more general formulation can be found in the literature [19] considering a more general deformation of the body:

$$Mq\varphi\int_{\Gamma_S}\left(\nabla P_0\right)n\varphi dS \Longrightarrow Mq\int_{\Gamma_S}\left(\nabla P_0\varphi\right)\left(\varphi n\right)dS. \tag{3-28}$$

Thus the dynamic condition equation at the 1st-order can be re-written combining (3-26) and (3-28) as:

$$M \int_{\Gamma_S} \left(-pI + \frac{1}{S_T} \left(\nabla u + \nabla^T u \right) \right) n\varphi dS - Mq \int_{\Gamma_S} \left(\nabla P_0 \varphi \right) (\varphi n) \, dS = f. \quad (3\text{-}29)$$

Recall that this equation represents the force made by the fluid on the solid. The two terms on the left hand side of this equation will be investigated in the next section.

The equations are simpler, and thus easier to solve. Moreover, they are linear as the hypothesis of small motion was used. The 0-order approximation is given by equation (3-20) and at the 1st-order by (3-21), (3-22), (3-23), (3-27) and (3-29). Those equations present a complete set of equations for small reduced velocity considering small motion of the solid. The dynamic condition at the 1st-order (3-29), presents some interesting phenomena that will be explained in the next sections.

3.1.1
Added stiffness

In (3-29), one can verify that the second term of the left-hand side does not depend on the dynamic of the fluid domain. Thus, it can be calculated without any fluid mechanics. This term represents a force since the right hand side of the equation is a force. Writing the force f as the sum two terms f_1 and f_2, one can write:

$$-Mq \int_{\Gamma_S} \left(\nabla P_0 \varphi \right) (\varphi n) \, dS = f_1. \quad (3\text{-}30)$$

Using (3-20), one can substitute P_0 and then write:

$$q \frac{M}{F_D^2} \int_{\Gamma_S} (\varphi e_z) (\varphi n) \, dS = f_1. \quad (3\text{-}31)$$

Here, one can see that the left hand side term involves the modal displacement q, then the integral with the dimensionless numbers ratio can be written as a stiffness, the added stiffness:

$$k_A = -\frac{M}{F_D^2} \int_{\Gamma_S} (\varphi e_z) (\varphi n) \, dS, \quad (3\text{-}32)$$

that can be easily computed since everything is know. Thus, from the solid point of view, moving in a fluid with a pressure gradient can be interpreted as being connected to an elastic spring. This is very useful since it simplifies a lot the equations and since this term should be calculated only once for a given problem.

3.1.2
High Stokes number: the added mass effect

The analysis of the remaining term of (3-29), called f_2, will reveal another interesting phenomenon. To calculate this term, one needs to solve a linearized fluid mechanics system that involves the pressure responsible for the pressure loading and, the velocity of the fluid responsible for the viscous shear loading. Recalling the equations of the fluid domain, the mass balance (3-21), the momentum balance (3-22) and, the equations at the interface, the kinematic condition (3-23), it is possible to write f_2 as:

$$M \int_{\Gamma_S} \left(-pI + \cancelto{0}{\frac{1}{S_T}} \left(\nabla u + \nabla^T u \right) \right) n\varphi dS = f_2. \qquad (3\text{-}33)$$

In this part, the focus will be only on high Stokes numbers, S_T, which is the case of many fluid-solid interaction problems. Considering that S_T is large, it is possible to rewrite the equation of momentum balance (3-22) neglecting the term that involves $\frac{1}{S_T}$. Then, one gets:

$$\frac{du}{dt} = -\nabla p. \qquad (3\text{-}34)$$

Recalling that S_T relates the density of the fluid ρ_F with the viscous coefficient μ, neglecting the term that involves the Stokes number means that the viscous effects are neglected. This consideration will impact the other equations. The term f_2 becomes:

$$M \int_{\Gamma_S} -pn\varphi dS = f_2. \qquad (3\text{-}35)$$

Here, as no viscous effects are considered (assumption of high Stokes number), no tangential force are taken into account. Then, the kinematic condition has to be a bit modified which leads to:

$$un = \frac{dq}{dt}\varphi n. \qquad (3\text{-}36)$$

Remark that equations (3-20), (3-34), (3-35) and (3-36), model linearized fluid mechanics problems with small reduced velocity, small motion of the solid and high Stokes number.

Using the separation of variables for u, the velocity field and p, the pressure field, it is possible to write each one of those functions as the product of two functions, one that depends only of space and other that depends only of time. The velocity field u can be written taking into account the original kinematic condition equation (3-23) which was stated for a single mode approximation of the solid dynamic, at the interface. But one can state the

velocity field in the same way in all the fluid as:

$$u(x,t) = \frac{d}{dt}q(t)\varphi_u(x) = \dot{q}(t)\varphi_u(x), \tag{3-37}$$

where φ_u is unknown. For the pressure field p, as it is related to acceleration (as presented in (3-34)), one gets:

$$p(x,t) = \frac{d^2}{dt^2}q(t)\varphi_p(x) = \ddot{q}(t)\varphi_p(x). \tag{3-38}$$

Then the equations on the fluid domain, respectively the mass balance and the momentum balance, can be simplified as:

$$div\,(u) = 0 \Longrightarrow div\,(\varphi_u) = 0, \tag{3-39}$$

$$\frac{du}{dt} = -\nabla p \Longrightarrow \varphi_u = -\nabla\varphi_p. \tag{3-40}$$

The equations at the interface can also be simplified. The kinematic condition and the fluid induced force equation (through the dynamic condition) become respectively:

$$un = \frac{dq}{dt}\varphi n \Longrightarrow \varphi_u n = \varphi n, \tag{3-41}$$

$$M\int_{\Gamma_S} -pn\varphi dS = f_2 \Longrightarrow -\ddot{q}M\int_{\Gamma_S} \varphi_p n\varphi dS = f_2. \tag{3-42}$$

Equation (3-42) is very interesting since it shows that the fluid induced force is written as function of the acceleration. As consequence, the term M times the integral over the interface can be seen as a mass (it multiplies an acceleration to give a force). It will be considered an added mass and it is given by:

$$m_A = M\int_{\Gamma_S} \varphi_p n\varphi dS. \tag{3-43}$$

The pressure force of the fluid on the solid can simply be seen as an added mass, see [17] and [43], on the solid. This simplifies a lot the equations.

3.1.3
Low Stokes number: the added damping effect

This section focuses only on systems with small Stokes number. Usually, this hypothesis of small Stokes number is valid for small systems, like vibrations inside a bearing involved by a very viscous fluid. In systems like that, the viscous effects are dominant in comparison to the acceleration in the momentum balance equation. Thus, it can be simplified and written as:

$$0 = -\nabla p + \frac{1}{S_T}\Delta u. \tag{3-44}$$

The equation for the mass balance and kinematic condition are not modified with the hypothesis of small Stokes number. They remain (3-21)

and (3-23). For the momentum balance and the dynamic condition at the interface, the pressure has to be rescaled, as $p \longleftarrow pS_T$, for compatibility. Then the simplified momentum balance can be rewritten as:

$$-\nabla p + \Delta u = 0. \tag{3-45}$$

The fluid induced force of the fluid on the solid (the term similar to a stiffness is not written here) is:

$$\frac{M}{S_T} \int_{\Gamma_S} \left(-pI + \nabla u + \nabla^T u\right) n\varphi dS = f_2. \tag{3-46}$$

Using separation of variables for the velocity field and the pressure field, it is possible to write:

$$u(x,t) = \dot{q}(t)\varphi_u(x), \tag{3-47}$$

$$p(x,t) = \dot{q}(t)\varphi_p(x). \tag{3-48}$$

This procedure is the same that was done in the previous section, however the pressure field is related to the velocity, not to the acceleration as before. It should be noted that the functions φ_u and φ_p will be different from the previous ones. Using the separation of variables, the equations on the fluid domain, respectively the mass balance and the momentum balance, can be simplified as:

$$div\left(u\right) = 0 \Longrightarrow div\left(\varphi_u\right) = 0, \tag{3-49}$$

$$0 = -\nabla p + \Delta u \Longrightarrow 0 = -\nabla\varphi_p - \Delta\varphi_u. \tag{3-50}$$

The equations at the interface can also be simplified, respectively the kinematic condition and the fluid induced force equation, as:

$$u = \frac{dq}{dt}\varphi \Longrightarrow \varphi_u = \varphi, \tag{3-51}$$

$$(3\text{-}46) \Longrightarrow \dot{q}\frac{M}{S_T} \int_{\Gamma_S} \left(-\varphi_p I + \nabla\varphi_u + \nabla^T\varphi_u\right) n\varphi dS = f_2 \tag{3-52}$$

Equation (3-52) shows that the fluid induced force is written as function of the velocity. Thus the term $\frac{M}{S_T}$ times the integral over the interface can be seen as a damping (it multiplies a velocity to give a damping force). It is written as:

$$c_A = \frac{M}{S_T} \int_{\Gamma_S} \left(-\varphi_p I + \nabla\varphi_u + \nabla^T\varphi_u\right) n\varphi dS, \tag{3-53}$$

and it behaves as an added damping, presented in [17], in a way that the pressure force of the fluid on the solid can simply be seen as an added damper on the solid.

3.1.4
Intermediate Stokes number: the memory effect

In this section, intermediate Stokes number will be briefly treated. Here neither the effects of viscosity are dominant nor they are small enough to be neglected. Indeed, the discussion was based on the momentum balance equation. For small Stokes number, the effect of the fluid acceleration was neglected whereas for high Stokes number, the viscous effects were neglected.

In this case nothing is neglected in the momentum balance equation (3-22). Thus the two terms involving velocity are present. One involves the spacial derivative of the velocity and the other its time derivative. In this region of intermediate Stokes number, the effects of added mass and added damping are in competition.

Indeed, here both time scales are present and none of them can be neglected. Then any motion of the solid will create perturbation in the fluid domain. This perturbation will occur respecting the characteristic fluid time, which means that it is not instantaneous. Then this perturbation in the fluid domain will create a variation of the flow induced force on the solid. The motion of the solid due to this force will occur respecting the characteristic solid time. Thus, as both time scales are present in this case, there is a time delay between the two dynamics. This means that what occurs in one domain is related to what happened previously in the other domain. This is called memory effect.

3.2
High reduced velocity: fixed solid

Now that the cases with small reduced velocity have been explored, one can try to do the same procedure for high reduced velocity. Recall that the reduced velocity is written as:

$$U_R = \frac{T_{solid}}{T_{fluid}}. \tag{3-54}$$

To consider that the reduced velocity is high means that the characteristic time of the solid is much longer than the characteristic time of the fluid. A limit case can be investigated when the dynamic of the fluid occurs with a fixed solid. Observe that this does not mean that the solid will not move, this just means that the motion of the solid is very slow in comparison to the one of the fluid.

With this hypothesis, as done in the previous section for low reduced velocity, the system can be seen as uncoupled since the velocity of the solid domain will not influence the fluid dynamic. Before starting the analysis, let's have a look on the dimensionless numbers involved in such cases. In the

standard fluid-solid interaction equations stated in (2-67), (2-78), (2-83), (2-88) and (2-93), it is possible to identify the Reynolds, the Cauchy and the Froude numbers. Observe that all those three dimensionless numbers are function of the fluid velocity U_0, which is convenient since, here, the solid motion will be neglected.

With this negligence, the time scale has to be changed. Then, one will scale the time using T_{fluid}. This leads to new dimensionless variables:

$$\tilde{t} = \frac{t}{T_{fluid}}, \tag{3-55}$$

$$\tilde{U} = \frac{U}{U_0}, \tag{3-56}$$

$$\tilde{P} = \frac{P}{\rho_F U_0^2}. \tag{3-57}$$

The specific set of equations for high reduced velocity will be written in terms of these new dimensionless variables. As before, one can use the boundary conditions of the fluid domain to express the order of magnitude of the fluid velocity at the fluid domain boundary, and at the interface. Then, at the fluid boundary, the velocity U can be written as:

$$U = o(U_0), \tag{3-58}$$

which leads to the following relation for the dimensionless formulation of the velocity field:

$$\tilde{U} = o\left(\frac{U_0}{U_0}\right) = o(1). \tag{3-59}$$

At the interface, the same thing can be done using the kinematic condition equation. Recalling that $\tilde{U} = \frac{d\bar{\xi}}{d\tilde{t}}$, it is possible to write

$$\tilde{U} = o\left(\frac{D}{U_R}\right). \tag{3-60}$$

Consider a high reduced velocity, which means $U_R >> D$, the velocity at the interface can be neglected. Then, in the kinematic condition, the solid is considered fixed from the point of view of the fluid dynamic. Consequently:

$$\tilde{U} = \frac{d\bar{\xi}}{d\tilde{t}} \approx 0. \tag{3-61}$$

Since the velocity of the interface is neglected and it does not interfere that much in the fluid domain, it is possible to consider a solid fixed in time in comparison with the fluid dynamics. This is a quasi-static aeroelasticity approximation.

Finally, although the system is coupled, two dynamics can be computed separately. As the motion of the solid is very small in comparison to the fluid motion, the interface can be considered fixed in time. This hypothesis could

be used thanks to the difference of the time scales in the two domains.

> **Specific set of equation for high reduced velocity:** using the new dimensionless variables, the mass balance and the momentum balance for the fluid domain become:
>
> $$div\left(\tilde{U}\right) = 0, \tag{3-62}$$
>
> $$\frac{d\tilde{U}}{d\tilde{t}} = -\frac{1}{F_R^2}e_z - \nabla\tilde{P} + \frac{1}{R_E}\Delta\tilde{U}. \tag{3-63}$$
>
> At the interface, one can rewrite the kinematic condition and the dynamic condition as:
>
> $$\tilde{U} = \frac{d\bar{q}}{d\tilde{t}}\varphi, \tag{3-64}$$
>
> $$\int_{\bar{\Gamma}_S} C_A\left(-\tilde{P}I + \frac{1}{R_E}\left(\nabla\tilde{U} + \nabla^T\tilde{U}\right)\right)n\varphi d\bar{S} = DF_{FS}. \tag{3-65}$$
>
> Finally, the equation for the solid is:
>
> $$U_R^2\frac{d^2\bar{q}}{d\tilde{t}^2} + \bar{q} = F_{FS}, \tag{3-66}$$
>
> where F_{FS} expresses the fluid-induced force on the solid. It will be called fluid load.

3.2.1
Flow-induced static instability with single mode approximation

As explained previously, with the consideration of a large reduced velocity, the velocity of the interface can be neglected in the fluid dynamic. Using once again the first-order approximation of the expansion (3-19) in the single mode approximation gives:

$$\xi(x,t) = Dq(t)\varphi(x). \tag{3-67}$$

One can find the expression of the fluid load and some consequences on the solid dynamics. As the interface is considered fixed at the position defined by the modal displacement q, the fluid variables are going to be functions of the quantity q. Thus the pressure field is defined as $\tilde{P}(Dq)$ and the velocity field as $\tilde{U}(Dq)$. Then, the fluid load F_{FS} is defined through those quantities as:

$$\int_{\bar{\Gamma}_S} C_A\left(-\tilde{P}I + \frac{1}{R_E}\left(\nabla\tilde{U} + \nabla^T\tilde{U}\right)\right)n\varphi d\bar{S} = F_{FS}(R_E, Dq, ...). \tag{3-68}$$

The fluid load, F_{FS}, at a given time depends of the position of the interface, through the quantity q. Rewriting the equation (3-68), the force can be expressed as the product:

$$F_{FS}(R_E, Dq, ...) = C_A F(R_E, Dq, ...). \tag{3-69}$$

Considering small motion of the solid which means small D, it is possible to use the asymptotic expansion of the function F with respect to D:

$$F_{FS} = C_A F_0 + D f_{FS} + ... \implies F_{FS} = C_A F_0 + Dq C_A \left(\frac{dF}{d(Dq)} \right) + ... \quad (3\text{-}70)$$

The first term corresponds to the fluid force with the original position of the interface and the second depends on the variation of the interface position. This second term is function of the modal displacement q which means that the flow induced force is a flow induced stiffness force, where:

$$f_{FS} = -k_F q \implies k_F = -C_A \left(\frac{dF}{d(Dq)} \right). \quad (3\text{-}71)$$

Thus, from the solid dynamic point of view, the flow induced force is equivalent to a stiffness force of a spring. This stiffness depends on the flow velocity through the Cauchy number, which varies with U_0^2. It can be negative or positive depending on the motion of the interface, which depends only on the fluid dynamics.

Now that the flow induced force has been expressed, let's analyze the influence of such force on the dynamic of the solid. As now the dynamic of the solid is the focus, it will be used the scaled time $\bar{t}$ instead of $\tilde{t}$. Thus, the solid dynamic equation can be re-written from (3-66), considering the characteristic solid time, as:

$$\frac{d^2 q}{d\bar{t}^2} + q = f_{FS}. \quad (3\text{-}72)$$

Then, using (3-71) one can write:

$$\ddot{q} + (1 + k_F)q = 0 \implies \ddot{q} + \left(1 - C_A \left(\frac{dF}{d(Dq)} \right) \right) q = 0. \quad (3\text{-}73)$$

Observing (3-73), it is possible to verify that the total stiffness of the solid system depends on the fluid characteristics. Indeed, in this expression, when the fluid velocity is increasing (so the Cauchy number increases too), the total stiffness term of the system is decreasing. As one can remark, there is a limit case where the system has no more stiffness. This specific condition, where $C_A \frac{dF}{d(Dq)} = 1$, means that the frequency of the system will have an imaginary part. This is called static instability since only stiffness terms are involved in this specific condition. In Fig. 3.2.1 the evolution of the frequency with respect to the normalized flow velocity looks like a parabola. This is completely normal since a linear variation of the flow velocity will produce a variation as a parabola of the normalized flow velocity presented in Fig. 3.2.1 due to the expression of C_A.
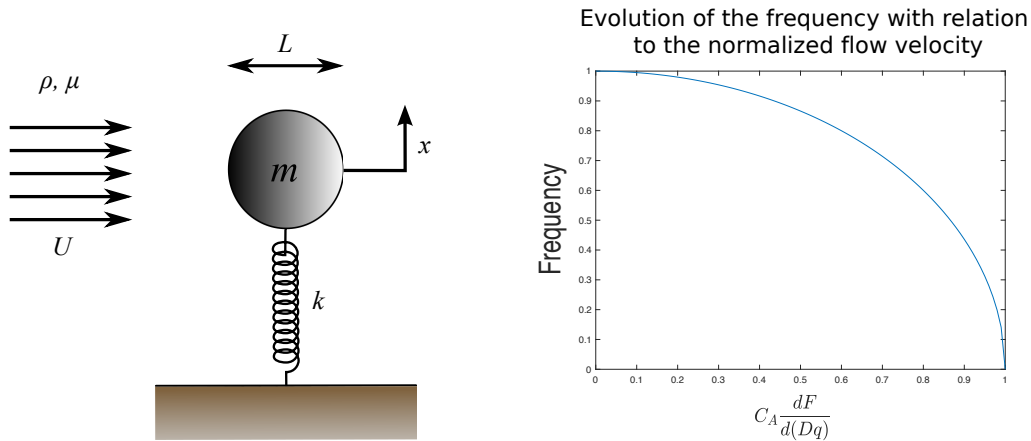
Figure 3.1: Left: Simple mass-spring system in a cross-flow / Right: Evolution of the frequency of the system with respect to the upstream velocity

Example of flow-induced static instability of a simple mass-spring system:
Consider the system presented in Fig. 3.2.1. The dynamic equation of this system is written as (3-72). The scaled natural frequency of the free system is one. Then considering (3-73), one can plot the evolution of the frequency of the system Fig. 3.2.1.

The evolution of the flow velocity is normalized with respect to the flow-induced force to simplify the representation. Without flow, the frequency of the system is one (as expected) but when the flow velocity increases the global stiffness of the system descreases and thus the frequency decreases too. The limit case is when the global stiffness becomes negative then the frequency starts to be imaginary.

This type of instability is an example of a phenomena that can occur in very flexible footbridges (studied in [39]) under the action of high velocity wind. Indeed, depending on the lift coefficient of the airfoil's section or of the footbridge's one, there will exist a critical fluid velocity (and thus a associated Cauchy number) which will cause the instability. At this point, the stiffness vanishes and, the amplitude of the solid displacement increases exponentially.

3.2.2
Flow-induced dynamic instability with two modes approximation

To observe more complex instabilities in the system response, a more complex formulation should be used. In this section, this will be explained considering two modes in the approximation of the displacement ξ. Indeed, the single mode approximation is not sufficient for some solid dynamics. Examples of such situations are the collapse of the Narrow Tacoma Bridge and the oscillation of a plane empennage under flutter effects [20]. One can easily see

that a combination of modes, bending ones in two different directions or even bending and torsional ones could better characterize the dynamic of the solid domain.

Thus, let's start with the two modes approximation to define the displacement ξ. The displacement is written as function of the projection of the modal displacements into two functions of space, the modes φ_1 and φ_2. Then:

$$\xi(x, t) = Dq_1(t)\varphi_1(x) + Dq_2(t)\varphi_2(x). \tag{3-74}$$

Using this approximation, the equation of motion of the solid should be written in term of both modal displacements q_1 and q_2 which leads to a system of two equations. The fluid load may also be projected in both modes. The approximation made before (the motion of solid is much slower than the motion of the fluid) is still valid which means that it remains in the quasi-static aeroelasticity approximation. The variables of the fluid domain must be written through the two modal displacements as made before for the single mode approximation. Thus:

$$\tilde{P}(Dq) \Longrightarrow \tilde{P}(Dq_1, Dq_2), \tag{3-75}$$

$$\tilde{U}(Dq) \Longrightarrow \tilde{U}(Dq_1, Dq_2). \tag{3-76}$$

For the single mode approximation, the flow induced force was calculated projecting on the single mode, as shown in (3-69). This time, the flow induced force will be calculated projecting on the two modes which leads to:

$$F_{FS}^i = C_A F_i\left(R_E, Dq_1, Dq_2, ...\right), \qquad i = 1, 2. \tag{3-77}$$

Using once again the asymptotic expansion as used for the single mode approximation (3-70), one can find:

$$F_{FS}^i = C_A F_0^i + Dq_1 C_A \left(\frac{dF_i}{d(Dq_1)}\right) + Dq_2 C_A \left(\frac{dF_i}{d(Dq_2)}\right) + ... \tag{3-78}$$

Once again, the first term is linked to the original force, and the other terms are related to the modal displacements q_i's. One can then define a stiffness operator K_{ij} such as:

$$K_{ij} = \frac{dF_i}{dq_j}. \tag{3-79}$$

Thus, as the single mode approximation led to a unique equation of motion, the two modes approximation leads to a system of two equations of motion. Usually, the term presented in (3-79) comes from experiments or numerical computations.

$$\begin{cases} m_1 \ddot{q}_1 + k_1 q_1 = f_{FS}^1 = C_A K_{11} q_1 + C_A K_{12} q_2 \\ m_2 \ddot{q}_2 + k_2 q_2 = f_{FS}^2 = C_A K_{21} q_1 + C_A K_{22} q_2 \end{cases} \tag{3-80}$$

Note that here the modal mass and the modal stiffness are not necessary equal to unit. This just happens for the single mode approximation. The equations presented in (3-80) are coupled since each of them contains both modal displacements. There is coupling through the flow induced stiffness forces. Then, depending on the variation of the fluid velocity value, the off-diagonal terms (K_{ij} for $i \neq j$) become closer and closer or more and more distant. Thus, the natural frequencies vary in a way that a coincidence between frequencies may occur. Let's have a look on what happens when the fluid velocity causes this coincidence of the two frequencies. Writing (3-80) as:

$$\begin{cases} m_1\ddot{q}_1 + (k_1 - C_A K_{11})\,q_1 = C_A K_{12}q_2 \\ m_2\ddot{q}_2 + (k_2 - C_A K_{22})\,q_2 = C_A K_{21}q_1 \end{cases}, \tag{3-81}$$

one can write:

$$\begin{cases} \ddot{q}_1 + \omega_1^2 q_1 = \frac{C_A K_{12}}{m_1}q_2 \\ \ddot{q}_2 + \omega_2^2 q_2 = \frac{C_A K_{21}}{m_2}q_1 \end{cases}. \tag{3-82}$$

To simplify the equations, the frequencies are scaled to unity, then $\omega = \omega_1 = \omega_2 = 1$, and, it is considered that the coupling stiffness terms (off diagonal terms of K_{ij}) are much smaller than the stiffness of the modes (the diagonal of K_{ij}). Thus, the off diagonal terms can be neglected and noted as ϵ.

Next, two cases will be analyzed. The symmetric case where the coupling stiffnesses are equal and the antisymmetric case where the stiffnesses have opposite sign. For each case, the natural frequencies and modes will be computed.

3.2.2.1
Symmetric case: equal coupling stiffnesses

In this case, the system of equations can be written as following with $\epsilon << 1$:

$$\begin{cases} \ddot{q}_1 + q_1 = \epsilon q_2 \\ \ddot{q}_2 + q_2 = \epsilon q_1 \end{cases}. \tag{3-83}$$

Stating that the modal displacements can be written as:

$$q_j = R_e\left[q_j e^{iwt}\right], \tag{3-84}$$

where $R_e\left[\Box\right]$ is the real part of the quantity, one can write:

$$\begin{cases} -\omega^2 q_1 + q_1 = \epsilon q_2 \\ -\omega^2 q_2 + q_2 = \epsilon q_1 \end{cases}. \tag{3-85}$$

The frequency of this system is the value ω that turns the determinant:

$$\begin{vmatrix} 1 - \omega^2 & -\epsilon \\ -\epsilon & 1 - \omega^2 \end{vmatrix} = 0. \tag{3-86}$$

Using the approximation $\epsilon \longrightarrow 0$, which gives $\sqrt{1+\epsilon} \approx 1 + \frac{\epsilon}{2}$, the natural frequencies are:

$$\omega \approx 1 \pm \frac{\epsilon}{2}. \tag{3-87}$$

Finally one can define the two frequency-mode couples as:

$$A = \left\langle 1 + \frac{\epsilon}{2}, \begin{pmatrix} 1 \\ -1 \end{pmatrix} \right\rangle, \tag{3-88} \qquad B = \left\langle 1 - \frac{\epsilon}{2}, \begin{pmatrix} 1 \\ 1 \end{pmatrix} \right\rangle. \tag{3-89}$$

These modes have real frequencies and are combinations of the original modes. Thus, there is a small coupling of the modes which makes the system a bit different compared to the original one. The modes here are qualified as neutral modes.

3.2.2.2
Antisymmetric case: opposite coupling stiffnesses

Doing exactly the same procedure for the case where the coupling stiffnesses have opposite sign, the system of equations can be written as following with $\epsilon << 1$:

$$\begin{cases} \ddot{q}_1 + q_1 = \epsilon q_2 \\ \ddot{q}_2 + q_2 = -\epsilon q_1 \end{cases}. \tag{3-90}$$

Stating that the modal displacements can be written as before, one looks for the following determinant to be zero:

$$\begin{vmatrix} 1 - \omega^2 & -\epsilon \\ +\epsilon & 1 - \omega^2 \end{vmatrix} = 0. \tag{3-91}$$

Then one can find the natural frequencies which have a complex part this time. Using the same approximation as before, it is possible to define the two couples frequency-mode as following.

$$A = \left\langle 1 + i\frac{\epsilon}{2}, \begin{pmatrix} 1 \\ -i \end{pmatrix} \right\rangle, \tag{3-92} \qquad B = \left\langle 1 - i\frac{\epsilon}{2}, \begin{pmatrix} 1 \\ i \end{pmatrix} \right\rangle. \tag{3-93}$$

Observe that the frequencies are complex and so are the modes. As it is well known, complex frequencies and complex modes are usually related to non-conservative modes. Taking for instance the first couple (3-92) defined before, one can, using (3-84), find the expression of the modal displacements as:

$$\begin{pmatrix} q_1 \\ q_2 \end{pmatrix}_A = \begin{pmatrix} \cos t \\ \sin t \end{pmatrix} e^{-\frac{\epsilon}{2}t}. \tag{3-94}$$

Plotting the phase diagram in the q_1q_2-plane, one can see that the dynamic is stable Fig. 3.2 and that the system is naturally damped.
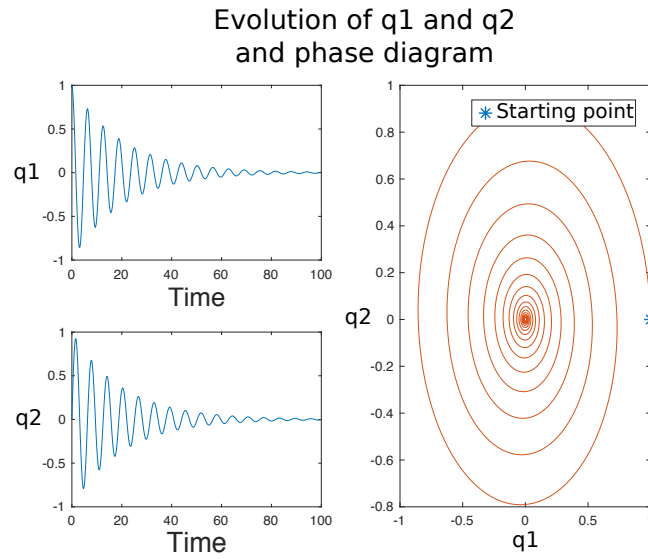
Figure 3.2: Time evolution of q_1 and q_2 and phase diagram in the q_1q_2-plane for the stable case, $\epsilon = 0.1$.
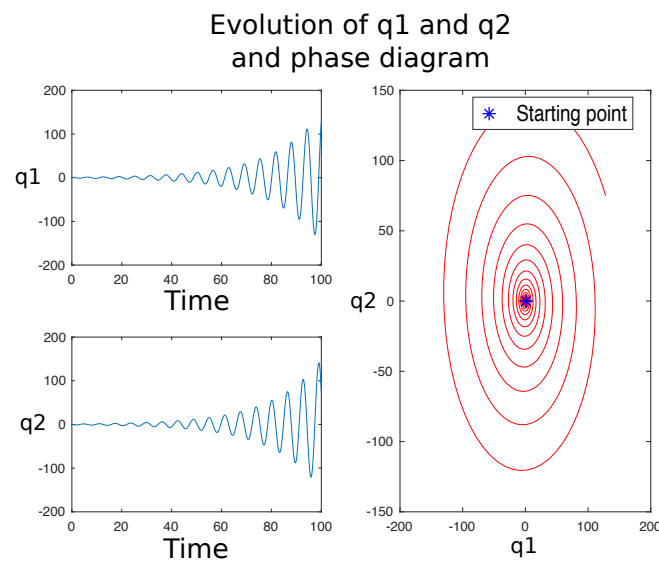
Figure 3.3: Time evolution of q_1 and q_2 and phase diagram in the q_1q_2-plane for the unstable case, $\epsilon = 0.1$.

Taking now the second couple (3-93), one can do exactly the same thing. This time, the modal displacements are:

$$\begin{pmatrix} q_1 \\ q_2 \end{pmatrix}_B = \begin{pmatrix} \cos t \\ -\sin t \end{pmatrix} e^{\frac{\epsilon}{2}t}. \tag{3-95}$$

Observing Fig. 3.3, one can see that the oscillations are growing exponentially, this mode is an unstable mode. To conclude, for the antisymmetric case, the system has a damped mode and an unstable mode which leads to a dynamic instability (with an exponential growth and oscillations).

Coming back to (3-82), one can notice that there is no reason for the coupling stiffnesses being equal or opposite. Considering that the coupling stiffness can vary in time, it is possible that there is an instant when they are equal and another when they are opposite. This way, an instability can occur. This dynamic instability is called the couple mode flutter. To occur it is required a coincidence of frequencies and a non-symmetric coupling stiffness.

3.3
Intermediate reduced velocity: a flow-induced dynamic instability

After the analysis of the two limit cases (low and high reduced velocity), one can investigate an intermediate case where the reduced velocity is neither very high nor very low. This case occurs when both time scales, the solid and the fluid have the same order of magnitude. Then, T_{solid} is not that large anymore and may change during the characteristic fluid time T_{fluid}. To simplify, one can consider that this change occurs at a constant rate. This time, neither the fluid velocity at the interface nor the velocity of the interface will be neglected. Let's note the rate of this change as γ which, using dimensionless variables, can be written as:

$$\tilde{\gamma} = \frac{d\tilde{U}}{d\tilde{t}}. \tag{3-96}$$

Combining it with the kinematic condition equation (2-84) and the order of magnitude of $\tilde{U}$ at the interface, one can easily find the order of magnitude of $\tilde{\gamma}$ (recall that $\tilde{t} = o(\frac{t}{T_{fluid}}) = o(U_R)$) as :

$$\tilde{\gamma} = o\left(\frac{D}{U_R^2}\right). \tag{3-97}$$

Then considering relative high flow velocity, which means $U_R^2 >> D$, one can say that $\tilde{\gamma}$ is negligible. This is equivalent to consider that the velocity of the interface is fixed in time. Thus, from the point of view of the fluid, the solid moves so slowly that it has a low deformation and its velocity is constant in time. This is the pseudo-static aeroelasticity approximation:

$$\Delta\tilde{U} = 0. \tag{3-98}$$

As seen before for the quasi-static aeroelasticity approximation, the two dynamics are coupled but, as the time scales are still different, they can be solved separately.

Let's have a look now on the consequences of such approximation on the dynamic of the solid. First, one can use here the single mode approximation defined before in (2-79). The difference here, is that the dimensionless variables of the fluid domain are dependent on the velocity of the interface. Thus, the pressure field and the velocity field can be written as:

$$\tilde{P}(Dq, D\dot{q}), \tag{3-99}$$

$$\tilde{U}(Dq, D\dot{q}). \tag{3-100}$$

Then, as made before for the previous single mode approximation for high reduced velocity, the flow induced force is calculated projecting on the single mode. One obtains the following expression:

$$\int_{\bar{\Gamma}_S} C_A \left(-\tilde{P}I + \frac{1}{R_E}\left(\nabla\tilde{U} + \nabla^T\tilde{U}\right)\right) n\varphi d\bar{S} = F_{FS}(R_E, Dq, D\dot{q}, ...). \tag{3-101}$$

As before, the flow induced force can be written as:

$$F_{FS} = C_A F(R_E, Dq, D\dot{q}, ...), \tag{3-102}$$

and then, using the asymptotic expansion in D as made several times before, $F_{FS} = C_A F_0 + D f_{FS} + ...$, one can find the expression of the non-constant flow induced force:

$$f_{FS} = C_A \left(\frac{dF}{d(Dq)}\right) q + C_A \left(\frac{dF}{d(D\dot{q})}\right) \dot{q}. \tag{3-103}$$

The first term is the flow induced stiffness force, which leads to flow induced static instability, and the second term is then a flow induced damping force since it is a function of $\dot{q}$. Knowing the flow induced force, one can study the dynamic of the solid through:

$$U_R^2 \frac{d^2q}{d\tilde{t}^2} + q = f_{FS}. \tag{3-104}$$

As the focus is on the dynamic of the solid, this equation can be rewritten using the solid time scale:

$$\ddot{q} + q = C_A \left(\frac{dF}{d(Dq)}\right) q + \frac{C_A}{U_R}\left(\frac{dF}{d(D\dot{q})}\right)\dot{q}. \tag{3-105}$$

A simpler form of this equation is:

$$\ddot{q} + c_F \dot{q} + (1 + k_F)q = 0, \tag{3-106}$$

where:

$$c_F = -\frac{C_A}{U_R}\left(\frac{dF}{d(D\dot{q})}\right). \tag{3-107}$$

As explained before in the case of the dynamic instability considering

high reduced velocity (using the two modes approximation), there is no reason for the damping force to be positive or negative. This force is function of the fluid dynamics. Finally, two cases are possible, one where $c_F > 0$ which will lead to damped mode and one, more critical, where $c_F < 0$ which leads to an unstable mode. In this case, the amplitude of the solid motion will increase exponentially in time.

Indeed, when there is damping in a mechanical system, one can say that the system is not conservative. If the damping is positive, the system will dissipate the energy brought by the force but when the damping is negative, the system will accumulate a part of the energy brought by the force and this will lead to an exponential increase of the motion.

This instability is also called flow induced dynamic instability and it is much more critical than the previous one since it can occur with only a single mode, and since no coincidence in frequency is required as in the previous case (the couple mode flutter). Besides of this, observe that the flow induced dynamic instability can occur with different reduced velocities. Every reduced velocity that turns the total damping of the system negative causes the instability. Remark that to compute these critical velocities, it is necessary to consider the total damping of the system, i.e. the sum of the damping coming from the solid and the fluid domain. Indeed, in (3-106) just the damping related with the fluid domain is taken into account.

3.4
Conclusions on the fluid-structure interaction consequences

As said in the introduction of this chapter, one of the objectives is to classify problems of fluid-structure interaction according to the value of the reduced velocity U_R. Three cases were investigated, the cases of small, high and intermediate reduced velocity.

For small reduced velocity, one has seen that the fluid could be considered as a still fluid. Using the approximation of small motion of the solid, several phenomena could be identified. The first one is the added stiffness effect which is linked to the original pressure field of the system. Others phenomena are related to the Stokes number.

– For high Stokes number, the fluid induced force behaves as an added mass effect.

– For low Stokes number, the fluid induced force behaves as an added damping effect.

– The case of intermediate Stokes number was briefly treated and the memory effect was quickly described.

For high reduced velocity, the solid can be considered fixed in relation to time which simplifies a lot the equations. This approximation was called the quasi-static approximation which means that the position of the interface is fixed at each time step. Then, using first the single mode approximation, one was able to determine a flow induced static instability which may occur with the diminution of the global stiffness of the solid domain.

Using the two modes approximation, an other interesting type of instability was identified. With these two modes, it exists a coupling between the modes related to the stiffness term. Also, this coupling may lead to a coincidence of the natural frequencies. In relation to the coincidence, two cases where investigated, the symmetric case where the coupling stiffness terms are equal and the case where they have opposite sign.

The symmetric case does not lead to an instability, it just leads to a small coupling between the modes which makes the response of the system slightly different than the original one. In the antisymmetric case, the coupling stiffness terms are opposite in sign which leads to two different modes, a damped one and an unstable one. The unstable mode causes flow induced dynamic instability. Note that, this instability occurs only if there is a coincidence of frequencies and also antisymmetry in the coupling stiffness terms.

Finally, the case of intermediate reduced velocity was investigated. In this case, the motion of the solid cannot be neglected and the velocity of the interface is considered constant. It has be shown that this instability is a result of negative flow induced damping force. Different from the other cases, this instability does not require a coincidence of frequencies.

Other types of instabilities were not treated here like vortex induced vibrations, as in [24]. This work gives an overview of what can occur for several values of reduced velocity. For each situation, the limit case was investigated with its dominant effect(s). In the real life, there is a transition between all these cases and, all these effects. According to the reduced velocity, for instance, some of them are dominant and others can be neglected.

Fluid-structure interaction problems have been presented, namely how to formulate them, and some of their consequences on the structure were also shown. Now, let's observe a structure that can suffer fluid-structure interactions and thus some instabilities. One proposes to study suspension bridges and namely their dynamic which is known for being very non-linear and quite particular.

Indeed, several examples of suspension bridges suffering fluid-structure interactions can be cited such as the case of the Tacoma Narrows Bridge which has collapsed in 1940. In all those cases, a common phenomenon was observed, as said in [32]: suspension bridges may suffer large oscillations that can appear suddenly.

In the next chapters, one will first present numerical models and one of them will be used to illustrate later this particular dynamic of suspension bridges. Also, the mathematical tools used to observe such dynamical behavior are given.

4
Numerical models for suspension bridges

4.1
Introduction

Before starting the description of the different simple numerical models used for suspension bridges, let's describe how a suspension bridge is usually made. The main elements and a global vision of such a structure are presented in Fig. 4.1. Usually the global structure of modern suspension bridges has a roadway (which does not have any structural function) which is supported by an element called the girder (usually made of stiffening trusses). Four towers sustain the two parallel sustaining cables. These two cables sustain the roadway and the girder through the hangers (usually smaller cables).
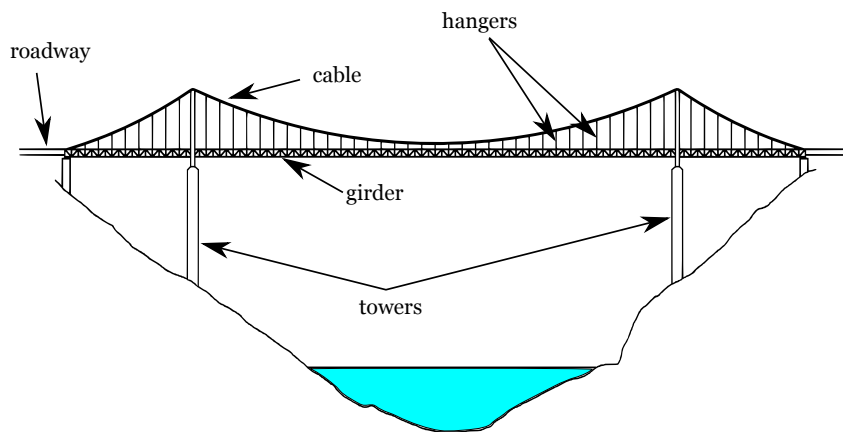
Figure 4.1: Classical view of suspension bridge.

The proper structure of suspension bridges makes them very vulnerable to fluid-structure interactions (which can interfere their sustainability that is studied in [2] and also explored in [28]) and quite hard to describe for dynamical studies through simple models. Moreover, because of the complex structure of suspension bridges, one may consider some non-linearities in the model which turns it more complex. As said in [32], non-linearities will allow to show some very interesting phenomena and mainly uncontrolled vibrations of the structure. Those vibrations are directly linked to the mechanical properties of

the bridge in a way that even common conditions (in the sense of non extreme conditions) of flow-induced excitation can create such instabilities.

As said before, the principal source of these instabilities are generally the fluid-structure interactions, but in some cases, the instability can be reached with other sources of excitation, for instance the case of the Millennium Bridge in London (excited by pedestrians through a coupling between the force generated by their steps and the dynamic of the bridge, as it shown in [1], [48] or [57]). As seen in the first chapters, fluid-structure interactions can act in different ways on the dynamic of the structure and large oscillations of the bridge may be expected due to negative damping effect or even due to the couple mode flutter effect for instance.

In the literature [32], one has shown that very large vertical oscillations can produce torsional oscillations in suspension bridges which are very critical for the sustainability of the structure. Indeed, as soon as a critical level of energy is brought to the structure, such instabilities can be observed. This energy can be brought by the wind through the lift effect or by more complex effect in the case of vortex induced instabilities. The objective of the following chapters is to build a simple model representing a suspension bridge and to observe large oscillations and non-linear behaviors.

As shown in [32] and [37] several types of model can represent suspension bridges. The simplest ones are one-dimensional models. Examples of more complex models are the ones that use fish-bone beam, the ones that use interacting oscillators or even use plate representation.

4.2
One-dimensional models

The simplest way to model suspension bridges is to consider the roadway and the girder as a unidimensional beam. Indeed, the length of the suspension bridge is much bigger than its width, then the approximation of considering the bridge deck as a beam is reasonable. But, as any consideration and simplification, some aspects of the real situation will be ruled out. In this specific case (Fig. 4.2), the torsion of the bridge cannot be observed, thus torsional vibrations will not be shown. But, once again as said in [32] and [45] large vertical oscillations are usually source of more complex torsional ones which are very critical for the structure. Vertical ones can also be very critical if their amplitude is important. From history, it was observed that it exists an instant where vertical oscillations suddenly change to torsional ones or more complex ones.

First, a brief presentation of the beam equations and also cable equations
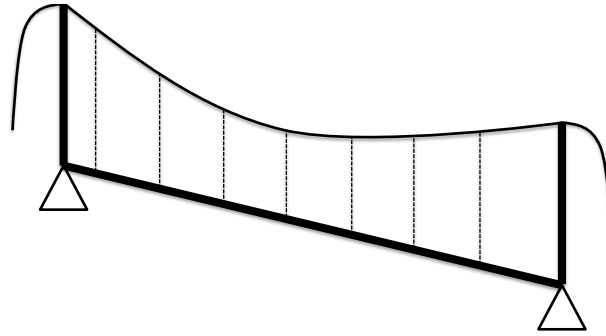
Figure 4.2: Schematic view of a one-dimensional model of suspension bridge

will be performed and then one will investigate one of the most known equations for suspension bridges using a one dimensional representation, the Meylan equation [31]. This representation combines cable and beam equations and a non linear formulation of the problem. From this formulation, a nonlinear nonlocal term appears due to the additional tension in the cable. This term can be approximated through different ways. This will be presented and explained in the next sections.

4.2.1
Linear beam equation

As defined in the literature, namely in [41], a beam as a prismatic body which is resistant to bending and twisting. During all this section one will consider that the x-axis and the beam axis are coincident and that the cross section of the beam is orthogonal to the x-axis. One will call w the deflection of the beam with respect to the z-direction from the horizontal equilibrium.

One can then define the elastic energy stored in the beam through the bending and the stretching energies (if the beam is not fixed at both endpoints, no stretching energy is expected). Finally,

$$\boxed{\text{considering small deformations } w \text{ of the beam}} \tag{4-1}$$

(in order to linearize the equations) one gets, as it is well known, the classical static equation for beams, the Euler-Lagrange equation that contains both, second and fourth order terms as following:

$$EI\frac{d^4w(x)}{dx^4} - T\frac{d^2w(x)}{dx^2} = f(x). \tag{4-2}$$

In this equation, E is the Young modulus (considered constant along the x-axis) and, I is the moment of inertia of the cross section of the beam (also considered constant all along the length of the beam). The term f represents

here the static vertical force on the beam. The term T represents the constant tension in the beam. Observe that $T = 0$ if the beam can move freely at, at least, one of the endpoints. Thus one gets a simpler form of the Euler-Lagrange equation:

$$EI\frac{d^4 w(x)}{dx^4} = f(x). \tag{4-3}$$

The equations (4-2) and (4-3) are the classical ones to represent the static deformation of a beam and may be combined to equations of the sustaining cable to build a complete model.

4.2.2
Cable under vertical loads

As found in the literature, for instance in [32] or [36], the sustaining cables are one of the main components of suspension bridges. Indeed, this element interacts with all the others of the bridge (towers, hangers and bridge deck) and also, because of the effect of the cables, the bridge deck may be designed considering the induced compression.

This section focuses on the deflection of cable (considered as a perfect flexible string) under vertical load. With this consideration, the cable has no resistance to bending and the only internal force is the tension called F. The tension acts tangentially to the position of the cable y. Let's call θ the angle between the horizontal x-direction and the curve of the cable then one can easily write:

$$\frac{d}{dx}y(x) = \tan \theta(x). \tag{4-4}$$

If the cable only suffers a vertical distributed load q, the horizontal component of the tension is constant along the cable:

$$F(x)\cos \theta(x) = H. \tag{4-5}$$

One considers that the load is distributed per horizontal unit which is exactly the case when a beam is suspended to a cable (see the following section). Neglecting the mass of the cable and considering that the space between the hangers is quite small (to really have a distributed load and not concentrated ones), the model is much simpler. One can then write the variation of the vertical component of the tension as:

$$\frac{d}{dx}[F(x)\sin \theta(x)] = -q(x). \tag{4-6}$$

Then, writing F in a different way thanks to (4-5), one gets, considering the positive vertical axis oriented downwards:

$$H\frac{d}{dx}[\tan \theta(x)] = -q(x), \tag{4-7}$$

and, finally, using (4-4) one obtains :

$$H\frac{d^2}{dx^2}y(x) = -q(x).$$ (4-8)

From (4-8) one can find the position of the cable y as a function of the vertical load q, the horizontal tension H and the length L between its two endpoints. Also, considering that both extremities of the cable are at the same height, one obtains:

$$y(x) = \frac{q}{2H}x(L-x).$$ (4-9)

4.2.3
Model of suspension bridge using beam and cable

The complete model consists of a combination of the sustaining cable and the roadway (modeled as a beam), see Figure 4.3. This is the topic of [44]. In this model, let us consider the orthogonal coordinate system (O, x, w) with the four characteristic points (O, O', M and M'). Note that the positive deflection of the beam is oriented downwards. The roadway, represented as a beam, is the
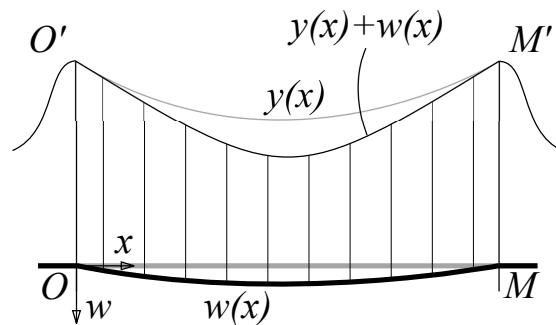
Figure 4.3: Beam sustained by a cable through parallel hangers.

segment connecting the points O and M. The cable is then suspended between the points O' and M' which are respectively the fixation points of the cable on the two towers OO' and MM'. In this initial position, the bridge deck is considered at the equilibrium position and no bending forces are present in the beam which means that the dead load of the bridge deck is all sustained by the cable itself (note that the dead load of the cable and the hangers is not considered here). From all these considerations, one can write the variables of the problem:

- L length of the beam;
- x position on the beam, $x \in [0, L]$;
- q dead load per unit length applied on the beam;
- p live load per unit length applied on the beam;

- y downwards displacement of the cable due to q;

- w downwards displacement of the beam due to the live load p;

- H horizontal tension in the cable due to the dead load only;

- h additional tension in the cable due to the live load p.

Here, it is necessary to mention that w will represent both vertical displacements of the cable and of the beam due to the live load since

$$\boxed{\text{the deformation of the hangers is neglected.}} \qquad (4\text{-}10)$$

As shown in the literature (namely by Gazzola in [32]), this assumption is quite common as long as the response of the bridge is contained in the lower modes and weakly stiffened bridges are involved. However, for more complex models, as the effect of the hangers is important, this assumption is removed because of the influence of the hangers on higher frequencies. This assumption is also removed for high stiffened bridges.

Then, reorganizing (4-8) and considering the dead load constant (since there is no mass variation), one can calculate the downwards displacement of the cable due to the dead load as:

$$\frac{d^2 y(x)}{dx^2} = -\frac{q}{H}. \qquad (4\text{-}11)$$

Thus, when a live load is added, a part of it, p_c is carried by the cable which leads to an additional tension h in the cable. The rest of the live load, called p_b, is carried by the bending stiffness of the beam. Due to this phenomena, the beam suffers a deflection w. The same deflection is added to the position of the cable y because the hangers are considered inextensible. Finally one can write the following equation:

$$(H + h(w(x))) \left(\frac{d^2 y(x)}{dx^2} + \frac{d^2 w(x)}{dx^2} \right) = -q - p_c(x). \qquad (4\text{-}12)$$

As seen before, the remaining part of the live load p_b is carried by the bending stiffness of the beam which leads to:

$$EI \frac{d^4 w(x)}{dx^4} = p_b(x). \qquad (4\text{-}13)$$

Finally, combining (4-12) and (4-13), one gets the following expression for this complete model presented by Fig. 4.3:

$$EI \frac{d^4 w(x)}{dx^4} - (H + h(w)) \frac{d^2 w(x)}{dx^2} + \frac{q}{H} h(w) = p(x), \qquad (4\text{-}14)$$

then the boundary conditions can be written as following when the beam is assumed to be hinged at the endpoints:

$$w(0) = w(L) = 0, \tag{4-15}$$

$$\frac{d^2w(0)}{dx^2} = \frac{d^2w(L)}{dx^2} = 0. \tag{4-16}$$

The equation, obtained considering (4-1) and (4-10), is a nonlinear fourth order equation (4-14) which is not that simple to integrate. Another simplification could be done considering h as a small constant. To by pass this simplification which would turn the problem linear, one needs to explain how to compute the additional tension in the cable due to the live load.

At this point, one can make some assumptions concerning the main cable of the bridge (which is extensible). Usually, the maximum deflection of the cable due to the dead load q is around $\frac{1}{10}$ of the total length L of the bridge. With this assumption, one can estimate the total length of the cable L_c and later estimate the additional tension h due to the live load p.

4.2.4
Additional tension in the cable

This section will present several ways to compute the additional tension h in the cable which is a function of the displacement w. First let's remind how to calculate the length of the cable, L_c. In [31] or [32], one can find that this length can be written as:

$$L_c = \int_0^L \sqrt{1 + y'(x)^2}\,dx. \tag{4-17}$$

Then, the additional tension in the cable is directly linked to the variation of the length ΔL_c from the initial position, due only to the dead load, to the new one, adding the live load. This can be written as:

$$\Delta L_c = \int_0^L \left(\sqrt{1 + [y'(x) + w'(x)]^2} - \sqrt{1 + y'(x)^2} \right) dx. \tag{4-18}$$

Finally, the tension is computed thanks to the mechanical properties of the cable as:

$$h(w) = \frac{E_c A_c}{L_c}\Delta L_c, \tag{4-19}$$

where E_c is the Young modulus of the cable material and A_c is the cross section area of the cable. Now, let's see some approximations used in the literature to compute this term which may be included in the equation (4-14).

First approximation: considering the following asymptotic expansion for any $\gamma \neq 0$ and applying it to (4-18),

$$\sqrt{1 + (\gamma + \epsilon)^2} - \sqrt{1 + \gamma^2} \approx \frac{\gamma\epsilon}{\sqrt{1 + \gamma^2}}, \tag{4-20}$$

for $\epsilon \longrightarrow 0$, one can write the variation of the cable length as:

$$\Delta L_c \approx \int_0^L \frac{y'(x)w'(x)}{\sqrt{1+y'(x)^2}}dx. \tag{4-21}$$

In the literature, a consideration is also made on the square of the first derivative of y. Neglecting this term and, integrating by parts one gets a first approximation. Then using (4-11) one can write:

$$\Delta L_c \approx -\int_0^L y(x)w''(x) \approx \frac{q}{H}\int_0^L w(x)dx. \tag{4-22}$$

Second approximation: from (4-18) one can reorganize the equation multiplying by the conjugate expression and to get:

$$\Delta L_c = \int_0^L \frac{2w'(x)y'(x)+w'(x)^2}{\sqrt{1+[y'(x)+w'(x)]^2}+\sqrt{1+y'(x)^2}}dx. \tag{4-23}$$

Neglecting the derivatives in the denominator and then integrating by parts leads to:

$$\Delta L_c \approx \int_0^L \left(w'(x)y'(x)+\frac{w'(x)^2}{2}\right)dx \approx \frac{q}{H}\int_0^L w(x)dx - \frac{1}{2}\int_0^L w(x)w''(x)dx. \tag{4-24}$$

Third approximation: another approximation can be done from (4-21). Integrating this equation by parts one can get:

$$\Delta L_c \approx -\int_0^L \frac{y''(x)w(x)}{(1+y'(x)^2)^{3/2}}dx. \tag{4-25}$$

Finally, using (4-11), the final expression of the variation of the cable length is:

$$\Delta L_c \approx \int_0^L \frac{w(x)}{\left[1+\frac{q^2}{H^2}\left(x-\frac{L}{2}\right)\right]^{3/2}}dx. \tag{4-26}$$

For further considerations, the first approximation (4-22), which is the simplest one, is taken into account. Indeed, the difference between the additional tensions computed with each of the three approximations is not that important according to [32]. The first approximation leads to a good enough estimation of the additional tension. Finally, modeling a suspension bridge with this one dimensional model using a beam suspended to a cable, one gets the following equation:

$$EIw''''(x) + (H+h(w))w''(x) + \frac{q}{H}h(w) = p(x), \tag{4-27}$$

where,

$$h(w) = \frac{E_c A_c}{L_c}\frac{q}{H}\int_0^L w(x), \tag{4-28}$$

with some boundary conditions. Here one considers the beam hinged at the

boundaries, then:

$$w(0) = w(L) = w''(0) = w''(L) = 0. \tag{4-29}$$

4.2.5
Dynamic equation

To describe the dynamic of the beam, the kinetic energy should be considered. Usually, dynamic of beams can be studied will two well known models, the Euler-Bernoulli one and the Timoshenko one. In the first model, shear stress and rotation of cross sections are neglected whereas in the Timoshenko model they are not. In this section the Euler-Bernoulli model is used.

The characteristics of the beam are as following, L is the length, ρ the mass per unit length (considered constant), A the area of the cross section (considered constant), the term f is the dynamic vertical force acting on the beam. The equation of motion of the beam, the Euler-Bernoulli equation, can then be written as:

$$EI\frac{d^4w(x,t)}{dx^4} + \rho A\frac{d^2w(x,t)}{dx^2} = f(x,t). \tag{4-30}$$

The initial conditions can bean initial deflection, velocity or acceleration. Then, to form the complete dynamic equation related to the static one (4-27), one neglected the kinetic energy from the cable (and from the hangers as said before). Indeed, the inertia and the mass of the cable are very small compared to the ones of the beam representing the bridge deck. Thus, the dynamic equation of this one dimensional model is:

$$\rho A\ddot{w}(x,t) + EIw''''(x,t) + (H + h(w))\,w''(x,t) + \frac{q}{H}h(w) = p(x,t), \tag{4-31}$$

where, the notation $\dot{\square}$ represents the time derivative, then $\ddot{\square}$ is the second order time derivative and the notation $\square'$ is the space derivative. Also:

$$h(w) = \frac{E_cA_c}{L_c}\frac{q}{H}\int_0^L w(x,t), \tag{4-32}$$

represents the additional tension due to the live load. The equation may be considered with the boundary conditions:

$$w(0,t) = w(L,t) = w''(0,t) = w''(L,t) = 0, \tag{4-33}$$

and the initial conditions:

$$w(x,0) = w_0, \quad \dot{w}(x,0) = \dot{w}_0, \quad \ddot{w}(x,0) = \ddot{w}_0, \tag{4-34}$$

4.2.6
Restriction on the additional tension in the cable

Considering only static models, for instance considering only (4-27) to (4-29), and applying a downwards load as traffic for instance, the additional tension will always be positive since the deformation of the bridge deck will be positive too. The formulation presented in the dynamics equations (4-31) - (4-34) can be used for any general cases of the live load (positive or negative). However, a correct interpretation of the additional tension and also of the load carried by the cable should be done.

Due to the considerations made on the hangers, which are considered as string or cable inextensible, they can only transmit vertical load to the main cable in one direction, the downwards one. Then, how to interpret $h < 0$? This should be interpreted as a diminution of the total tension in the sustaining cable. Of course the total tension in the cable cannot be negative, the cable cannot suffer compression. Thus an extra condition has to be added.

Then, at it was done in [52], one can define a function which will cancel the contribution of the cable when its computed total tension is negative. When this occurs, the total model is only a beam suffering vertical bending forces. To do this adds an other non-linearity to the equations presented before. Now, the problem can be written, considering the following function:

$$X^+ = \begin{cases} X, & X \geq 0, \\ 0, & X < 0. \end{cases} \tag{4-35}$$

as:

$$\rho A \ddot{w} + EI w'''' - H \left(1 + \frac{h}{H}\right)^+ w'' + q \left(\left(1 + \frac{h}{H}\right)^+ - 1\right) = p. \tag{4-36}$$

The equation for the additional tension (4-32), the boundary conditions (4-33) and the initial conditions (4-34) remain the same.

4.2.7
General stiffness factor

At this step, the complete equation governing the one dimensional model using a beam and a cable to represent a suspension bridge is formulated. In [52], a different organization of (4-36) is presented and permits to group the mechanical parameters. Indeed, rescaling the space interval to $[0, 1]$ instead of $[0, L]$, one can write (4-36) as:

$$\ddot{w} + C_1 w'''' - C_2 \left(1 + C_3 \int_0^1 w \, dx\right)^+ w'' + C_4 \left(1 + C_3 \int_0^1 w \, dx\right)^+ = p + C_4. \tag{4-37}$$

In (4-37), one can easily find the constants C_i's:

$$C_1 = \frac{gEI}{qL^4}, \quad C_2 = \frac{Hg}{qL^2}, \quad C_3 = \frac{E_cA_cqL}{H^2L^2}, \quad C_4 = g, \qquad (4\text{-}38)$$

where g represents the gravitational constant. An interesting parameter can thus be defined, the general stiffness factor. Indeed the ratio C_1/C_2 can be seen as a stiffness ratio between the bridge deck (in bending) and the cable (in traction), then the general stiffness factor K_{ind} can be written as:

$$K_{ind} = \sqrt{\frac{C_1}{C_2}}. \qquad (4\text{-}39)$$

Just to have an idea of the expected value for this parameter, in [52] the example of the George Washington Bridge between the New Jersey and the State of New York is given and its general stiffness factor is estimated at 0.029. Another example given in [32] with $EI = 57.10^6 kN.m^2$, $L = 460m$, $H = 97.75.10^3 kN$ and $q = 170kN/m$, considering a classical $g = 9.81m/s^2$, the general stiffness factor of this bridge is estimated as 0.052. Other examples can be found in [51].

4.3
Fish-bone beam model

Here, one will briefly present a two dimension model used for modeling suspension bridges. The bridge deck can be modeled through a fish-bone beam suspended to a cable on both sides, as done in [36] (Fig. 4.4). This custom beam is composed of a main central beam and several transversal perpendicular beams considered rigid. Thus, thanks to this representation, now the torsion is observable.
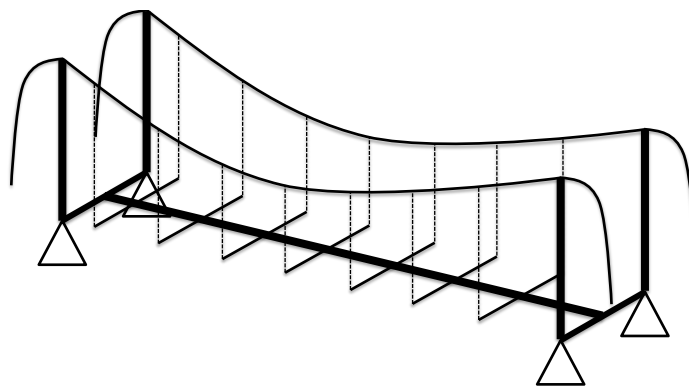
Figure 4.4: Schematic view of a fish-bone model of suspension bridge

Also, with this more complex model, it is possible to analyze the transfer of energy from vertical oscillations to torsional ones. Thus more complex effects like couple modeflutter for instance can be better understood and observed.

As shown in [32] for instance, the sudden change from vertical oscillations to torsional ones occurs when enough energy is present in the model. Then this model can allow to estimate this level of energy that will be the threshold of instability.

4.4
Models with interacting oscillators

Also, it is possible to model the suspension bridge using interacting oscillators. To do this, one investigates a single cross section of the bridge deck and then models it through a nonlinear double oscillator. In this configuration, both, vertical and torsional oscillations can be observed. Here, once again a transfer of energy from the vertical oscillations of the section to torsional ones is reached when a sufficient level of energy is present in the model. Then, instabilities such as couple mode flutter effect can be observed and better understood. Of course, a complete model of a bridge is made with several oscillators of this type.

4.5
Plate models

Finally, one can find plate models to represent suspension bridges (Fig. 4.5). These models use non linear plate equations and allow to show well some instabilities and large oscillations. Once again, with this type of model, instabilities such as couple mode flutter effects or/and torsionnal instabilities can be shown. Using this type of model, it is possible to verify that there is a critical level of energy that transforms vertical oscillations into torsionnal ones. This is coherent with what was presented in the two dimension models presented before.
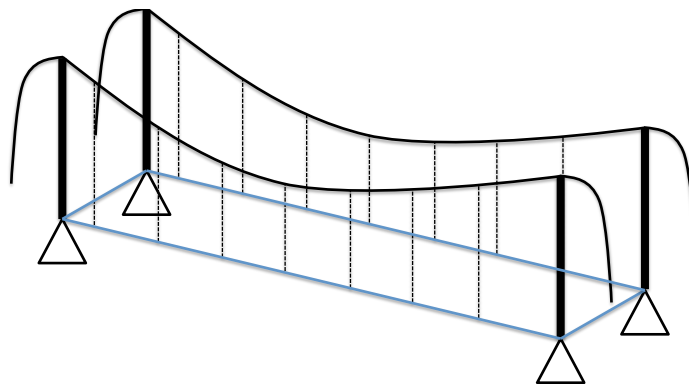
Figure 4.5: Schematic view of a plate model of suspension bridge

5
Finite element method and dynamic response analysis

5.1
Weak formulation

According to [4] and [40], the Finite Element Method (FEM) was first introduced in the 50's and 60's as a structural analysis tool. This method consists of a discretization technique of a given problem from its weak formulation or variational formulation [55] and, from its discretization, a approached solution can be obtained. To briefly explain the weak formulation, one will consider a uni-dimensional boundary value problem characterized by the equation defined for $x \in \mathcal{D}$, where $\mathcal{D} = [0, 1]$. This kind of problem is known as a Sturm-Liouville one. The classical formulation of such problem is:

$$-\frac{d}{dx}\left(p(x)\frac{du(x)}{dx}\right) + q(x)u(x) = f(x). \tag{5-1}$$

The functions u, p, q and f are also defined on the same domain $\mathcal{D}$ and the boundary conditions are defined as:

$$u(0) = 0, \quad \frac{du}{dx}(1) = 0. \tag{5-2}$$

For this example one will consider the simplest expression of (5-1) which is for $p(x) = 1$ and $q(x) = 0$. This leads to:

$$\frac{d^2u}{dx^2} + f = 0. \tag{5-3}$$

The equation (5-3) and the associated boundary conditions (5-2) are the strong formulation of the problem. To find the weak formulation of it, one needs to calculate the inner product of (5-3) with a weight function W such as:

$$\left\langle \frac{d^2u}{dx^2} + f, W \right\rangle = 0, \tag{5-4}$$

which is, developing, equivalent to:

$$\left\langle \frac{d^2u}{dx^2}, W \right\rangle + \langle f, W \rangle = 0. \tag{5-5}$$

Given the definition of the inner product, (5-5) can be written as:

$$\int_{\mathcal{D}} \frac{d^2u}{dx^2} W dx + \int_{\mathcal{D}} fW dx = 0. \tag{5-6}$$

Integrating by parts (5-6), such as $\int_{\mathcal{D}} u dv = uv|_{\mathcal{D}} - \int_{\mathcal{D}} v du$, one gets:

$$\int_{\mathcal{D}} \frac{du}{dx} \frac{dW}{dx} dx - W \frac{du}{dx}\Big|_{\mathcal{D}} = \int_{\mathcal{D}} fW dx. \tag{5-7}$$

The second term of the difference is directly linked to the boundary conditions of the problem. Indeed, in (5-2), it was defined a natural boundary condition and an essential one. It is important to notice that the weight function W has to respect the essential boundary conditions which is $u(0) = 0$ in this case but does not need to respect the natural ones. From these restrictions, one can define the space $\mathcal{V}$ of admissible weight functions. Finally, after reductions, the weak formulation of the problem is defined with $W \in \mathcal{V}$ as:

$$\int_{\mathcal{D}} \frac{du}{dx} \frac{dW}{dx} dx = \int_{\mathcal{D}} fW dx. \tag{5-8}$$

5.2
Weighted residual methods: Galerkin method

Given the weak formulation (i.e. (5-8)) of a problem, the finite element method, as a variational method, will lead to an approximation of the solution u of the problem initially described as (5-3). This approximated solution u_N will be calculated on the N discrete points of the domain $\mathcal{D}$ such as:

$$u_N(x) = \sum_{j=1}^{N} c_j \phi_j(x). \tag{5-9}$$

In (5-9), the c_j's are the coefficients to be determined and the ϕ_j's are the base functions that are linearly independent and previously defined on $\mathcal{D}$.

Of course, one wants this approximated solution such as it respects the weak formulation. The weight function W is also approximated by W_N which will be described with the ψ_i's functions ($i = 1, ..., N$) defined on $\mathcal{D}$. Thus (5-7) becomes:

$$\int_{\mathcal{D}} \frac{du_N}{dx} \frac{dW_N}{dx} dx = \int_{\mathcal{D}} fW_N dx, \tag{5-10}$$

which, replacing by (5-9) and considering the expression of the weight function, leads to:

$$\sum_{j=1}^{N} c_j \int_{\mathcal{D}} \frac{d\phi_j}{dx} \frac{d\psi_i}{dx} dx = \int_{\mathcal{D}} f\psi_i dx. \tag{5-11}$$

Simplifying one gets:

$$a_{ij} = \int_{\mathcal{D}} \frac{d\phi_j}{dx} \frac{d\psi_i}{dx} dx, \tag{5-12}$$

$$b_i = \int_{\mathcal{D}} f\psi_i dx, \tag{5-13}$$

and finally the expression is:

$$\sum_{j=1}^{N} a_{ij} c_j = b_i. \tag{5-14}$$

Using the matrix form one obtains the following expression:

$$[a]\{c\} = \{b\}, \tag{5-15}$$

where the coefficients $\{c\}$ (necessary to compute the approximated solution) are calculated by:

$$\{c\} = [a]^{-1}\{b\}. \tag{5-16}$$

The solution presented here is valid for a linear static problem. For dynamic problems the resolution might be done differently and for non-linear problems, an iterative process should be used.

5.3
Weak formulation of the equation of the one-dimensional model

In this part one will present the application of FEM to solve the non-linear equation of the one-dimensional model presented in the previous chapter (this was made by [33] for the static case), the equation (4-36) with (4-32), (4-33), (4-34) and (4-35). Just to remind the expression:

$$\rho A \ddot{w} + EI w'''' - H\left(1 + \frac{h}{H}\right)^{+} w'' + q\left(\left(1 + \frac{h}{H}\right)^{+} - 1\right) = p. \tag{4-36}$$

Then, calculating the inner product of the equation with the test functions ψ_i one obtains:

$$\left\langle \rho A \ddot{w} + EI w'''' - H\left(1 + \frac{h}{H}\right)^{+} w'' + q\left(\left(1 + \frac{h}{H}\right)^{+} - 1\right) - p, \psi_i \right\rangle = 0, \tag{5-17}$$

which can be written as:

$$\int_0^L \left[\rho A \ddot{w} + EI w'''' - H\left(1 + \frac{h}{H}\right)^{+} w'' + q\left(\left(1 + \frac{h}{H}\right)^{+} - 1\right) - p \right] \psi_i dx = 0. \tag{5-18}$$

Then, integrating twice by parts and considering the hinged-hinged boundary conditions (4-33), one gets:

$$\rho A \int_0^L \ddot{w} \psi_i dx + EI \int_0^L w'' \psi_i'' dx - H \int_0^L \left(1 + \frac{h}{H}\right)^{+} w'' \psi_i dx +$$
$$q \int_0^L \left(\left(1 + \frac{h}{H}\right)^{+} - 1\right) \psi_i dx - \int_0^L p \psi_i dx = 0. \tag{5-19}$$

Then, using the Galerkin method ($\psi_k = \phi_k$) and (5-9), it is possible to write:

$$\rho A \sum_{j=1}^{N} \ddot{w}_j \int_0^L \phi_i \phi_j dx + \sum_{j=1}^{N} w_j \left[EI \int_0^L \phi_i'' \phi_j'' dx - H \int_0^L \left(1 + \frac{h}{H}\right)^+ \phi_i \phi_j'' dx \right] +$$

$$q \int_0^L \left(\left(1 + \frac{h}{H}\right)^+ - 1 \right) \phi_i dx - \int_0^L p \phi_i dx = 0. \quad (5\text{-}20)$$

One can write this expression as a non-linear dynamic equation, which, using the matrix form, gives:

$$[m]\{\ddot{w}\} + [k]\{w\} + \left[k^{NL}(w)\right]\{w\} + \left\{f^{NL}(w)\right\} = \{f\}, \quad (5\text{-}21)$$

where,

$$m_{ij} = \rho A \int_0^L \phi_i \phi_j dx, \quad (5\text{-}22)$$

$$k_{ij} = EI \int_0^L \phi_i'' \phi_j'' dx, \quad (5\text{-}23)$$

$$k_{ij}^{NL} = -H \int_0^L \left(1 + \frac{h}{H}\right)^+ \phi_i \phi_j'' dx, \quad (5\text{-}24)$$

$$f_i^{NL} = q \int_0^L \left(\left(1 + \frac{h}{H}\right)^+ - 1 \right) \phi_i dx, \quad (5\text{-}25)$$

$$f_i = \int_0^L f \phi_i dx. \quad (5\text{-}26)$$

The matrices $[m]$ and $[k]$ are the global mass and stiffness matrices of the problem and $\{f\}$ is the global force vector. These three entities are the same as the ones that one could have found deriving all the equations and the weak formulation for a classical dynamic problem of a beam.

On the other hand, the matrix $\left[k^{NL}\right]$ represents a non-linear stiffness matrix, since it multiplies directly the displacement function w, which depends on the unknown of the problem itself through the function h. This term is directly linked to the extra stiffness coming from the cable (remember the additional tension in the cable) due to the displacement. Also, the term $\left\{f^{NL}\right\}$ is non-linear term since it also depends on the displacement through the function h. This is linked to the force of the cable on the beam. To solve such a non-linear dynamic equation, one will need to find the expression of the non-linear matrices at each time step.

The weak formulation of the problem is written using (4-37). Let's remind the equation:

$$\ddot{w} + C_1 w'''' - C_2 \left(1 + C_3 \int_0^1 w dx\right)^+ w'' + C_4 \left(1 + C_3 \int_0^1 w dx\right)^+ = p + C_4, \quad (4\text{-}37)$$

with,

$$C_1 = \frac{gEI}{qL^4}, \quad C_2 = \frac{Hg}{qL^2}, \quad C_3 = \frac{E_c A_c qL}{H^2 L^2}, \quad C_4 = g. \qquad (4\text{-}38)$$

The weak form of this expression is:

$$\sum_{j=1}^{N} \ddot{w}_j \int_0^L \phi_i \phi_j dx + \sum_{j=1}^{N} w_j \left[C_1 \int_0^L \phi_i'' \phi_j'' dx - C_2 \left(1 + C_3 \int_0^1 w dx \right)^+ \int_0^L \phi_i \phi_j'' dx \right] +$$

$$C_4 \left(1 + C_3 \int_0^1 w dx \right)^+ \int_0^L \phi_i dx = \int_0^L (p + C_4) \phi_i dx. \quad (5\text{-}27)$$

This forms the weak formulation of the problem and, it is written as:

$$[m]\{\ddot{w}\} + C_1 [k]\{w\} - C_2 \left(1 + C_3 \int_0^1 w dx \right)^+ \left[k^{NL} \right] \{w\} +$$

$$C_4 \left(1 + C_3 \int_0^1 w dx \right)^+ \left\{ f^{NL} \right\} = \{f\}, \quad (5\text{-}28)$$

where,

$$m_{ij} = \int_0^L \phi_i \phi_j dx, \qquad (5\text{-}29)$$

$$k_{ij} = \int_0^L \phi_i'' \phi_j'' dx, \qquad (5\text{-}30)$$

$$k_{ij}^{NL} = \int_0^L \phi_i \phi_j'' dx, \qquad (5\text{-}31)$$

$$f_i^{NL} = \int_0^L \phi_i dx, \qquad (5\text{-}32)$$

$$f_i = \int_0^L (p + C_4) \phi_i dx. \qquad (5\text{-}33)$$

The weak form presented in (5-27) (where the constants are defined by (4-38)) with (5-29)-(5-33) was used in the simulation routine implemented with the software Matlab. To check this simulation routine, the results obtained were compared with the results presented by [52].

5.4
Elementary functions

Here, the elementary functions ϕ_i's used to solve the problem are briefly presented. These functions are defined in (5-34)-(5-35) and are used to build the different matrices. To build these matrices, one needs to integrate the elementary functions. This integration will be better explain later.

To chose these functions one may keep in mind that they have to respect the boundary conditions of the problem. Also, to simplify the computation and save computational cost, they may be as simple as possible. Then, having

functions that are only different to zero in a small space of the domain will be very efficient during the computation.

As it is well explained in different books [4] and [40] or in the specialized literature concerning FEM, to build these functions, the domain should be discretized in elements, delimited by nodes, which create a mesh. Each node corresponds to one elementary function. Then, to be more efficient, the computation of the matrices is made through an elementary construction (thanks to the elementary functions). This means that elementary matrices are built and then assembled to form the global matrices of the problem.
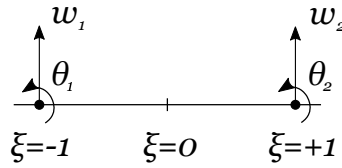
Figure 5.1: Local coordinate system.

Thus, instead of being defined in the whole domain, the functions are defined on elements, and as they are equal for all elements, this procedure is done only once. Then, an elementary description of the functions may be done. Due to the form of the equation to solve and its boundary conditions, Hermite functions will be used. Besides of this, the base functions are required to be continue with second derivative different from zero on the domain. Since it has been chosen to use linear elements with two nodes and the Euler-Bernoulli model, each element contains four degrees of freedom. The elementary functions used are preented in Fig 5.2 and are written as:

$$\begin{aligned}
\phi_1(\xi) &= \tfrac{1}{2} - \tfrac{3}{4}\xi + \tfrac{1}{4}\xi^3, \\
\phi_2(\xi) &= \tfrac{1}{4} - \tfrac{1}{4}\xi - \tfrac{1}{4}\xi^2 + \tfrac{1}{4}\xi^3, \\
\phi_3(\xi) &= \tfrac{1}{2} + \tfrac{3}{4}\xi - \tfrac{1}{4}\xi^3, \\
\phi_4(\xi) &= -\tfrac{1}{4} - \tfrac{1}{4}\xi + \tfrac{1}{4}\xi^2 + \tfrac{1}{4}\xi^3.
\end{aligned} \tag{5-34}$$

Their second derivative are:

$$\begin{aligned}
\phi_1''(\xi) &= \tfrac{3}{2}\xi, \\
\phi_2''(\xi) &= -\tfrac{1}{2} + \tfrac{3}{2}\xi, \\
\phi_3''(\xi) &= -\tfrac{3}{2}\xi, \\
\phi_4''(\xi) &= \tfrac{1}{2} + \tfrac{3}{2}\xi.
\end{aligned} \tag{5-35}$$

With these functions, defined on the elementary domain $\xi \in [-1; 1]$, it is necessary to change the coordinates in order to write the elementary matrices used to build the global ones.
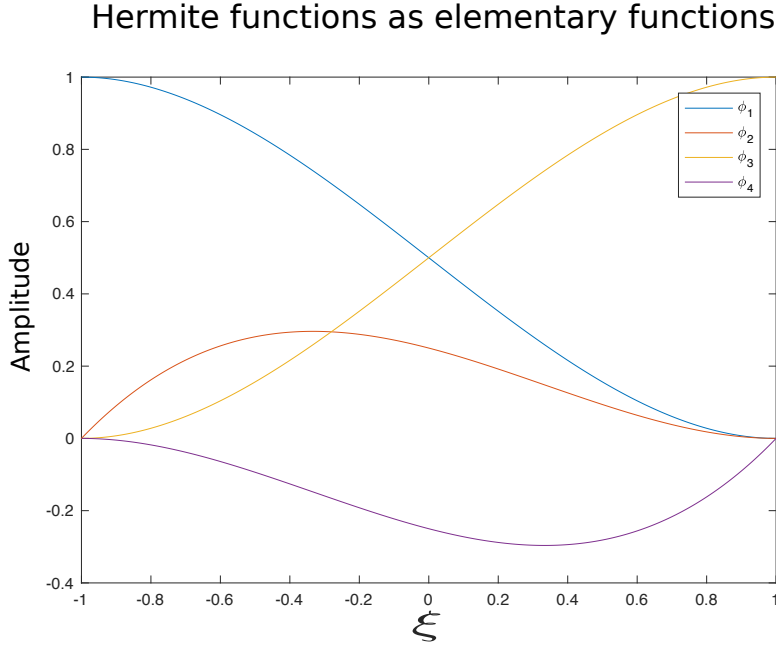
Figure 5.2: Hermite functions on the elementary domain.

5.5
Change of coordinates, from global to local

As explained previously, since the matrices will be computed for each element, local coordinates should be introduced. With this local coordinate system, the formulation of the matrices has to be modified since the size of the element is equal to one on the local system and can be different on the global one. Thus, the elementary matrices defined in (5-29)-(5-33) can be written as:

$$m_{ij}^{(e)} = \frac{l^{(e)}}{2} \int_{-1}^{1} \phi_i \phi_j d\xi, \tag{5-36}$$

$$k_{ij}^{(e)} = \left(\frac{2}{l^{(e)}} \right)^3 \int_{-1}^{1} \phi_i'' \phi_j'' d\xi, \tag{5-37}$$

$$k_{ij}^{NL(e)} = \frac{2}{l^{(e)}} \int_{-1}^{1} \phi_i \phi_j'' d\xi, \tag{5-38}$$

$$f_i^{NL(e)} = \frac{l^{(e)}}{2} \int_{-1}^{1} \phi_i d\xi, \tag{5-39}$$

$$f_i^{(e)} = \frac{l^{(e)}}{2} \int_{-1}^{1} (p + C_4) \phi_i d\xi, \tag{5-40}$$

where $l^{(e)}$ corresponds to the size between the two nodes of the element e. In the local coordinate system, the size of the element is always equal to 2, thus $d\xi = 2$ which led to the different forms of the elementary matrices.

5.6
Integration using the Gaussian quadrature

To build the elementary matrices, one needs to integrate quantities, on the local domain, in an efficient way since it may be done many times for refined meshes. A really common way to do this in FEM consists of using the Gaussian quadratic method [30]. This method evaluates the values of the fonction to integrate z at some points, called Gauss points, and then gives weight $\mathcal{W}$ to these values before summing them as:

$$\int_{-1}^{1} z(\xi)d\xi = \sum_{i=1}^{NGP} z(\xi_i)\mathcal{W}_i. \tag{5-41}$$

Here, NGP represents the number of Gauss points used for the approximation of the integral. Usually, NGP is, at least, twice the number of local nodes for each element, which should be $NGP = 4$ here. Then, for these values one can define the table used for the Gaussian quadrature method used in this case, cf. Table 5.1

i	ξ_i	$\mathcal{W}_i$
1	- 0.86113	0.347
2	- 0.33998	0.652
3	+ 0.86113	0.652
4	+ 0.33998	0.347

Table 5.1: Table for the Gaussian quadrature method with four points.

5.7
Modal analysis

For this section one will consider a linear problem in order to better explain the modal analysis that can be done thanks to the finite element discretization. Then, considering the classical equation of motion of a beam, see (4-30), one can define the weak formulation of the problem thanks to the boundary conditions. Here a hinged-hinged beam is considered for this section. Then, the equation of motion can be written, as it has been done for the non-linear equation (4-36), thanks to the mass and the stiffness matrices as:

$$[m]\{\ddot{w}\} + [k]\{w\} = \{f\}. \tag{5-42}$$

From this formulation one can write the eigenvalue problem associated to the free system and then, as it is well known, find when:

$$\det(-\omega^2[m] + [k]) = 0. \tag{5-43}$$

As the global mass and stiffness matrices are obtained through the finite element discretization, bigger is the number of elements N, better will be the approximation of the mode shapes and of the natural frequencies. Solving equation (5-43) one can obtain the normal modes Φ organized in columns and the associated natural frequencies Ω such as:

$$[\Phi] = \begin{bmatrix} | & | & & | \\ \Phi_1 & \Phi_2 & \ldots & \Phi_N \\ | & | & & | \end{bmatrix}, \quad [\Omega] = \begin{bmatrix} \omega_1^2 & 0 & \ldots & 0 \\ 0 & \omega_2^2 & & 0 \\ \vdots & & \ddots & \vdots \\ 0 & 0 & \ldots & \omega_N^2 \end{bmatrix}. \quad (5\text{-}44)$$

Note that all this section describes the modal analysis for linear problems. For non-linear ones, this procedure can be done but the interpretation is slightly different. Considering (5-21) and solving (5-43), the normal modes related to the linear system associated to the non-linear one are found. For non-linear systems, there is no constant mode shapes since everything depends on the excitation level. However, when the non-linearity is small, the normal modes can be used and a reduced order model built.

5.8
Dynamic response analysis through normal modes

Considering that the major contribution of the motion is contained in the first natural modes, one can reduce the model through the number of normal modes used to find the dynamic response of the beam. Thus, if one considers the same case as in the previous section, from (5-42) one obtains (5-43) which contains N normal modes. One can then reduce the problem to its n-first normal modes from Φ_1 to Φ_n ($n < N$) and then obtain:

$$[\Phi]_{red} = \begin{bmatrix} | & | & & | \\ \Phi_1 & \Phi_2 & \ldots & \Phi_n \\ | & | & & | \end{bmatrix}, \quad (5\text{-}45)$$

with the corresponding natural frequencies. Then the deflection of the beam $\{w\}$ can be represented through the modal coordinates $\{v\}$ such as:

$$\{w(t)\} = [\Phi]_{red}\{v(t)\}. \quad (5\text{-}46)$$

Using this expression in (5-42) one obtains:

$$[m]\,[\Phi]_{red}\,\{\ddot{v}(t)\} + [k]\,[\Phi]_{red}\,\{v(t)\} = \{f(t)\}, \quad (5\text{-}47)$$

and then multiplying by $[\Phi]_{red}^T$ one gets:

$$[\Phi]_{red}^T\,[m]\,[\Phi]_{red}\,\{\ddot{v}(t)\} + [\Phi]_{red}^T\,[k]\,[\Phi]_{red}\,\{v(t)\} = [\Phi]_{red}^T\,\{f(t)\}. \quad (5\text{-}48)$$

Reducing the equation (5-48), one can write the equation of motion as a system of uncoupled differential equations as:

$$[m_d]\{\ddot{v}(t)\} + [k_d]\{v(t)\} = \{q(t)\},\tag{5-49}$$

where $\{q(t)\}$ represents the force vector written with the modal coordinates. One also notes that, due to the orthogonality of normal modes, the mass and stiffness matrices are reduced to diagonal matrices respectively called $[m_d]$ and $[k_d]$. Using this reduction, the initial problem that should be solved through N coupled equations can be solved only with n uncoupled equations (5-50).

$$\begin{cases} m_{d_1}\ddot{v}_1(t) + k_{d_1}v_1(t) = q_1(t) \\ m_{d_2}\ddot{v}_2(t) + k_{d_2}v_2(t) = q_2(t) \\ \qquad\qquad \vdots \\ m_{d_n}\ddot{v}_n(t) + k_{d_n}v_n(t) = q_n(t) \end{cases}\tag{5-50}$$

Computationally speaking, this is a great improvement especially for complex cases which need more elements. Thus, solving (5-50), one gets the modal coordinates and, from them, can calculate the global dynamic response of the beam using (5-46).

5.9
Dynamic response analysis through the Newmark-beta method

In order to solve the non-linear problem described by (5-28), one can use the Newmark-beta method. As said in [12], this implicit method permits to compute non-linear terms quite easily and, depending on the characteristic parameters β and γ, can be unconditionally stable. Also, with this method, one can use relative important time increment without changing the solution for low frequency systems. Note that an implementation using the 4th and 5th order Runge-Kutta method (through the *ode45* function in Matlab) was made but the Newmark-beta method appeared to be more convenient for some specific cases. From initial conditions of displacement, velocity and acceleration, one can develop an implicit routine to solve the equation of motion.

Here, the characteristic parameters β and γ are defined by (5-51) which are common values that correspond to the linear acceleration method. With this combination of parameters, the method is stable and the time-step can be quite important.

$$\gamma = \frac{1}{2}, \qquad \beta = \frac{1}{4}.\tag{5-51}$$

According to [12] or [30], the method is unconditionally stable if $\gamma > \frac{1}{2}$ and $\beta > \frac{(2\gamma+1)^2}{4}$. Also, a numerical positive damping is introduced when $\gamma > \frac{1}{2}$ and a negative one if $\gamma < \frac{1}{2}$. The combination (5-51) leads to a unconditionally

stable resolution at the second order without numerical damping.

Concerning the time-step Δt used in the Newmark-beta method, it should be defined according to the maximal frequency that one wants to observe during the simulation. Indeed, as said in [30], the implicit methods tend to increase the characteristic time period of the system. Thus, it is recommended to respect (5-52), where f_{max} is the highest frequency that one wants to observe:

$$\Delta t < \frac{1}{10 f_{max}} \qquad to \qquad \frac{1}{100 f_{max}}. \tag{5-52}$$

Considering the dynamic equation (5-28) and introducing a damping matrix (for instance a proportional damping matrix) to be more general in the formulation, one can write the dynamic equation that will be solved with the Newmark-beta method:

$$[m] \{\ddot{w}\} + [c] \{\dot{w}\} + C_1 [k] \{w\} - C_2 \left(1 + C_3 \int_0^1 w dx\right)^+ \left[k^{NL}\right] \{w\} +$$
$$C_4 \left(1 + C_3 \int_0^1 w dx\right)^+ \left\{f^{NL}\right\} = \{f\}. \tag{5-53}$$

This expression is simplified as:

$$[m] \{\ddot{w}\} + [c] \{\dot{w}\} + C_1 [k] \{w\} + D_1 \left[k^{NL}\right] \{w\} + D_2 \left\{f^{NL}\right\} = \{f\}, \tag{5-54}$$

where:
$$D_1 = -C_2 \left(1 + C_3 \int_0^1 w dx\right)^+, \tag{5-55}$$

$$D_2 = C_4 \left(1 + C_3 \int_0^1 w dx\right)^+. \tag{5-56}$$

From (5-54), one can write a form in term of the increments (noted with $\delta\square$) of displacement, velocity, acceleration and non-linear terms for each time increment i with a time-step Δt as:

$$[m] \left\{\delta\ddot{w}^{(i)}\right\} + [c] \left\{\delta\dot{w}^{(i)}\right\} + C_1 [k] \left\{\delta w^{(i)}\right\} + D_1^{(i)} \left[k^{NL}\right] \left\{\delta w^{(i)}\right\} +$$
$$D_2^{(i)} \left\{f^{NL}\right\} = \left\{\delta f^{(i)}\right\}. \tag{5-57}$$

Here, the increment of each quantity is such as:

$$\delta\square^{(i)} = \square^{(i+1)} - \square^{(i)}. \tag{5-58}$$

The increments of velocity and acceleration are defined as:

$$\delta\ddot{w}^{(i)} = \frac{1}{\beta\Delta t^2} \delta w^{(i)} - \frac{\gamma}{\beta}\dot{w}^{(i)} - \frac{1}{2\beta}\ddot{w}^{(i)}, \tag{5-59}$$

$$\delta \dot{w}^{(i)} = \frac{\gamma}{\beta \Delta t} \delta w^{(i)} - \frac{\gamma}{\beta} \dot{w}^{(i)} + \Delta t \left(1 - \frac{\gamma}{2\beta} \right) \ddot{w}^{(i)}. \tag{5-60}$$

Using (5-59) and (5-60) in (5-57) gives:

$$\bar{K} \left\{ \delta w^{(i)} \right\} = \bar{R}, \tag{5-61}$$

where:

$$\bar{K} = \left[[m] \frac{1}{\beta \Delta t^2} + [c] \frac{\gamma}{\beta \Delta t} + C_1 [k] + D_1^{(i)} \left[k^{NL} \right] \right], \tag{5-62}$$

$$\bar{R} = \left\{ \delta f^{(i)} \right\} - D_2^{(i)} \left\{ f^{NL} \right\} + \left[[m] \frac{1}{\beta \Delta t} + [c] \frac{\gamma}{\beta} \right] \left\{ \dot{w}^{(i)} \right\} + \\ \left[[m] \frac{1}{2\beta} - [c] \Delta t \left(1 - \frac{\gamma}{2\beta} \right) \right] \left\{ \ddot{w}^{(i)} \right\}. \tag{5-63}$$

Then, for each time step, one may solve the equation (5-61) to find the variation of displacement and then velocity and acceleration. As the terms $D_1^{(i)}$ and $D_2^{(i)}$ are function of the unknown $w^{(i)}$, as shown in (5-55) and (5-56), the equation is non-linear. Here, considering that the time-step is small enough, it is possible to write $D_1^{(i)}$ and $D_2^{(i)}$ as functions of $w^{(i-1)}$. This is a good approximation that will be used in the simulation routine. Otherwise, one should find $D_1^{(i)}$ and $D_2^{(i)}$ through an iterative process, as explained in [60], for instance the Newton method, in order to find them as functions of $w^{(i)}$. Note that this iterative process has been implemented but the results were very similar. However, the computational cost was much more important which was responsible of slowing down the simulations. At the end of the all procedure, $\left\{ \delta w^{(i)} \right\}$ is found and, to find $w^{(i+1)}$ it is used:

$$\left\{ w^{(i+1)} \right\} = \left\{ w^{(i)} \right\} + \left\{ \delta w^{(i)} \right\}. \tag{5-64}$$

The velocities are found using (5-60):

$$\left\{ \dot{w}^{(i+1)} \right\} = \frac{\gamma}{\beta \Delta t} \left\{ \delta w^{(i)} \right\} + \left(1 - \frac{\gamma}{\beta} \right) \left\{ \dot{w}^{(i)} \right\} + \Delta t \left(1 - \frac{\gamma}{2\beta} \right) \left\{ \ddot{w}^{(i)} \right\}. \tag{5-65}$$

The acceleration has to satisfy the equation of motion then, as the displacement and the velocity are known, it is possible to compute the acceleration with:

$$\left\{ \ddot{w}^{(i+1)} \right\} = - [m]^{-1} \left[C_1 [k] \left\{ w^{(i+1)} \right\} + [c] \left\{ \dot{w}^{(i+1)} \right\} + D_1^{(i+1)} \left[k^{NL} \right] \left\{ w^{(i+1)} \right\} + \\ D_2^{(i+1)} \left\{ f^{NL} \right\} - \left\{ f^{(i+1)} \right\} \right]. \tag{5-66}$$

Now it is possible solve the dynamic equation presented in (5-28). A routine is developed using the software Matlab and presented in at the end of this document.

5.10
Algorithm used for the simulations

1 - Preprocessing

- Physical variables and geometry (beam & cable)
  - Computation of the C_i's
- Discretization of the space - creation of the mesh
- Definition of the assembly matrix
- Build the elementary matrices $M^{(e)}$, $K^{(e)}$, $K^{NL(e)}$, $F^{NL(e)}$
- Built the global matrices M, K, K^{NL}, F^{NL}
- Boundary conditions, reduction of matrices for modal analysis
- Modal analysis of the linear system

2 - Dynamic analysis

- Definition of the time vector
- Creation of the force matrix (function of time and space)
- Build the elementary matrix $F^{(e)}$
- Build the global matrix F
- Newmark-beta method
  - Initial conditions
  - Parameters of the Newmark-beta method : β and γ
  - Coefficients of the Newmark-beta method : a_i's
    - Loop on time t_i
      - Computation of the non-linear terms: from previous or actual time (iterative process)
      - Computation of K_{bar} and F_{bar}
      - Computation of δw
      - $w_{i+1} = w_i + \delta w$
      - Computation of $\delta(dw/dt)$
      - $(dw/dt)_{i+1} = (dw/dt)_i + \delta(dw/dt)$
      - Computation of (d^2w/dt^2)
    - end

3 - Post treatment

- Plots and figures

Figure 5.3: Algorithm used for the simulations.

5.11
Validation of the Matlab routine

5.11.1
Linear case of a hinged-hinged beam

A Matlab routine was developed, combining all the elements presented in this chapter, to solve (5-20) or, in a more convenient form, (5-28). To check the routine, one can verify that it works perfectly for the linear case. Considering the deflection w of a hinged-hinged beam (without cable, only a beam) defined with the following parameters:

$$L = 1m$$
$$E = 200GPa$$
$$I = 33.333.10^{-12}m^4 \tag{5-67}$$
$$A = 1.10^{-4}m^2$$
$$\rho = 7850kg.m^{-3}$$

The equation to solve is:

$$\rho A\ddot{w} + EIw'''' = p. \tag{5-68}$$

The boundary conditions and initial conditions are:

$$w(0,t) = w(L,t) = 0, \qquad w(x,0) = \dot{w}(x,0) = \ddot{w}(x,0) = 0. \tag{5-69}$$

Considering the free system of (5-68) that can be written as:

$$\ddot{w} + C_1 w'''' = 0, \tag{5-70}$$

which means that the other constants of (4-37) are then defined as:

$$C_2 = 0, \qquad C_3 = 0, \qquad C_4 = 0, \tag{5-71}$$

the natural frequencies can be found and compared to the analytical ones from [34]. The analytical form is:

$$f_i = \frac{1}{2\pi} \frac{(i\pi)^2}{L^2} \sqrt{\frac{EI}{\rho A}}. \tag{5-72}$$

The results are presented in Table 5.2. As another way to check the routine, the Power Spectral Density (PSD) of the response is plotted for a random excitation. The peaks of the PSD have to coincide with the natural frequencies of Table 5.2. For this simulation the parameters are: the number of elements $N_{ele} = 20$, the acquisition frequency $f_s = 3000Hz$, the time of simulation $T = 10s$. The excitation is a random distributed load generated through the random command of Matlab with the variance $\sigma_p = 1$ and the mean value

i	analytical frequency (Hz)	numerical frequency (20 el.) (Hz)
1	4.5776	4.5776
2	18.3105	18.3106
3	41.1985	41.2000
4	73.2419	73.2497
5	114.4404	114.4701

Table 5.2: Natural frequencies of a hinged-hinged beam.

$\hat{p} = 0$. Note that using this process to build the random excitation, due to the Nyquist condition, only frequency until half the acquisition one will be observable. After zooming on the region of interest, one can see that the PSD of the response (Fig. 5.4) is coherent with the natural frequencies of the system presented in Table 5.2.
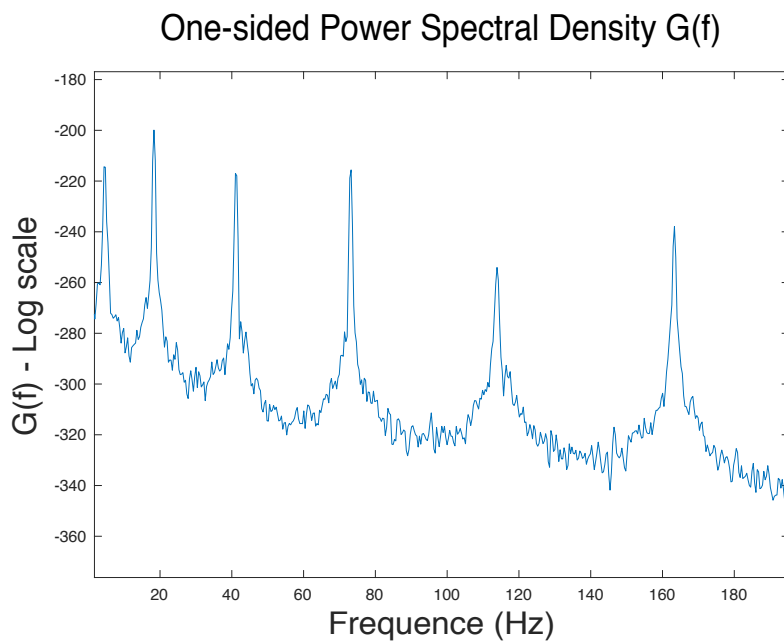
Figure 5.4: Power Spectral Density on a hinged-hinged beam using the routine.

Also, the response of the system to a specific frequency can be observed. Now the excitation as a unit distributed load only on the first half of the beam (in order to not force specifically in the first mode) with a periodic evolution in time of frequency μ, such as:

$$p(x, t) = P(x)\sin(2\pi\mu t), \tag{5-73}$$

where:

$$P(x) = \begin{cases} 1, & x \leqslant \frac{L}{2} \\ 0, & x > \frac{L}{2} \end{cases}. \tag{5-74}$$
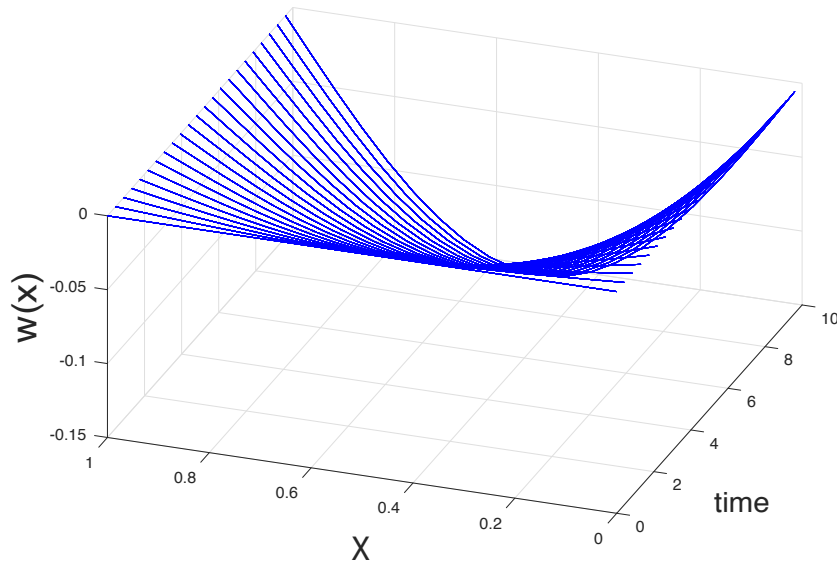
Figure 5.5: Evolution of $w(x)$ along the time (captured at 2μ), $\mu = 4.5776Hz$.
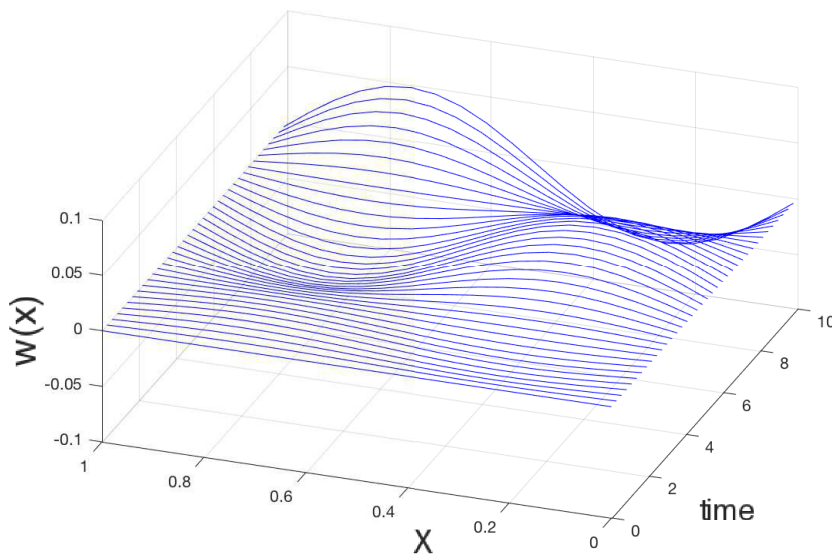
Figure 5.6: Evolution of $w(x)$ along the time (captured at 5μ), $\mu = 18.3106Hz$.

The Fig. 5.5 and 5.6 show that resonance occurs at these specific frequencies as expected. Thus, with all these considerations, the routine satisfies the linear case of a hinged-hinged beam.

5.11.2
Linear case of a hinged-hinged beam with axial tension

Considering the deflection w of a hinged-hinged beam, but this time with a axial tension $\mathcal{H}$, defined with the same physical parameters as before (5-67) with:

$$\mathcal{H} = 96.26N, \tag{5-75}$$

the equation to solve is:

$$\rho A\ddot{w} + EIw'''' - \mathcal{H}w'' = p. \tag{5-76}$$

The boundary conditions and initial conditions are:

$$w(0,t) = w(L,t) = 0, \qquad w(x,0) = \dot{w}(x,0) = \ddot{w}(x,0) = 0. \tag{5-77}$$

Considering the free system of (5-76) that can be written as:

$$\ddot{w} + C_1 w'''' - C_2 w'' = 0, \tag{5-78}$$

the other constants of (4-37) are then defined as:

$$C_3 = 0, \qquad C_4 = 0. \tag{5-79}$$

The natural frequencies can be found and compared to the analytical ones (cf. Table 5.3) that are found, according to [11], with:

$$f_i = \frac{1}{2\pi}(i\pi)^2 \sqrt{C_1 + \frac{C_2}{(i\pi)^2}}. \tag{5-80}$$

i	analytical frequency (Hz)	numerical frequency (20 el.) (Hz)
1	6.7097	6.7097
2	20.7735	20.7734
3	43.7495	43.7482
4	75.8325	75.8249
5	117.0685	117.0395

Table 5.3: Natural frequencies of a hinged-hinged beam with axial tension.
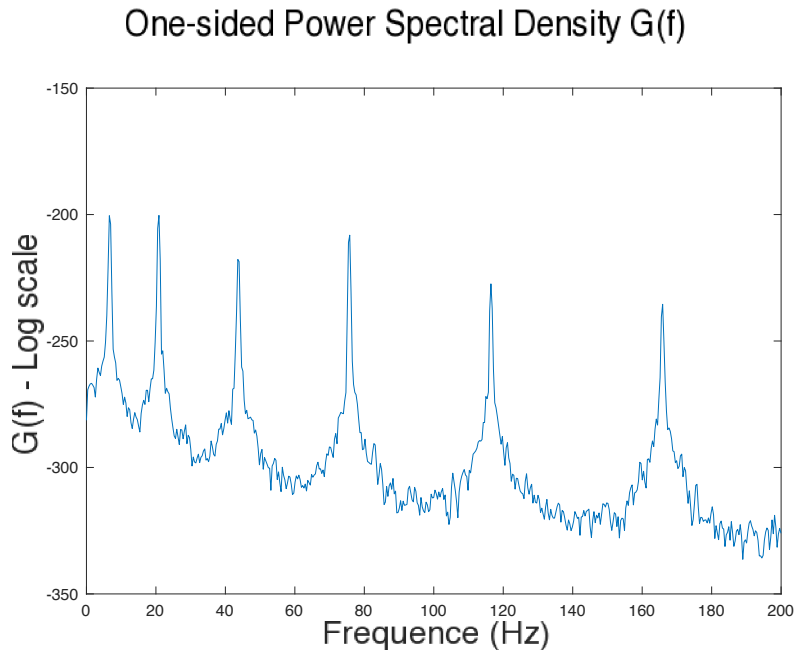
Figure 5.7: Power Spectral Density on a hinged-hinged beam with axial tension using the routine.

The same study as before, using the PSD, can be performed (cf. Fig. 5.7) and once again allows to validate the model for a hinged-hinged beam with axial tension. Also, using the same excitation as before (5-73) and (5-74), one can observe the resonance of the beam. Thus the routine can be validate for the case of hinged-hinged beam with axial tension.
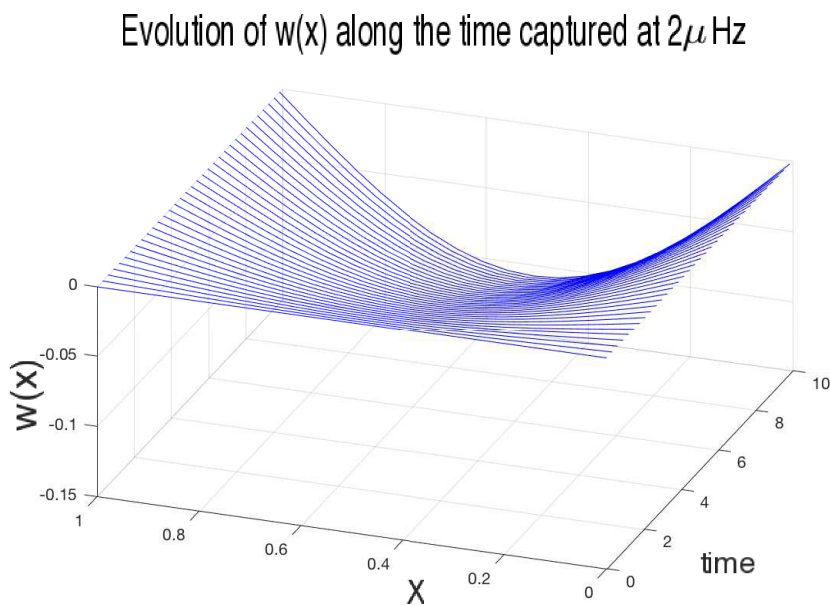

Figure 5.8: Evolution of $w(x)$ along the time (captured at 2μ), $\mu = 6.7097Hz$.
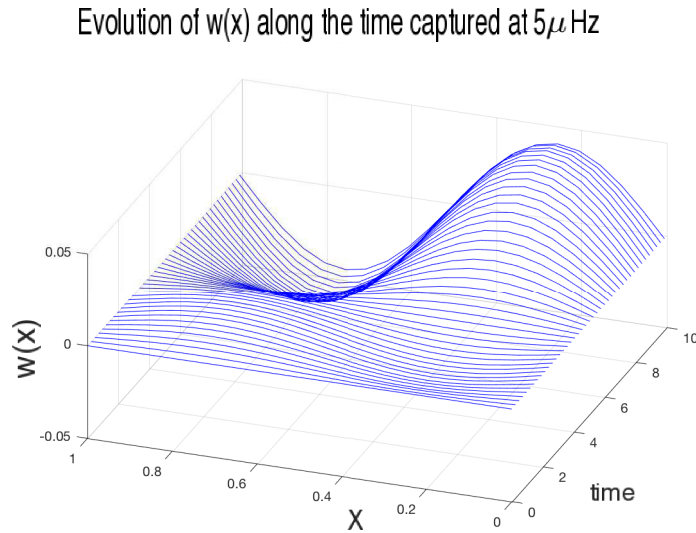
Figure 5.9: Evolution of $w(x)$ along the time (captured at 5μ), $\mu = 20.7734Hz$.

5.11.3
Non-linear case, one-dimensional model for suspension bridge

To validate this routine, the comparison of the results is made with [52], where another method is used to perform the dynamic analysis (the predictor-corrector method). In this case, the complete formulation of (4-37) is used and several combinations of the C_i's are investigated. In this section, the excitation is modeled with a vertical force defined with:

$$p(x,t) = \lambda sin(\pi x)sin(\mu t), \qquad x \in [0,1]. \tag{5-81}$$

Note that given the space domain, the excitation will force the system specifically in its first vibration mode. The boundary conditions and the initial conditions are defined with (5-69). The simulation is made for a time $T = 50s$ with a time increment $\Delta t = 0.005s$ (ten times smaller than in [52]). The spatial discretization is such that 21 nodes are used. The purpose of [52] is namely to investigate the influence of the ratio $\frac{C_1}{C_2}$ (in term of induced displacement) for $C_3 = C_4 = 1$.

Then, for each value of this ratio $\frac{C_1}{C_2}$, a map of the maximum induced displacement during the simulation, called w_{max}, can be plotted. The induced displacement is normalized with respect to the magnitude of the excitation λ as:

$$d_{max} = \frac{w_{max}}{\lambda}. \tag{5-82}$$

Thus, a map of the normalized induced displacement can be drawn for each ratio $\frac{C_1}{C_2}$ as a function of the frequency and the magnitude of the excitation.

Each point of the map represents the maximal displacement during the simulation for a given combination of λ and μ. As said in [52], large amplitude solution is considered when $d_{max} > 1$. The first case that will be investigated is for $C_1 = C_2 = 0.5$, which means $\frac{C_1}{C_2} = 1$, the results are plotted in Fig. 5.10.
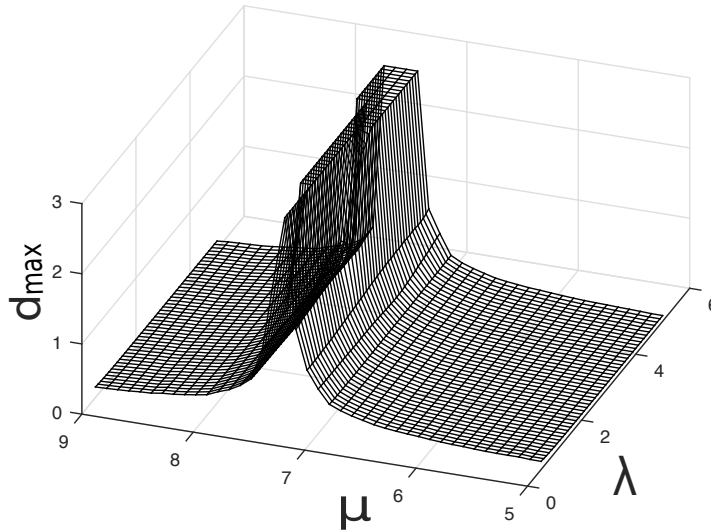
Figure 5.10: Normalized max. disp. d_{max} against μ and λ for $C_1/C_2 = 1.0$.

The peak observed in Fig. 5.10 corresponds exactly to the first natural frequency of a linear hinged-hinged beam with axial tension. This frequency can be approximated, as shown in [34], by:

$$\mu_{analytic} = \pi^2 \sqrt{C_1 + \frac{C_2}{\pi^2}}. \tag{5-83}$$

The second case considers $C_1 = 0.05$ and $C_2 = 0.5$. Then the ratio $\frac{C_1}{C_2} = 0.1$. The third case corresponds to $C_1 = 0.005$ and $C_2 = 0.5$ which means $\frac{C_1}{C_2} = 0.01$. The results are presented in Fig. 5.11 and 5.12. Here, it is interesting to note that decreasing the value of C_1 increases the role of the cable in the dynamic of the complete model. Also, the global stiffness of the model decreases when $\frac{C_1}{C_2}$ decreases then the natural frequency will be smaller. Therefore, the observation range of frequency is different.

For the second case, Fig. 5.11 , the main peak ($\mu = 3.1$) corresponds once again to the first natural frequency (5-83) of a linear hinged-hinged beam with axial tension, but, a second peak can be observed (at $\mu \approx 1.5$) and the frequency of this peak seems to vary according to the magnintude of the excitation.

Concerning the third case, Fig. 5.12, the results are even more interesting. For really small magnitude of the excitation, for instance $\lambda = 1$, the peak appears at $\mu = 2.3$ which corresponds exactly to (5-83). However for higher magnitude of the excitation, this peak seems to move to lower frequencies and also smaller peaks appear. As it is well said in [45] and [52] it seems that large amplitude oscillations may appear for any value of μ which is due to the non-linear nature of the model.
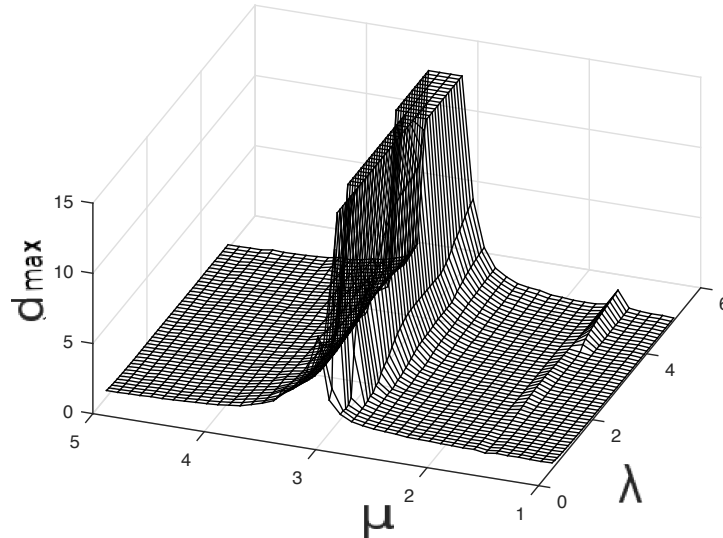
Figure 5.11: Normalized max. disp. d_{max} against μ and λ for $C_1/C_2 = .1$.
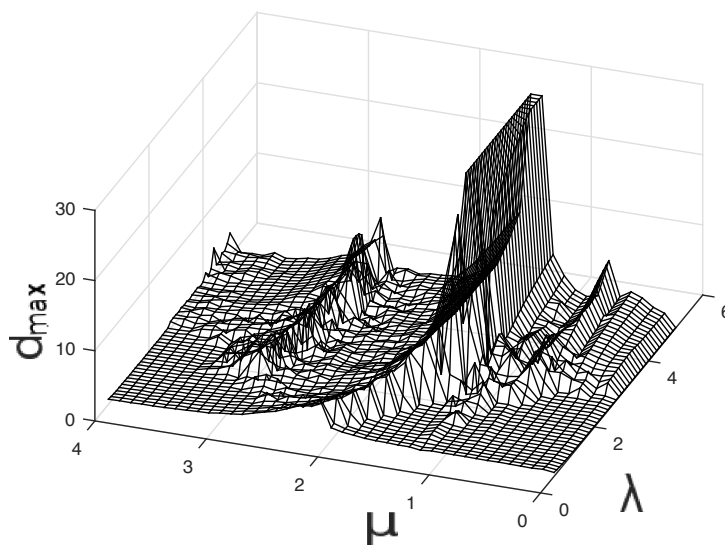
Figure 5.12: Normalized max. disp. d_{max} against μ and λ for $C_1/C_2 = .01$.

Note that for Fig. 5.10 to 5.12 the plots do not show very high values of d_{max}. This was done in order to see better the variation of d_{max} on the whole map. All the results presented here are perfectly equivalent to those presented in [52] calculated with an other method. Thus, from this, one can conclude that the routine developed for this work is perfectly working and can be validate.
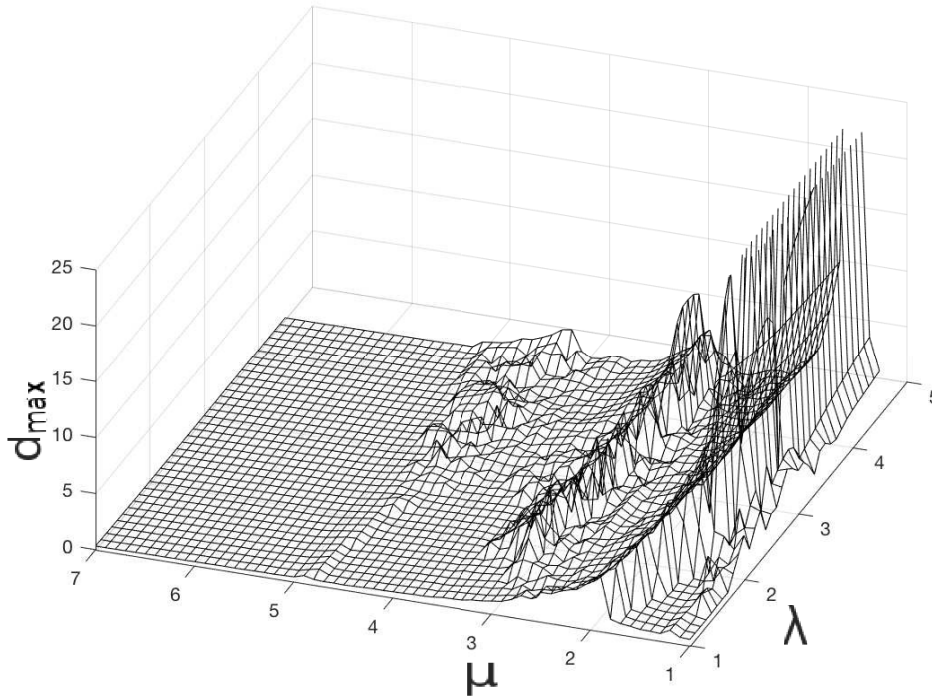
Figure 5.13: Normalized max. disp. d_{max} against μ and λ for $C_1/C_2 = .01$.

Also, the experiment was made for higher frequencies and interesting conclusions can be done. It seems that the second mode of the system is responsible for smaller displacements than the first one. Once again, for low level of excitation, the frequency of the peak in Fig. 5.13 corresponds to the second natural frequency of the linear system ($\mu \approx 4.9$). Finally, it seems that once again the frequency of the peak is changing with respect to the excitation level. From, this map, it is possible to identify regions where any frequency will produce large oscillation, once again this is due to the non-linear nature of the model.

Now that a simulation routine was built and verified, let's try to add

the fluid-structure interactions through simple models as presented in the first chapters. A discussion about the influence of the non-linearity will be done. Also, some comments are made on the influence of the fluid-solid interaction on the dynamic.

6
Simulations of the non-linear model with added stiffness

In this chapter, the routine developed with the software Matlab for a one-dimensional model of suspension bridges will be used to simulate a complete model of suspension bridge under wind load with the interaction between the fluid and the solid domains. The excitation will be modeled to represent the wind. First, one should explain how to model this excitation and, then, the interaction between the fluid and the solid domain will be defined using the first chapters. Finally, simulations will be realized for several combinations of the parameters governing the non-linearity of the model and also governing the fluid-structure interaction. As said before, it seems that for flexible suspension bridges or footbridges, the added stiffness is the effect that is the most likely to occur and it can be an important source of instability. In the next parts, an added stiffness term models the fluid-structure interaction. It will be added to the formulation of first, a hinged-hinged beam, and then to the complete non-linear model described before, for different combinations of parameters.

6.1
Definition of the excitation

There are many ways to model a wind excitation (as stochastic excitations using [18] for instance), and complex models are described in [56] to model wind in a three dimensional space with stochastic representation. Here a simpler representation will be used. First, as the wind is a lateral force (which may not be perfectly horizontal if different values of angle of attack are considered), and the simplified model used in the routine is one-dimensional representing the downwards coordinate, one needs to define a relation between the lateral force (from the horizontal) and the vertical force. This relation is the well known equation to compute the lift force:

$$F_z(x) = \frac{1}{2}\rho_F U^2(x) S C_L, \tag{6-1}$$

where ρ_F is the fluid density, U is the fluid velocity field, S is the area of the cross section, and C_L is the lift coefficient. As said before, the fluid is considered incompressible, then ρ_F is constant in time and space. As the model used in the routine does not represent the torsion and the rotation of the cross section

around the main axis, S is also considered constant in time and space. The lift coefficient depends on the profile of the cross section and on the angle of attack. As the angle of attack is considered fixed in time and space (no rotation of the cross section and no variation of the wind direction), the lift coefficient is constant. Here a qualitative study will be performed then the value of the lift coefficient and the aera of the cross section (in contact with the fluid) will be arbitrary defined. Thus, normalizing the lift force with respect to the lift coefficient, the area of the cross section and the density of the fluid, one obtains the normalized induced vertical force as a function of the fluid velocity field:

$$f_z(x) = U(x)^2. \tag{6-2}$$

The fluid velocity field is modeled as:

$$U(x) = \lambda_U sin(\pi x), \tag{6-3}$$

which is a similar approach to what was done in the previous chapters. Considering a periodic evolution in time, the normalized vertical induced force can be written as:

$$f_z(x, t) = (\lambda_U sin(\pi x))^2 sin(\mu_U t), \tag{6-4}$$

which is slightly different to [52]. It is the force that will enter in the routine simulation.

6.2
Simulation of a hinged-hinged beam with added stiffness

First, in order to observe and to quantify the effect of the added stiffness on the complete model, the simulation is made for an hinged-hinged beam with axial tension. Then the coefficients used in the routine are $C_1 = 0.5$, $C_2 = 0.5$ and $C_3 = C_4 = 0$. As shown in the first chapters of this document, to model the added stiffness as in (3-73), one needs to compute the term $C_A \frac{dF}{d(Dq)}$. Recall that C_A is function of the square of the magnitude of the flow velocity, here λ_U. This term, $C_A \frac{dF}{d(Dq)}$, is homogeneous to a stiffness, as seen before, and may be calculated from aerodynamics and fluid mechanics. Here this term will be approximated as a small percentage of $[k]$, presented in (5-53). This approximation does not represent the real fluid-solid interaction but may allow to observe some phenomena. Indeed, to compute the real fluid-solid interaction effect, fluid mechanics are used in order to find the added stiffness term $C_A \frac{dF}{d(Dq)}$. The deck shape, through its motion, will perturb the fluid flow and thus the flow induced force, as shown in [47]. Thus, several values of the percentage will be investigated and called, $p_\%$ such as:

$$\frac{dF}{d(Dq)} \approx p_\% C_1 \left[k\right].$$ (6-5)

The equation to solve can be written as:

$$[m]\{\ddot{w}\}+[c]\{\dot{w}\}+(C_1 - C_A p_\% C_1)[k]\{w\}+D_1\left[k^{NL}\right]\{w\}+D_2\left\{f^{NL}\right\} = \{f\},$$ (6-6)

where:

$$D_1 = -C_2 \left(1 + C_3 \int_0^1 w dx\right)^+,$$ (6-7)

$$D_2 = C_4 \left(1 + C_3 \int_0^1 w dx\right)^+.$$ (6-8)

Then the influence of the flow velocity and the frequency of the excitation will be studied using the map representation as in the previous chapter. In this part, this will allow to observe the influence of this approximation of the added stiffness with respect to μ_U and λ_U in terms of normalized maximal displacement as:

$$d_{max_2} = \frac{w_{max}}{\lambda_U^2}.$$ (6-9)

The boundary conditions and the initial conditions are exactly the same as in (5-60). The parameters of the simulation are: the time simulation $T = 20s$ and the time increment is $\Delta t = 0.005s$. The space discretization is the same as
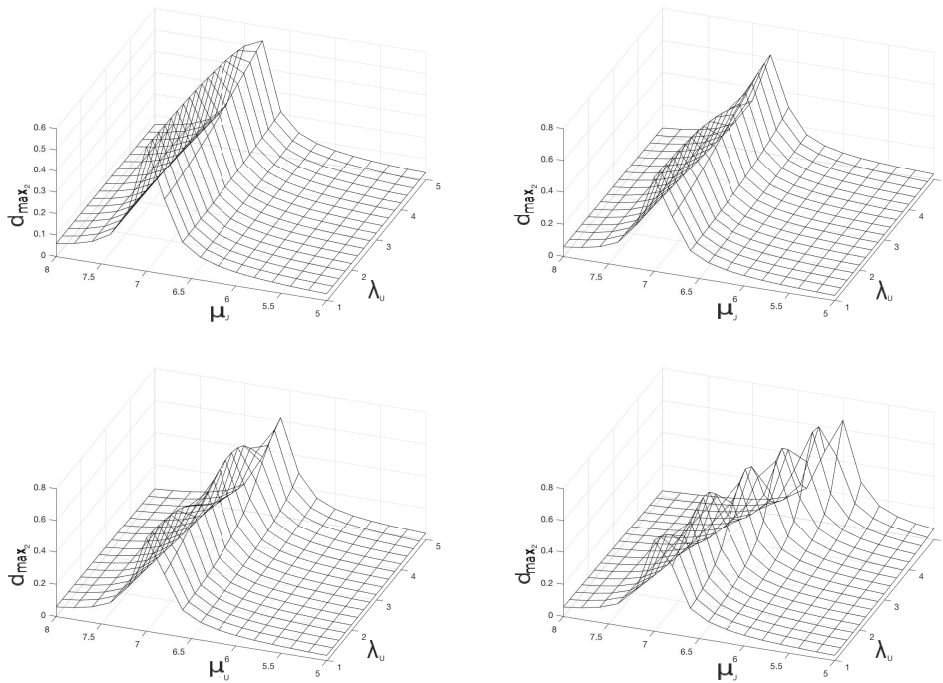
Figure 6.1: Case with $C_1 = 0.5$, $C_2 = 0.5$, $C_3 = 0$, $C_4 = 0$. Left-top: $p_\% = 0,1\%$ / Right-top: $p_\% = 0,2\%$ / Left-bottom: $p_\% = 0,4\%$ / Right-bottom: $p_\% = 1,0\%$

before with 21 nodes. In the previous chapter, large oscillations were considered when d_{max} was bigger than 1 for $T = 50s$. Here, as the simulation time is shorter (for computation time issues) and considering a linear evolution of the large oscillations in time, large oscillations are considered when $d_{max_2} > 0.4$.

Observing Fig. 6.1, representing several simulations for the hinged-hinged beam with axial tension, the expected effect of the added stiffness can be observed. Indeed, as shown in Fig. 3.2.1 and 3.2.1, increasing the flow velocity tends to decrease the global stiffness of the structure, thus the frequency, that generates large oscillations, will decrease. The same type of phenomena can be observed in Fig. 6.1. Varying the effect of the fluid-solid interaction through $p_\%$, it is possible to see how the decrease of the value of the large oscillation frequency occurs with respect to the flow velocity. One can see that for high $p_\%$, the peak frequency decreases relatively quickly when the flow velocity increases. Observe that this variation seems to follow a parabolic shape similar as Fig. 3.2.1. Now let's see if the same conclusions can be made considering the non-linear model.

6.3
Simulation of the non-linear model with added stiffness

In this section the entire non-linear model is used for the simulations. Two combinations of the parameters C_i's are studied and the influence of the flow velocity and the frequency of the excitation can be observed for different values of $p_\%$. Here, it is more difficult to draw the same conclusions as previously done observing Fig. 6.1. Indeed, as the fluid-solid interaction stiffness term is approximated as a percentage of the $[k]$ matrix, its influence is closely related to the ratio $\frac{C_1}{C_2}$. Bigger is this ratio, bigger is the effect of the fluid-solid interaction considering the approximation made here. Observe that this may not be verified for real cases of fluid-structure interaction problems.

Thus, observing Fig. 6.2 and 6.3, it is possible to see a small variation of the peak frequency according to the flow velocity. As said before, this variation is small and not as important as in Fig. 6.1 because the added stiffness is approximated with the beam stiffness term, which is decreasing comparing to the cable stiffness term from Fig. 6.1 to Fig. 6.2 and from Fig. 6.2 to 6.3.

However, modeling this time the excitation using (6-4), one can see that the range of large oscillations seems to be bigger than previously, in Fig. 5.11 and 5.12. This makes things even more difficult to visualize the effect of added stiffness in this region.
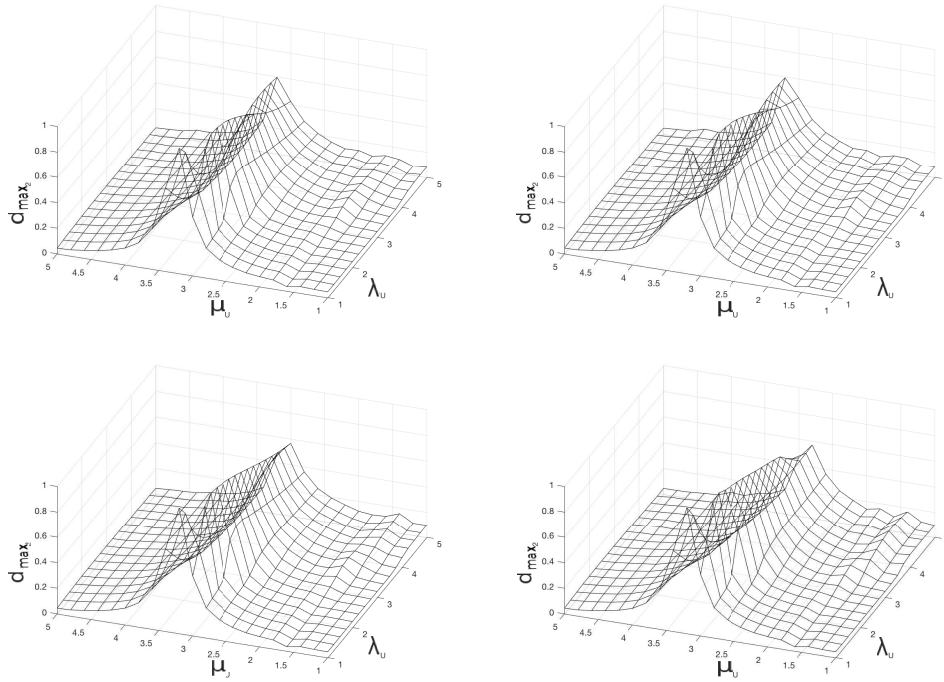
Figure 6.2: Case with $C_1 = 0.05$, $C_2 = 0.5$, $C_3 = 1$, $C_4 = 1$. Left-top: $p_{\%} = 0\%$ / Right-top: $p_{\%} = 0,1\%$ / Left-bottom: $p_{\%} = 0,4\%$ / Right-bottom: $p_{\%} = 1,0\%$
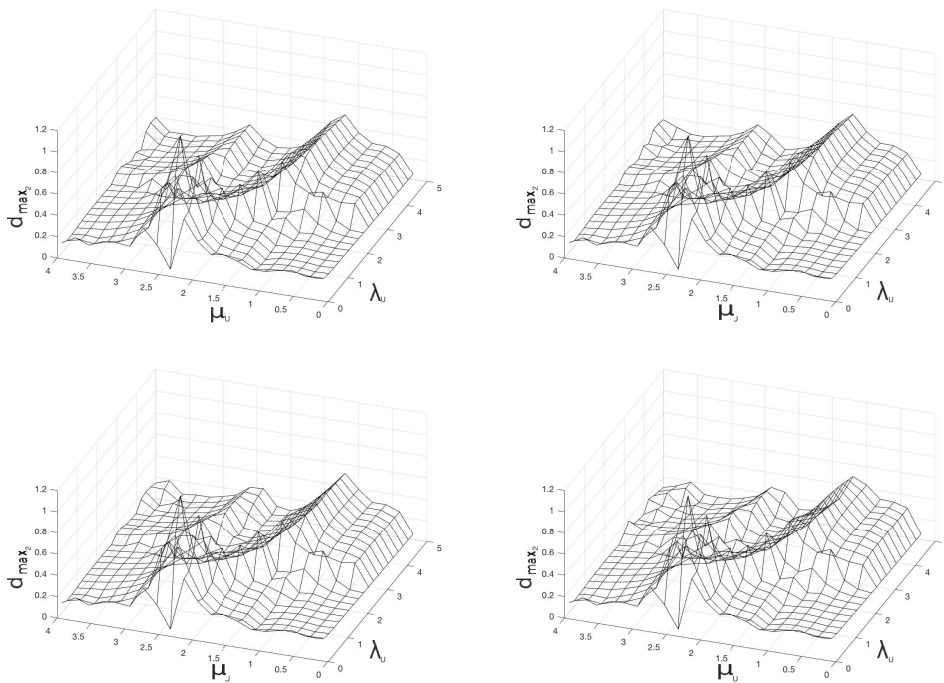

Figure 6.3: Case with $C_1 = 0.005$, $C_2 = 0.5$, $C_3 = 1$, $C_4 = 1$. Left-top: $p_{\%} = 0\%$ / Right-top: $p_{\%} = 0,1\%$ / Left-bottom: $p_{\%} = 0,4\%$ / Right-bottom: $p_{\%} = 1,0\%$

Here, the influence of a fluid-solid interaction effect, the added stiffness, was studied. As no fluid mechanics was used to quantify the added stiffness term, a rude approximation was used. Due to the nature of this approximation, the added stiffness effect was well observed for a high ratio $\frac{C_1}{C_2}$. However for smaller ones, the effect of the added stiffness was more difficult to observe. In future works, one could find an other way to approximate the added stiffness term to better suit the decreasing of the ratio $\frac{C_1}{C_2}$. Although the added stiffness effect is the most likely to occur for flexible suspension bridges or footbridges, one could have observed the effect of other fluid-solid interaction model such as the added damping for instance. This will be the purpose of future articles and experiments in the laboratory.

Now that the fluid-solid interaction was briefly studied using the non-linear model developed for this work, one will focus on the energy partition between modes during the simulations. As the model is non-linear, its dynamic is non-linear too. Thus, the tool used to study the energy partition may be able to work for non-linear systems. This is the reason why the Smooth Decomposition is presented and used to study the energy partition in the next chapter.

7
Energy partition with the Smooth Orthogonal Decomposition

As said before, this part will focus on the energy partition between modes during simulations or experiments. Once again, it appears that the Smooth Decompistion method is a suitable tool to make this kind of energy partition study since it works for linear and non-linear systems. Also, this method was a huge source of publication during the redaction of this work, the Smooth Orthogonal Decomposition (firstly introduce by [14] and also studied by [25]). Here, the base of the discussion is very similar to [26] and an application of the method to the mechanical system presented in the previous chapters is performed. The notation used here for the presentation of the method is equivalent to the one used in [26] in order to be coherent with what was done by the author on this subject. Thus it may be different from the notations used in the rest of this document.

7.1
Introduction

As said in [6], [10] and [50], the Smooth Decomposition (SD) is a multivariate data or statistical analysis method used to identify normal modes, natural frequencies and energy partition of systems. The method requires the knowledge of the system response (spatial data field) to a random excitation. It should be noted that only the output data of the system is needed for the identification. The excitation has to satisfy some properties, normally well met by a white noise, but doesn't need to be measured. This turns the method the ideal way to deal with the identification of systems under ambient excitations (considering Operational Modal Analysis as in [22], [58] or [59]), as wind or waves for instance, which can be hard to compute or to describe. Also, this family of methods can be used for damage detection such as in [23].

The output data of the system response is then projected into a basis and an optimization problem is created. It consists of finding the basis that gives the maximum variance of the displacement-projection and the minimum variance of the velocity-projection. This optimization problem can then be written as an eigenvalue problem with the covariance matrices of the displacement field, and of the corresponding velocity field. Solving this problem the system

is identified and no further considerations and approximations are needed. From the eigenvalues, the "energy" participation of each normal mode in the response during the simulation or the experimental test can be evaluated. Since this information is crucial for non-linear systems identification, the Smooth Decomposition method can be used to identify linear and non-linear systems. This is the reason why this method was used to study the energy partition of the non-linear model here. The method is a great tool for modal analysis as explained in this chapter.

First a description of the method is presented and how to interpret the results of the Smooth Decomposition, for linear systems, explained. Then, an application of Smooth Decomposition on a simulation using the one-dimensional model presented in the previous chapters is performed. Here the influence of the non-linearity on the energy partition will be discussed. Thus several combinations of parameters governing the non-linearity of the system are investigated. Also, the influence of the excitation energy on the results is discussed.

7.2
Description of the Smooth Decomposition

As the Karhunen-Loève Decomposition [7] or the Proper Orthogonal Decomposition (in [5], [16], [42] and [46]), the Smooth Decomposition, presented namely in [8], is based on the projection of the data field such as the generalized displacement field has the maximum variance in order to be sure that all the modes under interest are excited. Indeed, the bigger is the variance of the displacement field, the higher is the probability of a mode to be excited. The Smooth Decomposition method is a bit different because one also considers the derivative of this generalized displacement field, the velocity field. The objective is to find the basis that gives the maximum variance for the generalized displacement field and the minimum variance for the velocity field (in order to keep the motion as smooth as possible in time).

7.2.1
Decomposition principle

First, let's describe the data field used in this method. Recall that the notation in this chapter is slightly different than the one used before, in order to respect what was used in [26]. Let's consider the sampled scalar field $\mathbf{X}(t)$ formed of random values (in the matrix form) as a function of time t ($t \in \mathbb{R}$). This field is such as $\mathbf{X}(t) \in \mathbb{R}^{n \times m}$ where n represents the different instants and m represents the spacial points where the information is measured. The

displacement field is considered as a stationary second-order process with zero-mean value that admits a time derivative which is also a stationary zero-mean value process.

The central point of this method is to find a linear projections such as:

$$\mathbf{Y_X}(t) = \text{proj}_\phi \mathbf{X}(t) = \mathbf{X}(t)\phi, \quad (7\text{-}1) \qquad \mathbf{Y_{\dot{X}}}(t) = \text{proj}_\phi \dot{\mathbf{X}}(t) = \dot{\mathbf{X}}(t)\phi, \quad (7\text{-}2)$$

where $\mathbf{Y_X}(t) \in \mathbb{R}^{n \times m}$, $\mathbf{Y_{\dot{X}}}(t) \in \mathbb{R}^{n \times m}$ and $\phi \in \mathbb{R}^{m \times m}$ (representing a projection basis). Now, the objective of this method is to find this projection basis such as it keeps the maximum variance for the projection of the original field $\mathbf{X}(t)$ (the generalized displacement field) and the smallest projection of the velocity field in order to keep the variation in time as smooth as possible. The objective is to find $\max_\phi ||\mathbf{Y_X}(t)||^2$ and $\min_\phi ||\mathbf{Y_{\dot{X}}}(t)||^2$ which is exactly as maximizing $f(\phi)$ with:

$$f(\phi) = \frac{||\mathbf{Y_X}(t)||^2}{||\mathbf{Y_{\dot{X}}}(t)||^2} = \frac{||\mathbf{X}(t)\phi||^2}{||\dot{\mathbf{X}}(t)\phi||^2}. \tag{7-3}$$

Now let's simplify this ratio using the auto-correlation matrices $\mathbf{R_{XX}}$ and $\mathbf{R_{\dot{X}\dot{X}}}$ (cf. [18] or [54] for more details on correlation matrices), respectively, for the displacement field ($\mathbf{X}(t) \in \mathbb{R}^{n \times m}$) and the velocity field ($\dot{\mathbf{X}}(t) \in \mathbb{R}^{n \times m}$). Indeed, it is possible to write:

$$||\mathbf{X}\phi||^2 = (\mathbf{X}\phi)^T \mathbf{X}\phi = \phi^T \left(\mathbf{X}^T \mathbf{X}\right) \phi = n\phi^T \mathbf{R_{XX}}\phi, \tag{7-4}$$

$$||\dot{\mathbf{X}}\phi||^2 = \left(\dot{\mathbf{X}}\phi\right)^T \dot{\mathbf{X}}\phi = \phi^T \left(\dot{\mathbf{X}}^T \dot{\mathbf{X}}\right) \phi = n\phi^T \mathbf{R_{\dot{X}\dot{X}}}\phi. \tag{7-5}$$

Finally one gets this new expression for $f(\phi)$ (keeping in mind that n is the number of time samples, which is rather big, it can be simplified in the ratio even if the derivative method used does not conserve the same number of samples as in the original field). The objective is to find:

$$\max_\phi \left\{ f(\phi) = \frac{\phi^T \mathbf{R_{XX}}\phi}{\phi^T \mathbf{R_{\dot{X}\dot{X}}}\phi} \right\}. \tag{7-6}$$

In order to find the maximum of $f(\phi)$ one can express its derivative with respect to ϕ, called $\nabla f(\phi)$, such as:

$$\nabla f(\phi) = \frac{\partial f(\phi)}{\partial \phi} = \frac{2\left(\phi^T \mathbf{R_{\dot{X}\dot{X}}}\phi\right)\mathbf{R_{XX}}\phi - 2\left(\phi^T \mathbf{R_{XX}}\phi\right)\mathbf{R_{\dot{X}\dot{X}}}\phi}{\left(\phi^T \mathbf{R_{\dot{X}\dot{X}}}\phi\right)^2}, \tag{7-7}$$

and then find when $\nabla f(\phi)$ vanishes. One can also find this maximum using Lagrange multiples. In both cases one will find the following eigenvalue problem as the expression of the two initial propositions. The problem is equivalent to solve:

$$\mathbf{R_{XX}}\boldsymbol{\phi}_k = \lambda_k \mathbf{R_{\dot{X}\dot{X}}}\boldsymbol{\phi}_k, \qquad\qquad k = 1, ..., m. \qquad\qquad (7\text{-}8)$$

Solving this eigenvalue problem gives the eigenvalues, the λ_k's, and the eigenvectors, the $\boldsymbol{\phi}_k$'s, such as the λ_k's are in ascending order ($\lambda_1 > \lambda_2 > ... > \lambda_m$). In the literature [13], there is a relation between the auto-correlation of the velocity and the correlation of the acceleration and the displacement such as $\mathbf{R_{\dot{X}\dot{X}}} = -\mathbf{R_{\ddot{X}X}}$. From this relation, the following eigenvalue problem is written (7-9). This leads to the same results.

$$\mathbf{R_{XX}}\boldsymbol{\phi}_k = -\lambda_k \mathbf{R_{\ddot{X}X}}\boldsymbol{\phi}_k, \qquad\qquad k = 1, ..., m. \qquad\qquad (7\text{-}9)$$

Finally, using $\boldsymbol{\phi}_k$ it is possible to write the $\boldsymbol{\psi}_k$ such as:

$$\boldsymbol{\psi}_k = \mathbf{R_{\dot{X}\dot{X}}}\boldsymbol{\phi}_k. \qquad\qquad (7\text{-}10)$$

At this step several parameters from a displacement field of a mechanical system can be found: the λ_k (the Smooth Value - SV), the $\boldsymbol{\phi}_k$ (Smooth Mode - SM) and the $\boldsymbol{\psi}_k$ (Dual Smooth Mode - DSM). Depending on the characteristics of the system, one can interpret these parameters differently, as seen in [6], [8], [10], [25], [26] and also in [50].

7.2.2
Expansion Principle

From this decomposition two different bases are available, the smooth basis called $\boldsymbol{\Phi}$, formed with the $\boldsymbol{\phi}_k$'s, and the smooth dual basis, called $\boldsymbol{\Psi}$, formed with the $\boldsymbol{\psi}_k$'s (for $k = 1, ..., m$ with m as the number of measuring points). Now it is possible to use these two bases to find the smooth expansion of $\mathbf{X}(t)$ and its dual smooth expansion.

7.2.2.1
Expansion in the smooth basis

Considering the expansion of $\mathbf{X}(t)$ in the $\boldsymbol{\Phi}$-basis it is possible to write $\mathbf{X}(t) = \sum_{k=1}^{m} \xi_k(t)\boldsymbol{\phi}_k$, which can be simplified using the projection $\boldsymbol{\Pi}_1 = \boldsymbol{\Phi}\boldsymbol{\Psi}^T$ then one gets $\boldsymbol{\Pi}_1\mathbf{X}(t) = \sum_{k=1}^{m} \boldsymbol{\psi}_k^T\mathbf{X}(t)\boldsymbol{\phi}_k$. From these two expressions one can find the Dual Smooth Components (DSC) $\xi_k(t)$:

$$\xi_k(t) = \boldsymbol{\psi}_k^T\mathbf{X}(t). \qquad\qquad (7\text{-}11)$$

7.2.2.2
Expansion in the dual-smooth basis

Let's consider the $\boldsymbol{\Psi}$-basis to express $\mathbf{X}(t)$. The dual smooth expansion of this field into this basis can be written as $\mathbf{X}(t) = \sum_{k=1}^{m} \chi_k(t)\boldsymbol{\psi}_k$. Using the

oblique projection $\mathbf{\Pi}_2 = \mathbf{\Psi}\mathbf{\Phi}^T$, one gets $\mathbf{\Pi}_2\mathbf{X}(t) = \sum_{k=1}^{m} \boldsymbol{\phi}_k^T\mathbf{X}(t)\boldsymbol{\psi}_k$. Then from these equations the Smooth Components (SC) $\chi_k(t)$ is:

$$\chi_k(t) = \boldsymbol{\phi}_k^T\mathbf{X}(t). \tag{7-12}$$

One can notice an interesting property for the Smooth Components. Let's consider the square of it and develop in the following form:

$$\chi_k^2(t) = \left(\boldsymbol{\phi}_k^T\mathbf{X}(t)\right)^2 = \boldsymbol{\phi}_k^T\mathbf{X}(t)\left(\boldsymbol{\phi}_k^T\mathbf{X}(t)\right)^T = \boldsymbol{\phi}_k^T\mathbf{X}(t)\mathbf{X}(t)^T\boldsymbol{\phi}_k = \boldsymbol{\phi}_k^T\mathbf{R_{XX}}\boldsymbol{\phi}_k. \tag{7-13}$$

Now considering the original eigenvalue problem formulated in Eq.(7-8) it is possible to write:

$$\boldsymbol{\phi}_k^T\mathbf{R_{XX}}\boldsymbol{\phi}_k = \lambda_k\mathbf{R_{\dot{X}\dot{X}}}, \tag{7-14}$$

then considering the mean value (recall that the mean value of a random variable x is noted as $\mathbb{E}[x]$) of each part one gets:

$$\mathbb{E}\left[\boldsymbol{\phi}_k^T\mathbf{R_{XX}}\boldsymbol{\phi}_k\right] = \mathbb{E}\left[\lambda_k\mathbf{R_{\dot{X}\dot{X}}}\right]. \tag{7-15}$$

Considering (7-13) and the properties of the covariance matrices leads to:

$$\mathbb{E}\left[\chi_k^2(t)\right] = \mathbb{E}\left[\lambda_k\mathbf{R_{\dot{X}\dot{X}}}\right] \Rightarrow \mathbb{E}\left[\chi_k^2(t)\right] = \lambda_k. \tag{7-16}$$

7.2.3
Energetic point of view

An interesting thing with SD is the energetic study that can be made with this method. Let's call the "energy" of the field $\mathbf{X}(t)$ the expression $\mathbb{E}\left[||\mathbf{X}(t)||^2\right]$. From the dual smooth expansion one gets:

$$\mathbf{X}(t) = \sum_{k=1}^{m} \chi_k(t)\boldsymbol{\psi}_k \Rightarrow ||\mathbf{X}(t)||^2 = \sum_{k=1}^{m} ||\chi_k(t)\boldsymbol{\psi}_k||^2. \tag{7-17}$$

The expression of the "energy" can then be simplified using the previous formulation as:

$$\mathbb{E}\left[||\mathbf{X}(t)||^2\right] = \mathbb{E}\left[\sum_{k=1}^{m} ||\chi_k(t)\boldsymbol{\psi}_k||^2\right] = \sum_{k=1}^{m} \left[\mathbb{E}\left[\chi_k^2(t)\right]\mathbb{E}\left[||\boldsymbol{\psi}_k||^2\right]\right]. \tag{7-18}$$

Simplifying using (7-16) it is possible to find the final expression for the "energy" of $\mathbf{X}(t)$ as:

$$\mathbb{E}\left[||\mathbf{X}(t)||^2\right] = \sum_{k=1}^{m} \lambda_k ||\boldsymbol{\psi}_k||^2. \tag{7-19}$$

Note that, from this formula it is quite easy to find the energy captured in each mode (the identified mode with the SD which, sometimes, does not correspond to a physical mode) during the simulation since the expression:

$$E_i = \frac{\lambda_i \, ||\boldsymbol{\psi}_i||^2}{\sum\limits_{k=1}^{m} \lambda_k \, ||\boldsymbol{\psi}_k||^2}, \tag{7-20}$$

represents the fraction of energy captured by the mode i during the simulation. This value can help to verify if a mode has been well excited during a simulation (allows to judge the reliability of the results). This parameter is crucial for identification of non-linear systems since knowing the energy is essential.

7.3
Smooth Decomposition for modal analysis

From the formulation of the initial projection (7-1), it is possible to generalize this expression for m modes (with the $\boldsymbol{\Phi}$-matrix, such as $\boldsymbol{\Phi} \in \mathbb{R}^{m \times m}$) and get the following equation in the matrix form with $\mathbf{Q}$ as the SC-matrix ($\mathbf{Q} \in \mathbb{R}^{n \times m}$):

$$\mathbf{X} = \mathbf{Q}\boldsymbol{\Phi}^T. \tag{7-21}$$

As shown in [26], the interpretation of the results from the Smooth Decomposition is quite easy for linear systems a more complicated for non-linear ones. First, let's consider free linear undamped systems written in the matrix form as:

$$\mathbf{M}\ddot{\mathbf{X}} + \mathbf{K}\mathbf{X} = 0, \qquad k = 1, ..., m, \tag{7-22}$$

where $\mathbf{M}$ is the mass matrix, $\mathbf{K}$ is the stiffness, $\mathbf{X}$ and $\ddot{\mathbf{X}}$ represent respectively the displacement and the acceleration fields. From (7-22), the acceleration of the system (if the mass matrix $\mathbf{M}$ is not singular) can be written as:

$$\ddot{\mathbf{X}} = -\mathbf{X}\mathbf{K}^T\mathbf{M}^{-T}. \tag{7-23}$$

To apply the Smooth Decomposition to this kind of mechanical system means to maximize the function $f(\boldsymbol{\phi})$. Considering the original form of $f(\boldsymbol{\phi})$ defined in (7-3) and using the same property of correlation matrices used to write (7-9), one gets:

$$\max_{\boldsymbol{\phi}} \{f(\boldsymbol{\phi})\} = \max_{\boldsymbol{\phi}} \left\{ \frac{\boldsymbol{\phi}^T \mathbf{X}^T \mathbf{X} \boldsymbol{\phi}}{\boldsymbol{\phi}^T \mathbf{X}^T \mathbf{X} \mathbf{K}^T \mathbf{M}^{-T} \boldsymbol{\phi}} \right\}. \tag{7-24}$$

As shown before, solving this maximization problem is equivalent to solve the following eigenvalue problem (if the product $\mathbf{X}^T\mathbf{X}$ is invertible):

$$\mathbf{K}\boldsymbol{\Phi}^{-T} = \mathbf{M}\boldsymbol{\Phi}^{-T}\boldsymbol{\Lambda}. \tag{7-25}$$

Now, let's consider the initial mechanical system defined with (7-22). The associated eigenvalue problem is written with $\boldsymbol{\Omega}$ which is a diagonal matrix formed with the squares of the natural frequencies of the mechanical system (the ω_k^2's) associated to each column of $\boldsymbol{\Psi}$:

$$\mathbf{K\Psi} = \mathbf{M\Psi\Omega}. \tag{7-26}$$

Then the two expressions represent two equivalent eigenvalue problems (7-25) and (7-26). As they represent they same mechanical system they have to be equivalent, this leads to equivalences between the modal quantities, in terms of natural frequencies and mode shapes:

$$\mathbf{\Psi} = \mathbf{\Phi}^{-T}, \qquad \mathbf{\Omega} = \mathbf{\Lambda}. \tag{7-27}$$

Let's consider now general mechanical systems, the dynamic equation can be written as:

$$\mathbf{M\ddot{X}} + \mathbf{C\dot{X}} + \mathbf{KX} + \mathbf{AX} = \mathbf{F}, \tag{7-28}$$

where $\mathbf{M}$, $\mathbf{K}$ e $\mathbf{C}$ are the mass, the stiffness and the damping matrices of the system. $\mathbf{F}$ is the forcing vector which, in this specific case is not monitored (unknown excitation, characteristic of the output only methods). The term called $\mathbf{A}$ represents the nonlinearity of the mechanical system.

As shown in the literature [10], the interpretation for those cases is not as simple as for the linear ones. Indeed, one cannot find the simple equivalence shown with (7-27). These considerations come from the statistical linearization method thus they give results for a linear system. To apply the equivalences of (7-27) to non-linear systems gives the modal parameters for the linear equivalent system but not for the non-linear one.

If one considers a damped system with the $\mathbf{C}$-matrix as a linear combination of $\mathbf{M}$ and $\mathbf{K}$ (i.e. $\mathbf{C} = \alpha\mathbf{C} + \beta\mathbf{K}$) one can reach a similar interpretation as it was done for undamped systems. From this method it is possible to access the normal modes of the systems. For example, considering the $\mathbf{C}$-matrix as a combination of the $\mathbf{M}$-matrix only, one observes that for an α rather small ($0 \leq \alpha \leq 1$) the results still acceptable. This shows that the theory works perfectly for undamped systems but for damped ones the interpretation should be made carefully. Similar conclusions have been found [26].

Indeed, for damped systems, the modes have an imaginary part which cannot be expressed with normal modes and thus which cannot be found with SD (as the method was developed for undamped systems). It has be shown namely in article presented in Appendix D that this method works perfectly for continuous systems but one has to be careful with relation to the number of excited modes and the number of modes that are observed, but here this is not the focus of the discussion.

7.4

Application of Smooth Decomposition on a non-linear model

In this section, the Smooth Decomposition will be used to identify modal parameters of the non-linear one-dimensional model of a suspension bridge presented in the previous chapters. The equation (5-54) with (5-55) and (5-56) will be solved with the routine developed with Matlab. The boundary conditions are (5-69). Concerning the parameters of the Newmark-beta method, they are the same as before, $\gamma = \frac{1}{2}$ and $\beta = \frac{1}{4}$. With the acquisition frequency $f_s = 1500 Hz$, the maximal frequency that can be observed (according to (5-52)) is around $150 Hz$. As said before, the excitation has to satisfy some properties. Here the excitation will be a matrix defined with:

$$f(x, t) = s_0 \mathcal{N}(x, t), \qquad (7\text{-}29)$$

where s_0 is the excitation level or energy level and $\mathcal{N}$ is a Gaussian white-noise process with intensity one and zero-mean value. Here, the influence of the excitation level s_0 will be investigated for several combinations of the parameters C_i's. Recall that varying the values of these parameters one can control the non-linearity of the system. Observe that for time computing issues, the simulation time is reduced to $T = 10s$. Then, the number of samples is also reduced and may not be sufficient for a good approximation of the correlation matrices. However, the experiments was performed several times and similar results were observed. For this experiment, the excitation level s_0 is defined as a vector of equally spaced points between 0.0001 and 0.01. It has been verified that this level of excitation produces a acceptable displacement of the structure in this time interval (the order of magnitude of the maximum displacement for the maximal excitation is $\frac{L}{100}$, which is reasonable). The observation was reduced to the ten first modes found with the Smooth Decomposition (in order to respect (5-52) for all the combination cases).

Before starting the analysis, let's mention that the line connecting the markers always follows the mode with the major contribution for each excitation level (left hand side plot) and its associated frequency on the right hand side plot. Fig. 7.1, shows the results of the Smooth Decomposition in terms of modal energy of each identified mode and identified frequency. It can be observed that the first identified mode is dominant in the simulation (recall that longer simulations would be better) and that it is always the one with the major contribution. The energy is distributed only among the first mode.

Increasing the non linearity, in Fig. 7.2, one can see that now, that the second and the third modes are dominating. On the right hand side plot, it is possible to see the alternate domination of them. Also, one can see that the identification of higher modes, for instance the eighth and tenth, may vary with
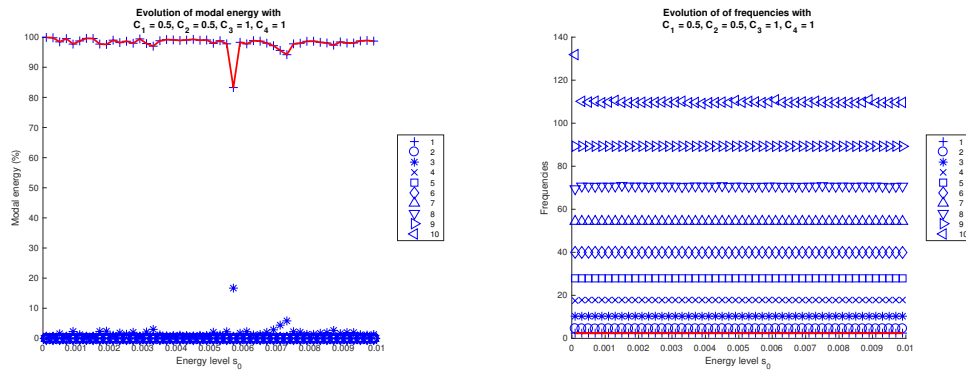
Figure 7.1: Case with $C_1 = 0.5$, $C_2 = 0.5$, $C_3 = 1$, $C_4 = 1$. Left: Evolution of the modal energy (%) of each identified mode with respect to s_0 / Right: Evolution of the identified frequencies with respect to s_0.

the excitation level. The energy is distributed among the three first modes. The same observations can be done concerning Fig. 7.3. Here it seems that the six first modes are competing the domination. As before, higher frequencies may vary with the excitation level.
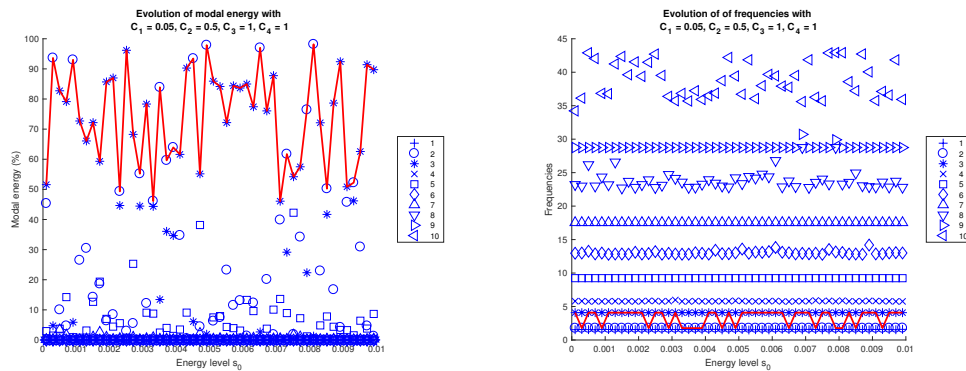
Figure 7.2: Case with $C_1 = 0.05$, $C_2 = 0.5$, $C_3 = 1$, $C_4 = 1$. Left: Evolution of the modal energy (%) of each identified mode with respect to s_0 / Right: Evolution of the identified frequencies with respect to s_0.

For Fig. 7.4, the conclusions are the same here, almost all the modes are dominant at least for one excitation level but the energy seems to be shared mostly between the modes 5 to 8.

These results are interesting and still have to be studied in future work. But it was possible to see, thanks to the Smooth Decomposition, that increasing the non-linearity of the system, higher modes may contribute to the response.

Keeping in mind the Fig. 5.12, it was expected a variation of the first frequency when increasing the excitation level. Zooming on the region of interest, one see variations of the first identified frequency. However, due to the number of samples used in the experiment, one cannot conclude on these
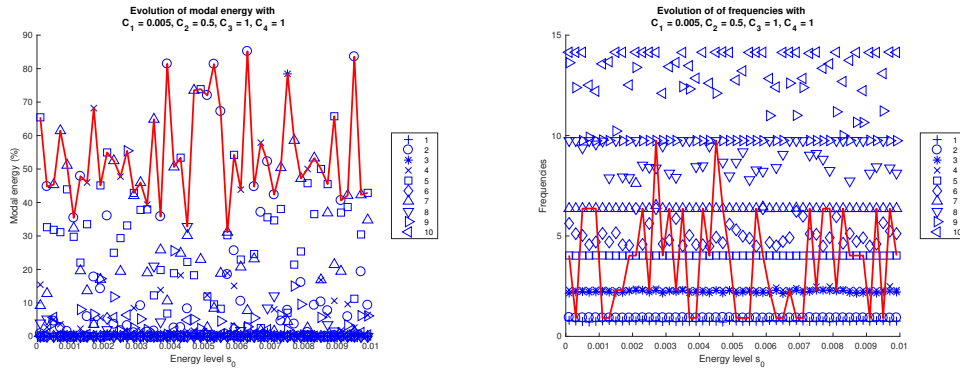
Figure 7.3: Case with $C_1 = 0.005$, $C_2 = 0.5$, $C_3 = 1$, $C_4 = 1$. Left: Evolution of the modal energy (%) of each identified mode with respect to s_0 / Right: Evolution of the identified frequencies with respect to s_0.
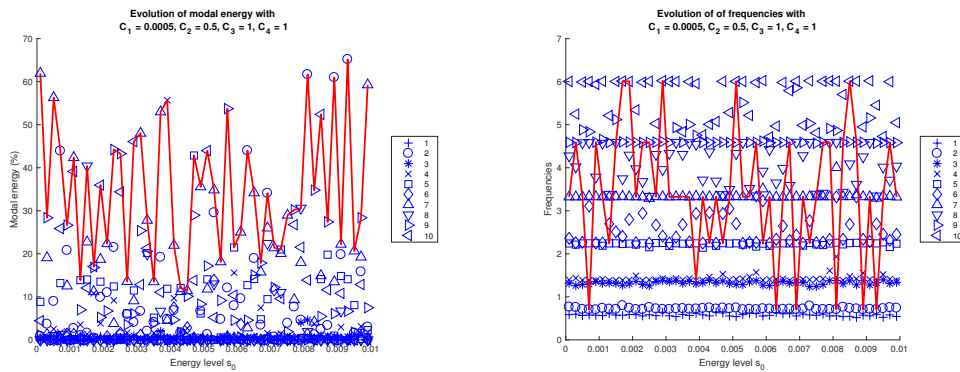

Figure 7.4: Case with $C_1 = 0.0005$, $C_2 = 0.5$, $C_3 = 1$, $C_4 = 1$. Left: Evolution of the modal energy (%) of each identified mode with respect to s_0 / Right: Evolution of the identified frequencies with respect to s_0.

variations. More work has to be done to understand better this point. However, these results can be interesting if one considers to use Smooth Decomposition for reduced order model [9]. Indeed, here, it has been shown that depending on the non-linearity and on the excitation level, the modes contributing the to response of the system may differ. Then, one may need to use a sufficient number of modes for the reduced order model.

8
Conclusions

As said in the introduction, fluid-solid interaction problems are very common, specifically in mechanical or civil engineering. It is important for the engineers to understand how such interactions occur and how they can affect the structure in order to avoid structural damages or failure.

In this work, the fluid-solid interaction problems were studied and, first the fundamentals of this type of problems were presented. In the first chapters, basic concepts of fluid-structure interactions were shown. One of them, the dimensional analysis, was performed for the fluid and the solid domains. Then, the equations governing the fluid-solid interaction problems were presented and a dimensionless formulation of them was written as a function of dimensionless parameters.

Next, these parameters were used as a comparison base to classify the fluid-solid interaction problems. The third chapter presented some approximations that can be made depending on several dimensionless numbers. Thus, some phenomena such as the added mass effect, the added stiffness or added damping and the memory effect were presented. These considerations permit to simplify the fluid-solid interaction problems and simpler formulations can be used. Also, in this chapter, some consequences of fluid-solid interactions were presented in terms of stability or instability. Then, limit cases were studied and some important flow induced instability were shown.

In the second part of this document, a structure that can suffer fluid-solid interactions was considered: a suspension bridge. The fourth chapter has presented the formulation of a non-linear one-dimensional model. A formulation that allows to write the dynamic equation of this system as a function of constant parameters was also presented. Later, these constants were used to study the influence of the non-linearity on the dynamic of the system.

Using this formulation, a routine (using the finite element discretization) was developed with the software Matlab, to solve the dynamic equation of the one-dimensional model presented before. After presenting some basic concepts of the finite element discretization, the routine was checked through several comparisons.

Then, this routine was used and a simple model of fluid-solid interactions, presented in the two first chapters, was added. A rude approximation of the added stiffness term was implemented to the simulation routine. Due to the nature of this approximation, the effect of the added stiffness term was quite hard to observe when an increasing non-linearity was investigated. However, for the linear case, a qualitative observation of the added stiffness effect was possible. Recall that the approximation made to compute the added stiffness does not represent at all the real formulation of the added stiffness term. For future works, more relevant computations of the added stiffness term should be presented in order to better observe the effect of the fluid-solid interaction.

The last part of this work presented a topic that was, as said before, an important source of publications during these years, the Smooth Decomposition. Using the routine developed in the previous chapters, a modal analysis was performed using the Smooth Decomposition. Some conclusions were made regarding the influence of the excitation level for the identification of modal parameters of this non-linear system. However, as said in this specific chapter, more work has to be done to draw better conclusions on the influence of the level excitation on the modal parameters identification. This is the subject of future works and will lead to some new publications.

For this work, many different aspects of engineering were used, such as fluid mechanics, solid mechanics, dynamic and modal analysis. The variety of the bibliography used for this work is attractive and reinforces the interest of the work. This document covers several types of discussions, from very theoretical ones to some direct numerical applications.

Through this entire work, it was possible to understand better the fluid-solid interactions and important elements were presented. For the future, this work will form a solid knowledge to explore more complex cases. Also, some conclusions were made on a specific non-linear structure: a suspension bridge. These conclusions will be used for future works and experimental studies at the laboratory where a suspension bridge test-rig was built. Indeed, now that some elementary concepts of suspensions bridges were shown, the understanding of the dynamic of the test-rig will be easier.

Bibliography

[1]   ABRAMS, D. M.. **Two coupled oscillator models: the millennium bridge and the chimera state**. 2006.

[2]   ALAMPALLI, S.; MOREAU, W. J.. **Inspection, Evaluation and Maintenance of Suspension Bridges**. CRC Press, 2015.

[3]   BARENBLATT, G. I.. **Scaling**, volumen 34. Cambridge University Press, 2003.

[4]   BATHE, K.-J.. **Finite element procedures**. Klaus-Jurgen Bathe, 2006.

[5]   BELLIZZI, S.; SAMPAIO, R.. **Poms analysis of randomly vibrating systems obtained from karhunen–loève expansion**. Journal of Sound and Vibration, 297(3):774–793, 2006.

[6]   BELLIZZI, S.; SAMPAIO, R.. **Smooth karhunen–loève decomposition to analyze randomly vibrating systems**. Journal of Sound and Vibration, 325(3):491–498, 2009.

[7]   BELLIZZI, S.; SAMPAIO, R.. **Karhunen–loève modes obtained from displacement and velocity fields: assessments and comparisons**. Mechanical Systems and Signal Processing, 23(4):1218–1222, 2009.

[8]   BELLIZZI, S.; SAMPAIO, R.. **Smooth decomposition of random fields**. Journal of Sound and Vibration, 331(15):3509–3520, 2012.

[9]   BELLIZZI, S.; SAMPAIO, R.. **Reduced models based on smooth decomposition for random mechanical systems**. International Review of Mechanical Engineering, 6 (1), p. 74–85, 2012.

[10] BELLIZZI, S.; SAMPAIO, R.. **The smooth decomposition as a non-linear modal analysis tool**. Mechanical Systems and Signal Processing, 64:245–256, 2015.

[11] BOKAIAN, A.. **Natural frequencies of beams under tensile axial loads**. Journal of sound and vibration, 142(3):481–498, 1990.

[12] BOYERE, E.; BOYERE, E.. **Algorithmes d'intégration temporelle de l'opérateur dyna_tran_modal date: 28/02/03**. Computer Methods in Applied Mechanics and Engineering, 23:259–279, 1980.

[13] BRINCKER, R.; VENTURA, C.. **Introduction to operational modal analysis**. John Wiley & Sons, 2015.

[14] CHELIDZE, D.; ZHOU, W.. **Smooth orthogonal decomposition-based vibration mode identification**. Journal of Sound and Vibration, 292(3):461–473, 2006.

[15] CHEN, Z.; XU, Y.; LI, Q. ; WU, D.. **Dynamic stress analysis of long suspension bridges under wind, railway, and highway loadings**. Journal of Bridge Engineering, 16(3):383–391, 2011.

[16] CHINESTA, F.; KEUNINGS, R. ; LEYGUE, A.. **The proper generalized decomposition for advanced numerical simulations: a primer**. Springer Science & Business Media, 2013.

[17] CONCA, C.; OSSES, A. ; PLANCHARD, J.. **Added mass and damping in fluid-structure interaction**. Computer methods in applied mechanics and engineering, 146(3-4):387–405, 1997.

[18] DE CURSI, E. S.; SAMPAIO, R.. **Uncertainty quantification and stochastic modeling with matlab**. Elsevier, 2015.

[19] DE LANGRE, E.. **Fluides et solides**. Editions Ecole Polytechnique, 2001.

[20] DE LANGRE, E.. **Frequency lock-in is caused by coupled-mode flutter**. Journal of Fluids and Structures, 22(6):783–791, 2006.

[21] DE LANGRE, E.; CHAIGNE, A.. **Dynamique et vibrations**. Editions Ecole Polytechnique, 2008.

[22] DE MAGALHÃES, F. M. R. L.. **Operational modal analysis for testing and monitoring of bridges and special structures**. PhD thesis, Universidade do Porto (Portugal), 2010.

[23] EFTEKHAR AZAM, S.. **Online damage detection in structural systems: applications of proper orthogonal decomposition, and kalman and particle filters**. 2014.

[24] FACCHINETTI, M. L.; DE LANGRE, E. ; BIOLLEY, F.. **Coupling of structure and wake oscillators in vortex-induced vibrations**. Journal of Fluids and structures, 19(2):123–140, 2004.

[25] FAROOQ, U.; FEENY, B.. **Smooth orthogonal decomposition for modal analysis of randomly excited systems**. Journal of Sound and Vibration, 316(1):137–146, 2008.

[26] FOINY, D.; WAGNER, G. B.; SAMPAIO, R. ; LIMA, R.. **Dynamical systems identification with smooth decomposition**. Proceedings of DINAME, 2017.

[27] FOX, R. W.; MCDONALD, A. T. ; PRITCHARD, P. J.. **Introduction to fluid mechanics**, volumen 5. John Wiley & Sons New York, 1998.

[28] FUJINO, Y.; KIMURA, K. ; TANAKA, H.. **Wind Resistant Design of Bridges in Japan: Developments and Practices**. Springer Science & Business Media, 2012.

[29] GATTI, P. L.. **Applied Structural and Mechanical Vibrations: Theory and Methods**. CRC Press, 2014.

[30] GAVIN, H.. **Numerical integration for structural dynamics**. Department of Civil and Environmental Engineering, Duke University, Durham, NC, 2001.

[31] GAZZOLA, F.; JLELI, M. ; SAMET, B.. **On the melan equation for suspension bridges**. Journal of Fixed Point Theory and Applications, 16(1-2):159–188, 2014.

[32] GAZZOLA, F.. **Mathematical models for suspension bridges**. MS&A Springer, 2015.

[33] GAZZOLA, F.; WANG, Y. ; PAVANI, R.. **Variational formulation of the melan equation**. Mathematical Methods in the Applied Sciences, 2016.

[34] GENTA, G.. **Vibration dynamics and control**. Springer, 2009.

[35] GIBBINGS, J. C.. **Dimensional analysis**. Springer Science & Business Media, 2011.

[36] GIMSING, N. J.; GEORGAKIS, C. T.. **Cable supported bridges: concept and design**. John Wiley & Sons, 2011.

[37] HARBI, H.; AHMED, N. U.. **Mathematical analysis of dynamic models of suspension bridges**. SIAM Journal on Applied Mathematics, 58(3):853–874, 1998.

[38] HÉMON, P.. **Vibrations des structures couplées avec le vent**. Editions Ecole Polytechnique, 2006.

[39] HUANG, M.-H.; THAMBIRATNAM, D. P. ; PERERA, N. J.. **Resonant vibration of shallow suspension footbridges**. Proceedings of ICE, Bridge Engineering, 158(BE4):201–209, 2005.

[40] HUGHES, T. J.. **The finite element method: linear static and dynamic finite element analysis**. Courier Corporation, 2012.

[41] INMAN, D. J.. **Engineering vibration**. 2014.

[42] KERSCHEN, G.; GOLINVAL, J.-C.. **Physical interpretation of the proper orthogonal modes using the singular value decomposition**. Journal of Sound and vibration, 249(5):849–865, 2002.

[43] KONSTANTINIDIS, E.. **Added mass of a circular cylinder oscillating in a free stream**. In: PROC. R. SOC. A, volumen 469, p. 20130135. The Royal Society, 2013.

[44] KUMAR, P.; GANGULI, A. ; BENIPAL, G. S.. **Mechanics of cable-suspended beams**. Latin American Journal of Solids and Structures, 14(3):544–559, 2017.

[45] LAZER, A. C.; MCKENNA, P.. **Large-amplitude periodic oscillations in suspension bridges: some new connections with nonlinear analysis**. Siam Review, 32(4):537–578, 1990.

[46] LENAERTS, V.; KERSCHEN, G. ; GOLINVAL, J.-C.. **Proper orthogonal decomposition for model updating of non-linear mechanical systems**. Mechanical Systems and Signal Processing, 15(1):31–43, 2001.

[47] LIN, Y.-Y.; CHENG, C.-M.; WU, J.-C.; LAN, T.-L. ; WU, K.-T.. **Effects of deck shape and oncoming turbulence on bridge aerodynamics**. Tamkang Journal of Science and Engineering, 8(1):43–56, 2005.

[48] MACDONALD, J. H.. **Lateral excitation of bridges by balancing pedestrians**. In: PROCEEDINGS OF THE ROYAL SOCIETY OF LONDON A: MATHEMATICAL, PHYSICAL AND ENGINEERING SCIENCES, p. rspa–2008. The Royal Society, 2008.

[49] PAÏDOUSSIS, M. P.; PRICE, S. J. ; DE LANGRE, E.. **Fluid-structure interactions: cross-flow-induced instabilities**. Cambridge University Press, 2010.

[50] SAMPAIO, R.; BELLIZZI, S.. **Analysis of nonstationary random processes using smooth decomposition**. Journal of Mechanics of Materials and Structures, 6(7):1137–1152, 2011.

[51] SARKER, J.; MANZUR, T.. **Optimum dimensions of suspension bridges considering natural period**. IOSR journal of Mech & Civil Engg, 6:67–76, 2013.

[52] SEMPER, B.. **A mathematical model for suspension bridge vibration**. Mathematical and computer modelling, 18(11):17–28, 1993.

[53] SIGRIST, J.-F.. **Fluid-structure interaction: an introduction to finite element coupling**. John Wiley & Sons, 2015.

[54] SOIZE, C.. **Fundamentals of random signal analysis, application to modal identification in structural dynamics, course given at puc-rio university, rio de janeiro, brazil, august 19-23, 1996**. Final Edition, Paris, France, 1997.

[55] SOUZA DE CURSI, E.. **Variational Methods for Differential Equations**. Wiley Online Library, 2015.

[56] STRØMMEN, E.. **Theory of bridge aerodynamics**. Springer Science & Business Media, 2010.

[57] VENUTI, F.; RACIC, V. ; CORBETTA, A.. **Modelling framework for dynamic interaction between multiple pedestrians and vertical vibrations of footbridges**. Journal of Sound and Vibration, 379:245–263, 2016.

[58] WAGNER, G. B.; FOINY, D.; SAMPAIO, R. ; LIMA, R.. **Operational modal analysis under wind load using stochastic sub-space identification**. Proceedings of DINAME, 2017.

[59] WAGNER, G.; FOINY, D.; LIMA, R. ; SAMPAIO, R.. **The robust smooth orthogonal decomposition method for operational modal analysis**.

[60] WRIGGERS, P.. **Nonlinear finite element methods**. Springer Science & Business Media, 2008.

[61] ZOHURI, B.. **Dimensional analysis and self-similarity methods for engineers and scientists**. Springer, 2015.

A
Dynamical Systems Identification with Smooth Decomposition - Article published for DINAME2017

Dynamical Systems Identification with Smooth Decomposition

Damien Foiny[1], **Gustavo B. Wagner**[1], **Rubens Sampaio**[1], **Roberta Lima**[1]

[1] Pontifical Catholic University of Rio de Janeiro (PUC-Rio), Department of Mechanical Engineering, Vibrations and Dinamics Laboratory, Rua Marquês de São Vicente, 225, Gávea - 22453-900, Rio de Janeiro - RJ, Brazil, damien.foiny@gmail.com, gustavo_gbw@hotmail.com, rsampaio@puc-rio.br, robertalima@puc-rio.br

Abstract: Smooth Decomposition (SD) is a multivariate data or statistical analysis method to find normal modes and natural frequencies in an spatial data field. The projection used for this method is made such as it keeps the maximum variance possible for the displacement vector and also as it keeps the smoothest motions along time. From this method we can get the "energy" participation in the response of each normal mode during the simulation or the experimental test which can be a relevant information to validate results concerning the identification process. This method of identification can be used for linear and nonlinear systems and uses only output data given that the excitation satisfies some properties normally met by a well chosen random excitation, as a white noise, for example. The objective of this method is to identify systems from their displacement field under ambient excitation which, in many cases, can be hard to compute or to describe. As the method is only based on the covariance matrices of the displacement field and the corresponding velocity field, it is no needed further considerations and approximations. In this point the method is a great tool for modal analysis and system identification. In this paper, the presentation of the method is firstly done which will show us how we can interpret the results of SD for different systems and then the application of SD on simulated multi-DoF damped and undamped systems is performed and discussed to understand how SD can be a great tool for modal analysis. A discussion about the quality of the excitation is also performed.

Keywords: Smooth Decomposition (SD), System Identification, Operational Modal Analysis (OMA), Nonlinear Parameters Identification

INTRODUCTION

The Smooth Decomposition (SD) is a statistical analysis technique for finding structures in an ensemble of spatially distributed data such that the vector displacement not only keeps the maximum possible variance but also the motion, as the velocity field, is as smooth in time as possible. Closely related with the SD are the dual smooth modes used in the framework of oblique projection to expand a random response of a system. The concept of dual mode with the associated decomposition defines a tool that transforms the SD in an efficient modal analysis tool. This method of identification can be used for linear and nonlinear systems and uses only output data as soon as the excitation satisfies some properties normally met by a well chosen random excitation, as a white noise, for example.

The main properties of the SD are discussed and some optimality characteristics of the expansion are deduced. The parameters of the SD (using the dual smooth modes and the smooth values) give access to a modal parameters of a linear system in terms of mode shapes, resonance frequencies and modal energy participations. This part is a remarkable improvement with respect to the standard modal analysis methods. This novel modal analysis of a linear system is illustrated by examples.

One of the examples, to show the main features of the method, is a simple multi-DoF undamped system subject to a random excitation that is identified from the output signal. Then, more complex examples of a multi-DoF system are identified. A discussion concerning the difficulty to identify systems with high damping coefficient is made. We also study a case which can be a first step before considering continuous systems with the partially observed case. Finally we will discuss about the importance of the excitation quality for such a method.

It is interesting to say that this is a new method, not yet compared with the methods known in the literature as Operational Modal Analysis (OMA). So far the only association between SD and OMA is the fact that both methods use output signals for the identification and they require random excitation. However the theories are different. SD is a type of Karhunen-Loève Decomposition, using correlations and projections in the modes whereas OMA uses the controllability matrix and correlations of the measured signals that are not necessarily the state of the system.

DESCRIPTION OF THE SMOOTH DECOMPOSITION METHOD

First we will present the basis of this method and its main objective. There is already another well known method called the "Karhunen-Loève Decomposition (KLD)" or the "Proper Orthogonal Decomposition (POD)" used to analyze random data. This method is not presented in this article. The main objective of KLD or POD consists in finding the base

B
Operational modal analysis under wind load using stochastic sub-space identification - Article published for DINAME2017

Operational modal analysis under wind load using stochastic sub-space identification

Gustavo B. Wagner[1]**, Damien Foiny**[1]**, Rubens Sampaio**[1]**, Roberta Lima**[1]

[1] Pontifícia Universidade Católica do Rio de Janeiro - Rua Marquês de São Vicente, 225, Gávea - Rio de Janeiro, RJ - Brasil - 22451-900 , gustavo_gbw@hotmail.com, damien.foiny@gmail.com, rsampaio@puc-rio.br, robertalima@puc-rio.br

Abstract: The extraction of modal parameters from a real structure represents an important step in modal analysis. When only the output signal is available in an experiment, the system identification process is referred as operation modal analysis (OMA). Applications of those cases are fond for structures where the ambient excitation (wind, traffic, waves, nearby systems, etc.) can not be removed or is the only possible one. Once the input signals can not be measured, some assumptions in their random nature are needed together with a stochastic modeling of the system. Among several methods, the stochastic subspace identification (SSI) has been shown to be a consistent one and, therefore, was chosen to be used in this paper. Here, the modal analysis of a system under wind load is studied. The fluid-structure interaction force is usually not easy to be represented and its whiteness (assumption made in most of OMA methods) can not be easily conformed. In this way, a two floor building model is used for experimental validation, where different fluid-structure interaction were created. The paper begins with a presentation of the discrete state space model followed by the SSI theory. Two popular SSI algorithms are presented: covariance-driven and data-driven. A efficient way to select the correct parameters for the method is discussed together with a procedure to analyze the results. To exemplify the identification process, experimental results are shown and the identified parameters are listed. As conclusion, the wind has been shown to be a good excitation source for OMA once the system has been correct identified.

Keywords: Operational modal analysis, System identification, Stochastic subspace methods, wind excitation, experimental validation

INTRODUCTION

Operational Modal Analysis (OMA) consist in find the dynamic characteristic of a structure through its modal parameters using output-only signals. Differently from the classical approach of Experimental Modal Analysis (EMA), where the input signal are also measured, OMA only uses the stochastic nature of the inputs, assumed to be random due the ambient conditions. This fact allows system identification to be done under circumstances where EMA is limited, which includes: large and heavy structures, where a controlled input is hard and expensive, and identification process of systems under operational conditions, where interferences from the location can not be eliminated.

With its majors developments happening in the early 1990s, applications of OMA in the structural dynamic field is far from reach its total potential. Nowadays, OMA has been used as tool in two main areas. The first is in the model validation of big structures such as bridges, tall buildings, stadiums and oil rigs (Rainieri and Fabbrocino, 2014)(Rodrigues, 2004)(Brincker and Ventura, 2015). These structures have in common the heavy weight and the acting ambient forces. The excitation are done by wind, traffic, and waves which are difficult to model and measure. Therefore, OMA methods for parameters estimations suits very well in those cases (Reynders et al.,2015) (Reynders et al.,2008a). Recent articles have also focused on the variance estimation of the modal parameters. Mellinger et al.(2016), for example, measured the uncertainties in the modal parameter of a aircraft during in-flight tests. Other main application where OMA has been developed in the recent years is in the field of structural health monitoring (SHM)(Liu, 2011)(Farrar, 2013)(Deraemacker, 2010). It is done by a periodic modal identification, which evaluates a possible change in the modal parameters. Cracks, corrosion, unfastened bolts and etc. usually reduces the system stiffness modifying natural frequencies and mode shapes.

The purpose of this article is to demonstrate a complete procedure of system identification in a real structure under wind load using stochastic subspace method. Becoming popular in the 2000s, stochastic subspace identification (SSI) consists in a collection of techniques that can be formulated in a consistent framework, where properties of the system can be estimated through matrix subspaces. The two principal subspace algorithms found in the literature are covariance-driven and data-driven, which consist in estimate the system controllability matrix using covariance matrices or orthogonal projections of the output signal. For a clear understanding of such methods, the extension of the state space model are done by the arrangement of the data in Hankel matrices. The methods performance heavily depends in the Hankel matrices dimension, since they are direct related to the number of elements in the estimation of covariances, the system order and the ratio between the interested frequency and the sampling frequency.

C
The Robust Smooth Orthogonal Decomposition Method for Operational Modal Analysis - Article published for IOMAC2017

IOMAC'17

7ᵗʰ *International Operational Modal Analysis Conference*
2017 May10-12 Ingolstadt - Germany

THE ROBUST SMOOTH ORTHOGONAL DECOMPOSITION METHOD FOR OPERATIONAL MODAL ANALYSIS

G.B. Wagner[1], D. Foiny[2], R. Lima[3], R. Sampaio[4]

[1] Master's student, Pontifícia Universidade Católica do Rio de Janeiro, Brazil, gustavo.wagner@aluno.puc-rio.br

[2] Master's student, Pontifícia Universidade Católica do Rio de Janeiro, Brazil, damien.foiny@gmail.com

[3] Prof. , Pontifícia Universidade Católica do Rio de Janeiro, Brazil, robertalima@puc-rio.br

[4] Prof. , Pontifícia Universidade Católica do Rio de Janeiro, Brazil, rsampaio@puc-rio.br

ABSTRACT

The smooth orthogonal decomposition (SOD) method has been studied in the last past years as an output-only modal parameters identification technique for linear normal modes and natural frequencies extraction. Seen as a variant of the proper orthogonal decomposition (POD), the SOD method consists in the identification of a projection base that not just maintain the maximum variance of a scalar field, but also perform it in the smoothest possible way. In this paper a new implementation of the method is proposed to overcame its noise sensitivity problem. This new implementation also allows the modal parameters uncertainties to be quantified. With a numerical simulation and an experimental test, the method's performance is demonstrated and validated.

Keywords: smooth orthogonal decomposition, system identification, noise control

1.   INTRODUCTION

In *operational modal analysis* (OMA), orthogonal decomposition methods are a recent family of identification techniques based on a multivariate statistics method. They all have been developed as extension of the *proper orthogonal decomposition* (POD) to overcome some of its limitations when applied to modal analysis. For linear structures, POD requires a priori knowledge of the system's inertial matrix to relate the *proper orthogonal modes* (POMs) to the *linear normal modes* (LNMs), as presented in [1][2][3]. Another inherent limitation consists in the fact that the *proper orthogonal values* (POVs) contains only informations about the energy of the POMs in the acquired data, and therefore are not uniquely related to them. Those disadvantages were first overcome by the *smooth orthogonal decomposition* method (SOD) in [4] and after by the *state-variable modal decomposition* method (SVMD) in [5][6].

The smooth orthogonal decomposition (SOD), also known as smooth Karhunen-Loève decomposition [7], consists in the identification of a projection base that not just maintain the maximum variance of a scalar field (in case of modal analysis, the structure displacement, velocity or acceleration), but also

D
Dynamical System Identification and Modal Analysis using Smooth Decomposition - Article submitted to Scientist Review

Dynamical System Identification and Modal Analysis using Smooth Decomposition

Damien Foiny[1], Gustavo B. Wagner[1], Roberta Lima[2], Rubens Sampaio[2,*]

Pontifical Catholic University of Rio de Janeiro (PUC-Rio)
Department of Mechanical Engineering
Vibrations and Dynamics Laboratory
Rua Marquês de São Vicente, 225, Gávea - 22453-900, Rio de Janeiro - RJ, Brazil

Abstract

Smooth Decomposition (SD) is a multivariate data or statistical analysis method to find normal modes, natural frequencies and energy partition in a spatial data field. The projection used for this method is chosen to keep the maximum variance possible for the generalized displacement vector and also to keep the smoothest motions along time. This method gives the "energy" participation of each normal mode in the response during the simulation or the experimental test which is a crucial information for identification of non-linear systems. This method of identification can be used for linear and nonlinear systems (since we do have access to the energy partition) and uses only output data provide the excitation satisfies some properties normally met by a well chosen random excitation, as a white noise, for example. The objective of this method is to identify systems from their generalized displacement field under ambient excitation which, in many cases, can be hard to compute or to describe. As the method is only based on the covariance matrices of the generalized displacement field and the corresponding velocity field, no further considerations and approximations are needed. Due to this feature, the method is a great tool for modal analysis and system identification. In this paper, the presentation of the

---

[*]Corresponding author. Postal address defined before. Tel.: +55 (21) 3527-1172
  Email address: `rsampaio@puc-rio.br` (Rubens Sampaio)
  [1]Master's student, Pontifical Catholic University of Rio de Janeiro, Brazil
  [2]Professor, Pontifical Catholic University of Rio de Janeiro, Brazil

E
Comparison of the modal identification of a test rig of a suspension bridge using ouput-only methods - Abstract written for COBEM 2017

Comparison of the modal identification of a test rig of a suspension bridge using output-only methods

Damien Foiny, Gustavo B. Wagner, Pablo Milheiro, Roberta Lima, Rubens Sampaio

PUC-Rio, Department of Mechanical Engineering
Rua Marquês de São Vicente, 225, Gávea - 22453-900
Rio de Janeiro, RJ - Brazil
damien.foiny@gmail.com, gustavo_gbw@hotmail.com, pablomilheiro@gmail.com,
robertalima@puc-rio.br, rsampaio@puc-rio.br

Abstract: Using a test rig of a suspension bridge several methods of identification using output-only data are compared. The methods compared stem from the Karhunen-Loève decomposition. They use random signals and correlations of the system response to extract the signals from noise. Their ability to deal with noise vary and the methods are compared on this basis. Their sensitivity to noise is discussed as well as their similarities and differences using a test rig of a suspension bridge that challenges the identification.

Keywords: Operational Modal Analysis, System Identification, Decomposition Methods, Identification, Suspension Bridge.

Introduction

The methods of identification used will be referred here as Proper Orthogonal Decomposition (POD). The PODs will be described and how to use them in modal analysis explained. All methods deal with stochastic signals and the main difference among them is how they treat noisy signals.

To simplify the understanding of the methods, they are applied to a test rig representing a suspension bridge. The methods need only output data, so the excitation (with a white noise for the numerical examples and with a wind load for the experimental model) will be not monitored. So the methods are in the class of Operational Modal Analysis (OMA).

Experimental Procedure or Computational Procedure

First, to better explain the similarities and differences among the methods, they will be applied in some toy-problems designed to show how the PODs work. The problems may include damping or not, may be linear or not. For our cases the non-linearity is constructed with a cubic non-linear spring. The computational procedure necessary for the estimation of modal parameters will be shown.

After dealing with the toy-problems, the same methods will be applied on a test rig representing a suspension bridge under not-monitored wind load (Fig.1). This part is a real-life experiment and some difficulties, as noisy signals, will appear.

Results and Discussion

Our results for the identification will be presented in terms of modal parameters. The evaluation of our estimated modal parameters will be made through a comparison of the ones we get from analytic solutions (for numerical examples) and from the numerical model for the

F
Matlab Codes

```
%%%%%%%%%%%%%%%%%%%%%%%%%%%%%%%%%%%%%%%%%%%%%%%%%%%%%%%%%%%%%%
% CODE FIG. 3.2
%%%%%%%%%%%%%%%%%%%%%%%%%%%%%%%%%%%%%%%%%%%%%%%%%%%%%%%%%%%%%%
clear all
clc
close

u = 0:0.01:1;
om = zeros(1,length(u));
for i = 1:length(u)
    om(i) = sqrt((1- u(i)^2));
end

plot(u, om, '-')
suptitle('Evolution of the frequency with relation to the normalized flow velocity');
xlabel('$C_A\displaystyle\frac{dF}{d(Dq)}$','interpreter','latex');
ylabel('Frequency');

%%%%%%%%%%%%%%%%%%%%%%%%%%%%%%%%%%%%%%%%%%%%%%%%%%%%%%%%%%%%%%
% CODE FIG. 3.3
%%%%%%%%%%%%%%%%%%%%%%%%%%%%%%%%%%%%%%%%%%%%%%%%%%%%%%%%%%%%%%
clear all
close all
clc

t = 0:0.01:100;

eps = 10^(-1);
q1 = cos(t).*exp(-eps/2.*t);
q2 = sin(t).*exp(-eps/2.*t);

figure(),
subplot(2,2,1)
plot(t,q1)
xlabel('Time');
ylabel('q_1');

subplot(2,2,3)
plot(t,q2)
xlabel('Time');
ylabel('q_2');

subplot(2,2,[2 4]),
plot(q1(1),q2(1),'*','MarkerSize',10);
hold on
plot(q1,q2)
suptitle('Time evolution of q_1 and q_2 and phase diagram in the q_1q_2-plane');
legend('Starting point');
xlabel('q_1');
ylabel('q_2');

%%%%%%%%%%%%%%%%%%%%%%%%%%%%%%%%%%%%%%%%%%%%%%%%%%%%%%%%%%%%%%
% CODE FIG. 3.4
%%%%%%%%%%%%%%%%%%%%%%%%%%%%%%%%%%%%%%%%%%%%%%%%%%%%%%%%%%%%%%
clear all
```

```matlab
close all
clc

t = 0:0.1:100;

eps = 10^(-1);
q1 = cos(t).*exp(eps/2.*t);
q2 = -sin(t).*exp(eps/2.*t);

figure(),
subplot(2,2,1)
plot(t,q1)
xlabel('Time');
ylabel('q_1');

subplot(2,2,3)
plot(t,q2)
xlabel('Time');
ylabel('q_2');

subplot(2,2,[2 4]),
plot(q1(1),q2(1),'b*','MarkerSize',10);
hold on
plot(q1,q2,'r')
hold on
plot(q1(1),q2(1),'b*','MarkerSize',10);
suptitle('Time evolution of q_1 and q_2 and phase diagram in the q_1q_2-plane');
legend('Starting point');
xlabel('q_1');
ylabel('q_2');

%%%%%%%%%%%%%%%%%%%%%%%%%%%%%%%%%%%%%%%%%%%%%%%%%%%%
% BASIC FUNCTIONS
%%%%%%%%%%%%%%%%%%%%%%%%%%%%%%%%%%%%%%%%%%%%%%%%%%%%

function [PHI,DGradPHI] = BasicFunc (XI,h)

    PHI(1) =  (1/2) - (3/4)*XI + (1/4)*XI^3;
    PHI(2) =  (1/4) - (1/4)*XI - (1/4)*XI^2 + (1/4)*XI^3;
    PHI(3) =  (1/2) + (3/4)*XI - (1/4)*XI^3;
    PHI(4) = -(1/4) - (1/4)*XI + (1/4)*XI^2 + (1/4)*XI^3;

    DGradPHI(1) =  (3/2)*XI;
    DGradPHI(2) = -(1/2) + (3/2)*XI;
    DGradPHI(3) = -(3/2)*XI;
    DGradPHI(4) =  (1/2) + (3/2)*XI;

end

%%%%%%%%%%%%%%%%%%%%%%%%%%%%%%%%%%%%%%%%%%%%%%%%%%%%
% GLOBAL POINTERS
%%%%%%%%%%%%%%%%%%%%%%%%%%%%%%%%%%%%%%%%%%%%%%%%%%%%

function [ASSMtrx, DomNodeID,NGDOF] = GlobalPointers(NELE)

DomNodeID = zeros(2,NELE);
```

```
ASSMtrx = zeros(4,NELE);
for iele = 1:NELE
   DomNodeID (1,iele) = iele;
   DomNodeID (2,iele) = iele + 1;

   ASSMtrx (1,iele) = 2*iele - 1;
   ASSMtrx (2,iele) = 2*iele;
   ASSMtrx (3,iele) = 2*iele + 1;
   ASSMtrx (4,iele) = 2*iele + 2;
end
NGDOF = max(max(ASSMtrx));

%%%%%%%%%%%%%%%%%%%%%%%%%%%%%%%%%%%%%%%%%%%%%%%%%%%%%%%
% VARIABLES
%%%%%%%%%%%%%%%%%%%%%%%%%%%%%%%%%%%%%%%%%%%%%%%%%%%%%%%

L = 1;

B = 50e-3;
h = 2e-3;
E = 200e9;
rho = 7850;
grav = 9.81;

I = B*h^3/12;
A = B*h;

q = rho*A*grav;
H = 5/4*L*q;

Ec = 200e9;
rc = 1.5e-3;
Ac = pi*rc^2;
Lc = 1.026*L;

w0 = .5;
wc = @(x) -q/2/H .* x.*(L-x) + w0;

C1 = 0.5;
C2 = 0.5;
C3 = 1;
C4 = 1;

%%%%%%%%%%%%%%%%%%%%%%%%%%%%%%%%%%%%%%%%%%%%%%%%%%%%%%%
% GAUSS VALUES
%%%%%%%%%%%%%%%%%%%%%%%%%%%%%%%%%%%%%%%%%%%%%%%%%%%%%%%

NGP = 4;
XIGP = [-0.86113631 -0.33998104 0.33998104 0.86113631];
WGP = [0.34785485  0.65214515  0.65214515 0.34785485];

%%%%%%%%%%%%%%%%%%%%%%%%%%%%%%%%%%%%%%%%%%%%%%%%%%%%%%%
% GET ELEM AB
%%%%%%%%%%%%%%%%%%%%%%%%%%%%%%%%%%%%%%%%%%%%%%%%%%%%%%%

function [M,K,Knl,Fnl] = GetElemAb(iele, NGP, XIGP, WGP)
```

```matlab
global DX

M = zeros(4);
K = zeros(4);
Knl = zeros(4);
Fnl = zeros(4,1);

for igp = 1:NGP
   XI = XIGP(igp);
   W = WGP(igp);
   [Phi,DDPhi] = BasicFunc(XI,DX(iele));
   for ilnode = 1:4
      for jlnode = 1:4
         M(ilnode, jlnode) = M(ilnode, jlnode) + ...
            W*(Phi(ilnode) * Phi(jlnode)* (DX(iele)/2));

         K(ilnode, jlnode) = K(ilnode, jlnode) + ...
            W*(DDPhi(ilnode) * DDPhi(jlnode)* (2/DX(iele))^3);

         Knl(ilnode, jlnode) = Knl(ilnode, jlnode) + ...
            W*(Phi(ilnode) * DDPhi(jlnode)* 2/DX(iele));

      end
      Fnl(ilnode) =  Fnl(ilnode) + ...
         W*(Phi(ilnode)*DX(iele)/2);
   end
end

%%%%%%%%%%%%%%%%%%%%%%%%%%%%%%%%%%%%%%%%%%%%%%%%%%%%%%%%%%%%
% GET ELEM F
%%%%%%%%%%%%%%%%%%%%%%%%%%%%%%%%%%%%%%%%%%%%%%%%%%%%%%%%%%%%

function [F] = GetElemF(iele, NGP, XIGP, WGP,f)

global DX

F = zeros(4,1);

for igp = 1:NGP
   XI = XIGP(igp);
   W = WGP(igp);
   [Phi,~] = BasicFunc(XI,DX(iele));
   for ilnode = 1:4
      F(ilnode) =  F(ilnode) + W*(f(ilnode,:)*Phi(ilnode)*DX(iele)/2);
   end
end

%%%%%%%%%%%%%%%%%%%%%%%%%%%%%%%%%%%%%%%%%%%%%%%%%%%%%%%%%%%%
% GLOBAL MAT
%%%%%%%%%%%%%%%%%%%%%%%%%%%%%%%%%%%%%%%%%%%%%%%%%%%%%%%%%%%%


function [M,K,Knl,Fnl] = GlobalMat(ASSMtrx,NGDOF,NELE,NGP,XIGP,WGP)

M = zeros(NGDOF);
```

```matlab
    K = zeros(NGDOF);
    Knl = zeros(NGDOF);
    Fnl = zeros(NGDOF, 1);

    for iele = 1:NELE
       [Me,Ke,Knle,Fnle] = GetElemAb(iele, NGP, XIGP, WGP);
       for ildof = 1:4
          igdof = ASSMtrx(ildof,iele);
          for jldof = 1:4
             jgdof = ASSMtrx(jldof,iele);
             M(igdof,jgdof) = M(igdof,jgdof) + Me(ildof,jldof);
             K(igdof,jgdof) = K(igdof,jgdof) + Ke(ildof,jldof);
             Knl(igdof,jgdof) = Knl(igdof,jgdof) + Knle(ildof,jldof);
          end
          Fnl(igdof) = Fnl(igdof) + Fnle(ildof);
       end
    end

    %%%%%%%%%%%%%%%%%%%%%%%%%%%%%%%%%%%%%%%%%%%%%%%%%%%%%%%%
    % GLOBAL F
    %%%%%%%%%%%%%%%%%%%%%%%%%%%%%%%%%%%%%%%%%%%%%%%%%%%%%%%%

    function [F] = GlobalF(ASSMtrx,NDOF,NELE,NGP,XIGP,WGP,f)

    F = zeros(NDOF, 1);

    for iele = 1:NELE
       [Fe] = GetElemF(iele, NGP, XIGP, WGP,f(ASSMtrx(:,iele),:));
       for ildof = 1:4
          igdof = ASSMtrx(ildof,iele);
          F(igdof) = F(igdof) + Fe(ildof);
       end
    end

    %%%%%%%%%%%%%%%%%%%%%%%%%%%%%%%%%%%%%%%%%%%%%%%%%%%%%%%%
    % NEWMARK ROUTINE
    %%%%%%%%%%%%%%%%%%%%%%%%%%%%%%%%%%%%%%%%%%%%%%%%%%%%%%%%

    function [x,dx,ddx] = newmarkmodif(t,M,K,C,Knl,Fnl,dof,F)

    global X
    variables

    gamma = 1/2;
    beta = 1/4;

    dt = t(2)-t(1);
    Nt = length(t);

    % ALLOCATION
    x = zeros(dof,Nt); dx = zeros(dof,Nt); ddx = zeros(dof,Nt); tens = zeros(1,Nt);

    % INITIAL CONDITIONS
    x(:,1) = zeros(dof,1); dx(:,1) = zeros(dof,1); ddx(:,1) = zeros(dof,1);

    % NEWMARK COEFFICIENTS
```

```matlab
a0 = 1/beta/dt/dt; a1 = gamma/beta/dt; a2 = 1/2/beta;
a3 = -dt*(1 - gamma/2/beta); a4 = 1/beta/dt; a5 = gamma/beta;

fac = 1;
func = @(u) fac*trapz(X,u);

for i = 1:Nt-1

   dF = F(:,i+1) - F(:,i);

   testval1 = 1 + C3*func([0;x(2:2:end-1,i);0]);
   if testval1 <= 0
      g = 0;
   else
      g = testval1;
   end

   Kbar = a0*M + a1*C + C1*K - C2*g*Knl;
   Fbar = dF - C4*g*Fnl + (a2*M + a3*C)*ddx(:,i) + (a4*M + a5*C)*dx(:,i);

   Dx = Kbar\Fbar;
   x(:,i+1) = x(:,i) + Dx;

   Ddx = a1*Dx - a5*dx(:,i) - a3*ddx(:,i);
   dx(:,i+1) = dx(:,i) + Ddx;

   testval2 = 1 + C3*func([0;x(2:2:end-1,i+1);0]);
   if testval2 <= 0
      g = 0;
   else
      g = testval2;
   end

   ddx(:,i+1) = - M\(C1*K*x(:,i+1) ...
      - C2*g*Knl*x(:,i+1) ...
      + C*dx(:,i+1) ...
      + C4*g*Fnl ...
      - F(:,i+1) );
end

%%%%%%%%%%%%%%%%%%%%%%%%%%%%%%%%%%%%%%%%%%%%%%%%%%%%%%%%%
% MAIN CODE CHAP5
%%%%%%%%%%%%%%%%%%%%%%%%%%%%%%%%%%%%%%%%%%%%%%%%%%%%%%%%%

clear all
close all
clc

global X DX

%-------------------------------------------------------------------%
% PRE PROCESSING
%-------------------------------------------------------------------%

% GEOMETRY
variables
```

```matlab
% MESH
NELE = 20;
NODES = NELE+1;
X = linspace(0,L,NODES);
DX = diff(X);
[ASSMtrx, DomNodeID,NGDOF] = GlobalPointers(NELE);

% GAUSS INT
GaussVal

% GLOBAL MATRICES
[M,K,Knl,Fnl] = GlobalMat(ASSMtrx,NGDOF,NELE,NGP,XIGP,WGP);

% BOUNDARY CONDITIONS
fixedNodeU = [1 NGDOF-1]';
fixedNodeV = []';

% REDUCED MATRICES
prescribedDof = [fixedNodeU;fixedNodeV];
activeDof = setdiff([1:NGDOF]', prescribedDof);
M = M(activeDof,activeDof);
K = K(activeDof,activeDof);
Knl = Knl(activeDof,activeDof);
Fnl = Fnl(activeDof,1);

% DAMPING
aM = 0; aK = 0;
C = aM*M + aK*K;

% MODAL ANALYSIS LINEAR
[V,D] = eig(C1*K - C2*Knl,M);
freqMAT = sqrt(sort(diag(D)))/2/pi;

%-----------------------------------------------------------------------%
% DYNAMICAL ANALYSIS
%-----------------------------------------------------------------------%
% TIME
fs = 200;
tend = 50;
t = linspace(0,tend,tend*fs);
Nt = length(t);

% FORCE
lambda = 1:0.1:5;
mu = 5:0.1:9;

maxdefl = zeros(length(lambda),length(mu));
pd = zeros(length(lambda),length(mu));

ind = 0;
for ilam = 1:length(lambda)
   for imu = 1:length(mu)
   ind = ind + 1
   f = zeros(NGDOF,Nt);
```

```matlab
        ii = 0;
        for i = 1:2:NGDOF
            ii = ii + 1;
            for j = 1:Nt
                f(i,j) = lambda(ilam) * sin(pi*X(ii)) * sin(mu(imu)*t(j)) + C4;
            end
        end

        F = zeros(NGDOF,Nt);
        for i = 1:Nt
            [F(:,i)] = GlobalF(ASSMtrx,NGDOF,NELE,NGP,XIGP,WGP,f(:,i));
        end
        F = F(activeDof,:);

        dof = length(activeDof);
        % SOLVING VIA NEWMARK
        [x,dx,ddx] = newmarkmodif(t,M,K,C,Knl,Fnl,dof,F);
        disp = zeros(NGDOF,length(t));
        disp(activeDof,:) = x;

        maxdefl(ilam,imu) = max(max(abs(disp)));
        pd(ilam,imu) = maxdefl(ilam,imu)/lambda(ilam);

    end
end

%----------------------------------------------------------------------%
% POST PROCESSING
%----------------------------------------------------------------------%

figure(),
[xlam,ymu] = meshgrid(lambda,mu);
Z = pd';
hSurface = surf(xlam,ymu,Z);
set(hSurface,'FaceColor',[0 0 1],'FaceAlpha',0);
az = -70;
el = 45;
view(az, el);
axis([lambda(1) lambda(end) mu(1) mu(end) 0 max(max(maxdefl))])
xlabel('\lambda');
ylabel('\mu');
zlabel('pd');

%%%%%%%%%%%%%%%%%%%%%%%%%%%%%%%%%%%%%%%%%%%%%%%%%%%%%%%%%%%%%%%
% MAIN CODE CHAP6
%%%%%%%%%%%%%%%%%%%%%%%%%%%%%%%%%%%%%%%%%%%%%%%%%%%%%%%%%%%%%%%

clear all
close all
clc

global X DX

% GEOMETRY
variablesBis
```

```matlab
% MESH
NELE = 20;
NODES = NELE+1;
X = linspace(0,L,NODES);
DX = diff(X);
[ASSMtrx, DomNodeID,NGDOF] = GlobalPointers(NELE);

% GAUSS INT
GaussVal

% GLOBAL MATRICES
[M,K,Knl,Fnl] = GlobalMat(ASSMtrx,NGDOF,NELE,NGP,XIGP,WGP);

% BOUNDARY CONDITIONS
fixedNodeU = [1 NGDOF-1]';
fixedNodeV = []';

% REDUCED MATRICES
prescribedDof = [fixedNodeU;fixedNodeV];
activeDof = setdiff([1:NGDOF]', prescribedDof);
M = M(activeDof,activeDof);
K = K(activeDof,activeDof);
Knl = Knl(activeDof,activeDof);
Fnl = Fnl(activeDof,1);

% DAMPING
aM = 0; aK = 0;
C = aM*M + aK*K;

% MODAL ANALYSIS LINEAR
[V,D] = eig(C1*K - C2*Knl,M);

% [V,D] = eig(K,M);
freqMAT = sqrt(sort(diag(D)))/2/pi;

%----------------------------------------------------------------------%
% DYNAMICAL ANALYSIS
%----------------------------------------------------------------------%
% TIME
fs = 200;
tend = 20;
t = linspace(0,tend,tend*fs);
Nt = length(t);

U = 1:.25:5;
ptk = 0.001;
mutab = 1:0.2:4;
maxtab = zeros(length(U),length(mutab));
ind = 0;
for iu0 = 1:length(U)
   U0 = U(iu0);
   CL = 1;
   S = 1;
   rhof = 1;
   for imu = 1:length(mutab)
      ind = ind + 1
```

```matlab
            mu = mutab(imu);
            f = zeros(NGDOF,Nt);
            ii = 0;
            for i = 1:2:NGDOF
                ii = ii + 1;
                for j = 1:Nt
                    f(i,j) = 1/2*rhof*CL*(U0*sin(pi*X(ii)))^2 * sin(mu*t(j)) + C4;
                end
            end

            F = zeros(NGDOF,Nt);
            for i = 1:Nt
                [F(:,i)] = GlobalFBis(ASSMtrx,NGDOF,NELE,NGP,XIGP,WGP,f(:,i));
            end
            F = F(activeDof,:);

            dof = length(activeDof);
            % SOLVING VIA NEWMARK
            [x,dx,ddx] = newmarkmodifBis(t,M,K,C,Knl,Fnl,dof,F,U0,rhof,ptk);
            disp = zeros(NGDOF,length(t));
            disp(activeDof,:) = x;

            maxdisp = max(max(disp(1:2:NGDOF,:)));
            maxdisp = maxdisp/U0^2;
            maxtab(iu0,imu) = maxdisp;
        end

    end

    figure(),
    [xU,ymu] = meshgrid(U,mutab);
    Z = maxtab';
    hSurface = surf(xU,ymu,Z);
    set(hSurface,'FaceColor',[0 0 1],'FaceAlpha',0);
    az = -70;
    el = 45;
    view(az, el);
    xlabel('\lambda_U');
    ylabel('\mu_U');
    zlabel('pd_2');


    %%%%%%%%%%%%%%%%%%%%%%%%%%%%%%%%%%%%%%%%%%%%%%%%%%%%%%%%%%%%%%
    % MAIN CODE CHAP7
    %%%%%%%%%%%%%%%%%%%%%%%%%%%%%%%%%%%%%%%%%%%%%%%%%%%%%%%%%%%%%%

    clear all
    close all
    clc

    global X DX


    %----------------------------------------------------------------------%
    % PRE PROCESSING
    %----------------------------------------------------------------------%
```

```matlab
% GEOMETRY
variables

% MESH
NELE = 20;
NODES = NELE+1;
X = linspace(0,L,NODES);
DX = diff(X);
[ASSMtrx, DomNodeID,NGDOF] = GlobalPointers(NELE);

% GAUSS INT
GaussVal

% GLOBAL MATRICES
[M,K,Knl,Fnl] = GlobalMat(ASSMtrx,NGDOF,NELE,NGP,XIGP,WGP);

% BOUNDARY CONDITIONS
fixedNodeU = [1 NGDOF-1]';
fixedNodeV = []';

% REDUCED MATRICES
prescribedDof = [fixedNodeU;fixedNodeV];
activeDof = setdiff([1:NGDOF]', prescribedDof);
M = M(activeDof,activeDof);
K = K(activeDof,activeDof);
Knl = Knl(activeDof,activeDof);
Fnl = Fnl(activeDof,1);

% DAMPING
aM = 0; aK = 0;
C = aM*M + aK*K;

[V,D] = eig(C1*K - C2*Knl,M);

freqMAT = sqrt(sort(diag(D)))/2/pi;

%------------------------------------------------------------------------%
% DYNAMICAL ANALYSIS
%------------------------------------------------------------------------%
% TIME
fs = 1500;
tend = 10;
t = linspace(0,tend,tend*fs);
Nt = length(t);

% FORCE
factab = 0.0001:0.0002:0.01;

enertab = zeros(10,length(factab));
freqtab = zeros(10,length(factab));
for ifac = 1:length(factab)
    ifac
    fac = factab(ifac);
    f = zeros(NGDOF,Nt);

    for i = 1:2:NGDOF
```

```matlab
        for j = 1:Nt
            f(i,j) = fac*(rand(1,1)-.5);
        end
    end

    F = zeros(NGDOF,Nt);
    for i = 1:Nt
        [F(:,i)] = GlobalF(ASSMtrx,NGDOF,NELE,NGP,XIGP,WGP,f(:,i));
    end
    F = F(activeDof,:);

    dof = length(activeDof);

    % SOLVING VIA NEWMARK
    [x,dx,ddx] = newmarkmodif(t,M,K,C,Knl,Fnl,dof,F);
    disp = zeros(NGDOF,length(t));
    disp(activeDof,:) = x;

    %------------------------------------------------------------------------%
    % SMOOTH DECOMPOSITION
    %------------------------------------------------------------------------%

    ySD = disp(3:2:end-2,:)';
    [Ns,n_dof] = size(ySD);

    for i = 1:n_dof
        ySD(:,i) = ySD(:,i) - mean(ySD(:,i));
    end
    dy = timediff(ySD,fs,'Remez');
    [ldy,cdy] = size(dy);
    temp = ySD;
    clear('y');
    tronc = 20;
    ySD = temp(tronc+1:end,:);
    Ru = (1/Ns).*ySD'*ySD;
    Rdu = (1/ldy).*dy'*dy;
    [gamma_des,lambda_des] = eig(Ru,Rdu);
    [lambda,ind] = sort(diag(lambda_des),'descend');
    gamma = gamma_des(:,ind);
    psi = Rdu*gamma;
    xi = ySD(:,1:n_dof)*psi;
    zeta = ySD(:,1:n_dof)*gamma;

    omega = zeros(n_dof,1);
    freq = zeros(n_dof,1);
    for i = 1:n_dof
        omega(i,1) = sqrt(1/lambda(i,1));
        freq(i,1) = omega(i,1)/(2*pi);
    end

    E = zeros(1,n_dof);
    for i = 1:n_dof
        E(1,i) = lambda(i,1)*(norm(psi(:,i)))^2;
    end

    fE = zeros(1,n_dof);
```

```matlab
    for i = 1:n_dof
        fE(1,i) = E(1,i)/sum(E);
    end

    enertab(:,ifac) = fE(1:10);
    freqtab(:,ifac) = freq(1:10);

end

%------------------------------------------------------------------------%
% POST PROCESSING
%------------------------------------------------------------------------%

[M,I] = max(enertab);

set(0,'DefaultAxesLineStyleOrder',{'+','o','*','x','s','d','^','v','>','<','p','h'});
figure(),
for j = 1:10
    hold on
    plot(factab,freqtab(j,:),'b','MarkerSize',10);
end
hold on
maxfreq  = zeros(1,length(freqtab));
for i = 1:length(freqtab)
    maxfreq(1,i) = freqtab(I(i),i);
end
plot(factab,maxfreq,'r-','LineWidth',2);
legend('1','2','3','4','5','6','7','8','9','10','Location','eastoutside')
xlabel('Energy level s_0');
ylabel('Frequencies');
title({'Evolution of of frequencies with ',['C_1 = ',num2str(C1),', C_2 = ',num2str(C2),', C_3 =
',num2str(C3),', C_4 = ',num2str(C4),]});

set(0,'DefaultAxesLineStyleOrder',{'+','o','*','x','s','d','^','v','>','<','p','h'});
figure(),
for j = 1:10
    hold on
    plot(factab,100*enertab(j,:),'b','MarkerSize',10);
end
hold on
plot(factab,100*max(enertab),'r-','LineWidth',2);
legend('1','2','3','4','5','6','7','8','9','10','Location','eastoutside')
xlabel('Energy level s_0');
ylabel('Modal energy (%)');
title({'Evolution of modal energy with ',['C_1 = ',num2str(C1),', C_2 = ',num2str(C2),', C_3 =
',num2str(C3),', C_4 = ',num2str(C4),]});


%%%%%%%%%%%%%%%%%%%%%%%%%%%%%%%%%%%%%%%%%%%%%%%%%%%%%%%%%%%%%%
% NEWMARK ROUTINE MODIFIED FOR CHAP6
%%%%%%%%%%%%%%%%%%%%%%%%%%%%%%%%%%%%%%%%%%%%%%%%%%%%%%%%%%%%%%

function [x,dx,ddx] = newmarkmodifBis(t,M,K,C,Knl,Fnl,dof,F,U0,rhof,ptk)

global X
variablesBis
```

```matlab
gamma = 1/2;
beta = 1/4;

dt = t(2)-t(1);
Nt = length(t);

% ALLOCATION
x = zeros(dof,Nt); dx = zeros(dof,Nt); ddx = zeros(dof,Nt); tens = zeros(1,Nt);

% INITIAL CONDITIONS
x(:,1) = zeros(dof,1); dx(:,1) = zeros(dof,1); ddx(:,1) = zeros(dof,1);

% NEWMARK COEFFICIENTS
a0 = 1/beta/dt/dt; a1 = gamma/beta/dt; a2 = 1/2/beta;
a3 = -dt*(1 - gamma/2/beta); a4 = 1/beta/dt; a5 = gamma/beta;

fac = 1;
func = @(u) fac*trapz(X,u);

for i = 1:Nt-1

    dF = F(:,i+1) - F(:,i);

    testval1 = 1 + C3*func([0;x(2:2:end-1,i);0]);
    if testval1 <= 0
        g = 0;
    else
        g = testval1;
    end
    Kbar = a0*M + a1*C + C1*(K - rhof*U0^2*ptk*K) - C2*g*Knl;
    Fbar = dF - C4*g*Fnl + (a2*M + a3*C)*ddx(:,i) + (a4*M + a5*C)*dx(:,i);

    Dx = Kbar\Fbar;
    x(:,i+1) = x(:,i) + Dx;

    Ddx = a1*Dx - a5*dx(:,i) - a3*ddx(:,i);
    dx(:,i+1) = dx(:,i) + Ddx;

    testval2 = 1 + C3*func([0;x(2:2:end-1,i+1);0]);
    if testval2 <= 0
        g = 0;
    else
        g = testval2;
    end
    ddx(:,i+1) = - M\(C1*(K - rhof*U0^2*ptk*K)*x(:,i+1) ...
        - C2*g*Knl*x(:,i+1) ...
        + C*dx(:,i+1) ...
        + C4*g*Fnl ...
        - F(:,i+1) );
end
```